Chapter 11

Structural Insight Into the Viral 3C-Like Protease Inhibitors: Comparative SAR/QSAR Approaches

Nilanjan Adhikari*, Sandip K. Baidya*, Achintya Saha**, Tarun Jha*
*Jadavpur University, Kolkata, West Bengal, India; **University of Calcutta, Kolkata, West Bengal, India

1 INTRODUCTION

In early 2003, about 8500 people were diagnosed across the world with severe acute respiratory syndrome (SARS). Among them, almost 800 died due to its first outbreak. The disease was broken out and turned into an epidemic in Guangdong of South China. Two cases of SARS infections were noticed in Taiwan and Singapore due to improper handling of the samples in the research laboratory. During April 2004, a "mini outbreak" of infections took place in a research laboratory of Beijing that, in turn, led to a chain of infections across three generations. Fortunately, the total number of SARS-infected people was only nine that time. This incidence threatens us about the mini outbreaks of SARS globally at any time (Anand et al., 2005). The SARS is caused by the SARS-coronavirus (SARS-CoV) that belongs to the family of Coronaviridae. This family also includes viruses, such as feline infectious peritonitis virus, murine hepatitis virus, bovine coronavirus, transmissible gastroenteritis virus (TGEV), as well as human coronavirus 229E (Kim et al., 2015). The SARS is considered as a global threat to the health (Khan, 2013; Perlman and Netland, 2009). Moreover, water and food-borne viral gastroenteritis may be caused by the noroviruses that belong to the family Calciviridae (Atmar, 2010; Patel et al., 2009). Therefore, there is an urgent need to develop small molecule antiviral drugs to combat these viruses. The picornavirus belongs to the family of viruses namely Picornaviridae, Calciviridae, and Coronaviridae (Mandadapu et al., 2013a). A number of pathogeneses in human may occur due to these viruses leading to economic and medical burden. For example, human rhinovirus (HRV) is the major reason

for upper respiratory tract infection (Ren et al., 2012; Turner and Couch, 2007; Winther, 2011) whereas nonpolio enteroviruses are responsible for symptomatic infections with 10–15 million cases per year in United States (McMinn, 2012; Solomon et al., 2010). Depending on the similarity of the polycistronic organization of the genome, common and posttranscriptional strategies along with the conserved region of domain homology in viral proteins, the virus families are related phylogenetically though these families are not related morphologically (Anand et al., 2005; Cavanagh, 1997; Cowley et al., 2000). Coronavirus is found to be responsible for causing a number of diseases not only in human but also in animals, though the human coronavirus has not been taken into account seriously before the SARS outbreak (Anand et al., 2005). Human coronavirus (HCoV) OC43 and 229E may be responsible for illness in the upper portion of the respiratory tract along with common cold-like conditions (Myint, 1995). The HCoV 229E is the only strain till date that can be cultured in cell culture technique efficiently. The symptoms of SARS include rigor, malaise, high degree of fever, cough, headache, and dyspnoea. The symptoms may also lead to produce interstitial infiltrates in lungs that may be treated through ventilation and intubation (Lee et al., 2003). Not only the lungs but also other organs may be affected by SARS infection (such as liver, kidney, and gastrointestinal tract). Therefore, the SARS infection may be treated as a cause of systemic infection. Face-to-face contacts may be supposed to be the reason for transmission of the pathogen though other routes are also possible. A number of inhibitors against SARS-CoV 3CL^{pro} and HRV 3C^{pro} were reported and the process of development of new antivirals against this class has been continued for a decade. In the present report, quantitative structure–activity relationships (QSARs) techniques have been explored to understand the relation between the SARS-CoV 3CL^{pro} and HRV 3C^{pro} enzyme inhibitory activity with the physicochemical and structural properties of these inhibitors developed till now. This approach may be a useful strategy to design and develop novel and potential SARS-CoV 3CL^{pro} and HRV 3C^{pro} inhibitors to combat the dreadful viral infections.

2 GENOME STRUCTURE OF SARS-CoV AND ITS REPLICATIONS

Among the known RNA viruses, the coronaviruses are enveloped, (+) stranded RNA viruses with the largest single-stranded RNA genome (27–31 kb approximately). The RNAs are polyadenylated and 5′capped. These are translated into large polyproteins following their entry into the host cell. The polyproteins are proteolytically cleaved by viral proteinases resulting in viral gene products. The RNA polymerase (pol) is found to be encoded by the genome of SARS-CoV and four structural proteins that commonly include the spike glycoprotein (S), envelope (E), membrane (M), and nucleocapsid (N) proteins in the order of Pol-S-E-M-N. The spike protein (S) is the antigenic determinant for coronavirus and is found to be involved in receptor binding. The E protein plays a significant role during viral assembly. The M glycoprotein transmembrane envelope is found abundantly

and is responsible for budding of the virus, and the N protein is related to the viral RNA packaging (Holmes, 2003; Shigeta and Yamase, 2005; Zhai et al., 2007).

3 STRUCTURE AND FUNCTIONS OF CORONAVIRUS MAIN PROTEASES

Coronavirus contains a positive-stranded RNA with a single-stranded, large size (27–31 kb) RNA genome. Two overlapping polyproteins, that is, pp1a (450 kDa approx.) and pp1ab (750 kDa approx.) are encoded by the replicase gene with more than 20,000 nucleotides (Herold et al., 1993). These two polyproteins regulate the replication, as well as transcription processes in the virus (Thiel et al., 2001). Proteolysis helps to liberate nonstructural proteins (nsp) from these polyproteins. The proteolytic cleavage is mainly controlled by the viral protein-ase termed as M^{pro} (Anand et al., 2005). The M^{pro} is a cysteine proteinase which is synonymous or rather called as 3C-like protease ($3CL^{pro}$) as the substrate specificity resembles picornavirus 3C-protease ($3C^{pro}$), though both of these vi-ruses are structurally less similar (Anand et al., 2002, 2005). The $3CL^{pro}$ is found to cleave the polyprotein at 11 conserved region including Leu-Gln↓ sequences which are initiated by the autolytic cleavage of the enzyme from pp1a and pp1ab (Hegyi and Ziebuhr, 2002b; Ziebuhr et al., 2000). The pp1a and pp1ab poly-proteins help to release functional polypeptides by papain-like protease (PL^{pro}) and $3CL^{pro}$ is located in the nonstructural protein regions, namely nsp3 and nsp5 (Fig. 11.1) via proteolytic reaction mechanisms (Grum-Tokars et al., 2008).

These PL^{pro} and $3CL^{pro}$ are processed by the replicase through autocatalytic mechanisms. The PL^{pro} is found to be responsible for cleaving 3 sites, whereas $3CL^{pro}$ cleaves 11 sites in the viral genome (Grum-Tokars et al., 2008). The SARS-$3CL^{pro}$ cleavage sites are shown in Table 11.1. This type of cleavage is found to be conserved in the $3CL^{pro}$ as evidenced from the experimental data
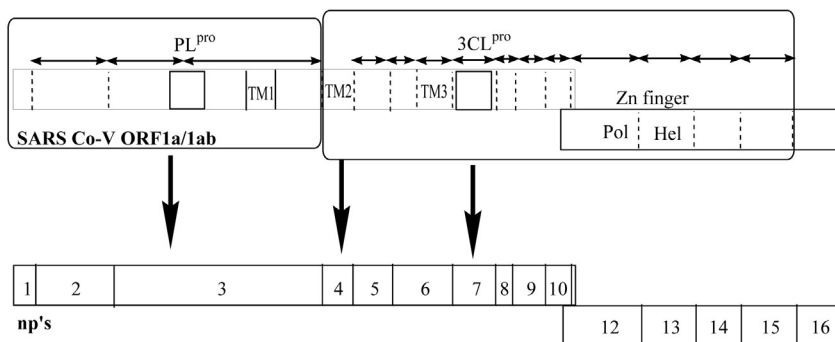
FIGURE 11.1 **SARS-CoV genomic RNA encoding viral replicase polyproteins pp1a and pp1ab (3 and 11 sites are recognized and processed by PL^{pro} and $3CL^{pro}$, respectively).** Hel, Helicase coding regions; Pol, polymerase; TM, transmembrane. *(Adapted from Grum-Tokars, V., Ratia, K., Begaye, A., Baker, S.C., Mesecar, A.D., 2008. Evaluating the 3C-like protease activity of SARS-Coronavirus: recommendations for standardized assays for drug discovery, Virus Res. 133, 63–73.)*

TABLE 11.1 SARS-CoV 3CL^pro Cleavage Sites and the Canonical Recognition Sequences (11 Recognition Sequences are Shown from P5′ to P6 Positions at the Respective Locations)

Sl. No.	3CL^pro cleavage sites	P5′	P4′	P3′	P2′	P1′	P1	P2	P3	P4	P5	P6
01	nsp4/5	LYS	ARG	PHE	GLY	SER	GLN	LEU	VAL	ALA	SER	THR
02	nsp5/6	LYS	LYS	PHE	LYS	GLY	GLN	PHE	THR	VAL	GLY	SER
03	nsp6/7	ASP	SER	MET	LYS	SER	GLN	VAL	THR	ALA	VAL	LYS
04	nsp7/8	GLU	SER	ALA	ILE	ALA	GLN	LEU	THR	ALA	ARG	ASN
05	nsp8/9	SER	LEU	GLU	ASN	ASN	GLN	LEU	LYS	VAL	ALA	SER
06	nsp9/10	THR	ALA	ASN	GLY	ALA	GLN	LEU	ARG	VAL	THR	ALA
07	nsp10–12	SER	ALA	ASP	ALA	SER	GLN	MET	LEU	PRO	GLU	ARG
08	nsp12/13	CYS	ALA	GLY	VAL	ALA	GLN	LEU	VAL	THR	HIS	PRO
09	nsp13/14	THR	VAL	ASN	GLU	ALA	GLN	LEU	THR	ALA	VAL	ASN
10	nsp14/15	VAL	ASN	GLU	LEU	SER	GLN	LEU	ARG	THR	PHE	THR
11	nsp15/16	TRP	ALA	GLN	SER	ALA	GLN	LEU	LYS	PRO	TYR	PHE

Source: Adapted from Grum-Tokars, V., Ratia, K., Begaye, A., Baker, S.C., Mesecar, A.D., 2008. Evaluating the 3C-like protease activity of SARS-Coronavirus: recommendations for standardized assays for drug discovery, Virus Res. 133, 63–73.

(Anand et al., 2003) and the sequence of genomic structure (Marra et al., 2003; Rota et al., 2003).

Three noncanonical M^pro cleavage sites are observed in SARS coronavirus polyproteins having Val, Met, or Phe amino acid residues at P2 position whereas the same cleavage site is found dissimilar in other coronaviruses. Therefore, the structural and functional criteria of M^pro helps to identify it as an important target for developing anti-SARS drugs or other anticoronaviral drugs (Anand et al., 2005). The structures of HCoV 229E M^pro, TGEV M^pro, and SARS-CoV M^pro demonstrate that these enzymes have three distinct domains. The first two domains (domain I and II) together possess similarity with chymotrypsin whereas the third one consists of an α-helical fold which is unique (Anand et al., 2005). The active site which is situated between the first two domains possesses a Cys-His catalytic site. Antiparallel β-barrels with six strands are composed of the domain I and II (residues 8–99 of I and 100–183 of II, respectively). The domain II is connected to domain III (residues 200–300) through a long loop (residues 184–199) (Anand et al., 2005). The hydrophobic amino acid residues are found to compose the domain I β-barrel. The α-helix (residues 53–58) helps to close the β-barrel like a lid. The domain I is bigger than domain II, as well as the homologous domain II of chymotrypsin and 3C^pro of HAV (Allaire et al., 1994; Bergmann et al., 1997; Tsukada and Blow, 1985). Moreover, a number of secondary

structural elements are found to be missing in coronavirus M^{pro} compared to HAV 3C^{pro} (such as strands b2II and cII along with the linking loop). The Gly135 to Ser146 form a portion of the barrel though domain II possesses maximum consecutive turns and loops. Moreover, the structural alignment of coronavirus M^{pro} domain II with the picornavirus 3C^{pro} domain II is found to be different. Superimposition of domain I of TGEV M^{pro}, with HAV 3C^{pro} domain I results in a root mean square deviation (rmsd) of 1.85 Å whereas superimposition of domain II of both of these enzymes yields a rmsd of 3.25 Å. The overall rmsd for the C$_{\alpha}$ atoms between their structures is >2 Å for all 300 C$_{\alpha}$ positions and the three M^{pro} structures possess similarity among themselves (Anand et al., 2005). The helical domain III is the most variable domain that exhibits a better overlapping between HCoV M^{pro} and TGEV M^{pro} compared to the SARS-CoV M^{pro}, with each other. Moreover, TGEV and HCoV 229E (belongs to group I coronavirus) show 61% sequence similarity whereas SARS-CoV (belongs to group II coronavirus) exhibits 40% and 44% sequence similarity with HCoV 229E and TGEV, respectively (Anand et al., 2003). A high degree of conserved region (42%–48%) between the domain I and II is observed while comparing group I coronavirus M^{pro}, and group II SARS-CoV M^{pro}. The domain III comparatively exhibits a lower degree of sequence similarity (36%–40%) between these two groups coronaviral enzymes (Anand et al., 2005). The X-ray crystallography structures of SARS-CoV M^{pro}, TGEV M^{pro}, and HCoV 229E M^{pro} show that these form dimers (Anand et al., 2002, 2003; Yang et al., 2003). Moreover, it was also confirmed that the dimer form is enzymatically active but the monomeric form is not active (Anand et al., 2005; Fan et al., 2004). The dimerization process is found to be mandatory for enzyme activity and this process helps to discriminate the coronavirus M^{pro}, and the picornavirus M^{pro} distinctly.

4   CATALYTIC SITE OF SARS-CoV M^{PRO}

A catalytic dyad is formed by Cys145 and His41 at the SARS-CoV active site, whereas other cysteine and serine protease are found to form a catalytic triad. A water molecule is found to have hydrogen bonding interaction with His41 and Asp187. Moreover, if the cysteine residue is replaced with serine at the enzyme active site, the enzymatic activity of SARS-CoV M^{pro} is decreased. For coronaviral main protease, as well as the picornaviral protease, the cysteine residue is located at the same place of the active site of the His41 imidazole ring plane (distance 3.5–4 Å). For hydrogen bonding interaction between the side chains, the sulfur atom of cysteine residue should be along with the same plane of imidazole function (Anand et al., 2005).

5   SUBSTRATE BINDING SITES OF SARS-CoV M^{PRO}

The substrate binding sites are found to be conserved in all coronavirus main proteases as suggested by the experimental observations (Anand et al., 2003, 2005). The X-ray crystallographic study between the inhibitor-SARS CoV M^{pro} suggests

that the imidazole function of His163 is located at the bottom of the S1 site of M^{pro} to donate hydrogen bond to the backbone carbonyl function of glutamine. For interaction with glutamine at S1 site, the histidine amino acid residue has to be remained unaltered over a broad range of pH. This may be possible through two interactions involved in the imidazole ring. It may either stack to the phenyl ring of Phe140 or may accept a hydrogen bond from the hydroxyl function of Tyr161. Replacement of the His163 is found to abolish the proteolytic activity (Hegyi et al., 2002a; Ziebuhr et al., 2000). All these residues discussed are found to be conserved not only in SARS-CoV M^{pro} but also in all other coronavirus main proteases. Moreover, residues Ile51, Met151, Glu166, and His172 of the S1 pocket take part in the conformation of SARS-CoV M^{pro} (Anand et al., 2005). Regarding the S2 specificity site, all the coronaviruses M^{pro} consists of a leucine residue at the S2 cleavage site. This S2 site is hydrophobic in nature and is composed of side chain amino acid residues, such as His41, Thr47, Met49, Tyr53, and Met165. The longer methionine residue may restrict the S2 pocket and requires slight spatial orientation to accommodate the substrate leucine residue. Due to the presence of Ala46 residue and differences in amino acid sequences, the S2 pocket is bigger in SARS-CoV M^{pro} compared to HCoV 229E M^{pro} and TGEV M^{pro}. In SARS-CoV M^{pro}, a stretch of amino acid sequences is observed in 40–50 residues that help to enlarge the size by forming a helix which is not observed in other coronaviruses. This bigger size may be effective in the substrate binding (Anand et al., 2005). Apart from the S1 and S2 pockets, some other substrate binding pockets should be taken into consideration. At the P4 position, small amino acid residues may be preferable (such as Val, Thr, Ser, and Pro) whereas no specificity at the P3 position is observed for coronavirus M^{pro}. At the P4 position, some amino acid residues are found to be conserved in SARS-CoV M^{pro} (such as Met165 and Thr190). Moreover, P5 amino acid side chains are found to interact with the main chain at Pro168, Thr190, and Gln192 in SARS-CoV M^{pro}, and help like a linker between domain II and III.

6 RNA INTERFERENCE AND VACCINES OF SARS-CoV

Apart from antivirals to fight against these coronaviruses, RNA interference (RNAi) and vaccine development may be a useful strategy though it is a challenging task. The RNAi is an important tool for gene silencing. Apart from the use of RNAi in cancer and genetic disorder (Wang et al., 2004), development of siRNA inhibitors in SARS infection may be a boon for the treatment of the disease (Li et al., 2005). The replication of the SARS may be inhibited effectively through RNAi in vero cells. Therefore, siRNA therapy may be effective to combat SARS infection (Wang et al., 2004). Short hairpin RNA (shRNA) may be useful to target the N gene sequence of SARS coronavirus and to inhibit shRNA of SARS-CoV antigen expression (Tao et al., 2005; Zhai et al., 2007). These results suggest that gene silencing through RNAi may effectively inhibit the SARS-CoV antigen expression, and, therefore, RNAi approach may

be effectively utilized as possible therapy for inhibiting SARS-CoV infection. Moreover, the RNAi is used to target the replicase enzyme of human SARS virus. It not only targets the hSARS gene but also produces inhibitory effects on the SARS RNA virus expression (Zhai et al., 2007). As far as the development of SARS vaccines is concerned, the inactivated SARS-CoV along with the full-length S protein and an attenuated weak virus, and recombinant SARS protein may be used (Jiang et al., 2005; Zhai et al., 2007). The S protein and the inactivated virus were reported to be used to neutralize antibodies. The attenuated or the weak form of the virus might be used to induce immunity, as well as to neutralize antibodies (Finlay et al., 2004). The development of recombinant vaccines may be a useful strategy to prevent SARS infections. It mainly depends on the best antigen identification, as well as the choice of expression system. The S glycoprotein of SARS-CoV along with its truncated form may be targeted for development of recombinant vaccine as the best candidate (Babcock et al., 2004; Bisht et al., 2004; Buchholz et al., 2004; Yang et al., 2004; Zhai et al., 2007). A number of reports were published regarding recombinant S protein vaccine against different SARS-CoV through aryl delivery system (Pogrebnyak et al., 2005; Tuboly et al., 2000).

7 DEVELOPMENT OF QSAR MODELS

QSAR is a useful tool to understand the relation between the structural and physicochemical properties of the drug molecules, and their biological activity which may be useful for predicting the activity or toxicity profile of drugs (Gupta, 2007; Verma and Hansch, 2009). The data required for developing the QSAR models are collected from the literature (see individual QSAR for corresponding references). The IC_{50} (molar concentration required to produce 50% inhibition of the enzyme), EC_{50} (effective concentration), or K_i (binding affinity) data are obviously considered as the biological activity term or dependent variable. The independent variables include physicochemical parameters [such as hydrophobicity, molar refractivity, dipole moment along with different axes, molecular weight (MW), polar surface area (PSA), and polar volume, as well as surface area (SA) and volume] and many topological parameters, such as Kier's molecular connectivity indices, Balaban indices, etc. Regarding the statistics of QSAR models, N is used to indicate the number of compounds in the set, R to indicate the correlation coefficient of the QSAR model obtained, R^2 refers to the squared correlation coefficient exhibiting the goodness of fit, q^2 indicates square of the leave-one-out cross-validated correlation coefficient (represents the internal validation of the model), R_A^2 refers to the adjusted R^2, F value represents the Fischer statistics (Fischer ratio) that actually means the ratio between the explained and unexplained variance for a particular degree of freedom, P stands for the probability factor related to F-ratio, SEE means the standard error of estimate, Q is the quality factor that can be a measure of chance correlation. A high Q represents the high predictivity, as well as the lack of over-fitting of the model.
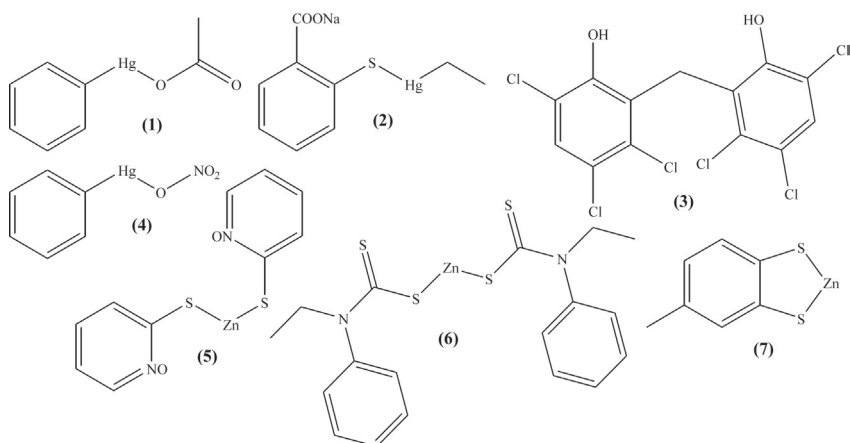
FIGURE 11.2   **Metal-conjugated SARS 3CL^{pro} inhibitors.**

Compounds that misfit in the correlation are considered as outliers and are usually removed from the regression. We discuss here the QSAR models obtained for different categories of SARS-CoV 3CL^{pro} and HRV 3C^{pro} inhibitors.

7.1   Coronaviral 3CL^{pro} Inhibitors

7.1.1   Metal-Conjugated SARS-CoV 3CL^{pro} Inhibitors

Hsu et al. (2004) reported some metal-conjugated compounds as promising SARS-CoV 3CL^{pro} inhibitors (Fig. 11.2; Table 11.2). The model obtained was as shown by Eq. (11.1):

$$pK_i = 4.806 (\pm 0.369) + 0.013 (\pm 0.003) PSA \qquad (11.1)$$

$N = 5$, $R = 0.910$, $R^2 = 0.828$, $R_A^2 = 0.771$, $F(1, 3) = 14.459$, $P < 0.03195$, SEE = 0.229, $q^2 = 0.643$, $Q = 3.974$, Outlier = Compounds **1**, **3**

   This model suggested that the increasing value of the PSA may contribute positively to the binding enzyme. Compounds with a higher PSA (Compounds **4–6**, Table 11.2) have higher activity than compounds with a lower PSA (Compounds **2**, **7**, Table 11.2). Compound **1** has a lower PSA but higher activity whereas compound **3** having the higher PSA has lower activity. These molecules are not explained properly by this model. Therefore, these molecules (Compounds **1**, **3**, Table 11.2) were considered as outliers. They may have different mechanism(s) of action(s).

7.1.2   Some Small Molecule SARS-CoV 3CL^{pro} Inhibitors

Blanchard et al. (2004) reported some SARS-CoV 3CL^{pro} inhibitors (Fig. 11.3; Table 11.3). The QSAR model for these compounds was as shown by Eq. (11.2).

$$pIC_{50} = 4.845 (\pm 0.064) + 0.002 (\pm 0.000) PSA \qquad (11.2)$$

TABLE 11.2 The Biological Activity and Physicochemical Parameters of Metal-Conjugated SARS-CoV 3CL[pro] Inhibitors (Fig. 11.2) for QSAR Model [Eq. (11.1)]

| Compound	Obsd[b]	Calcd[c]	Res[d]	Del res[e]	Pred[f]	PSA
1[a]	6.155	5.625	0.530	0.716	5.439	69.998
2	5.620	5.511	0.109	0.168	5.452	61.487
3[a]	4.863	5.791	−0.928	−1.124	5.987	82.389
4	6.523	6.506	0.017	0.029	6.494	135.592
5	6.770	6.444	0.326	0.514	6.256	130.932
6	6.000	6.213	−0.213	−0.267	6.267	113.794
7	5.854	5.694	0.160	0.204	5.649	75.130

[a]Considered as outliers.
[b]Observed or experimental activity.
[c]Calculated activity of compounds according to Eq. (11.1).
[d]Difference between the observed and calculated activity.
[e]Difference between the observed and leave-one-out cross-validated activity.
[f]Leave-one-out cross-validated activity.
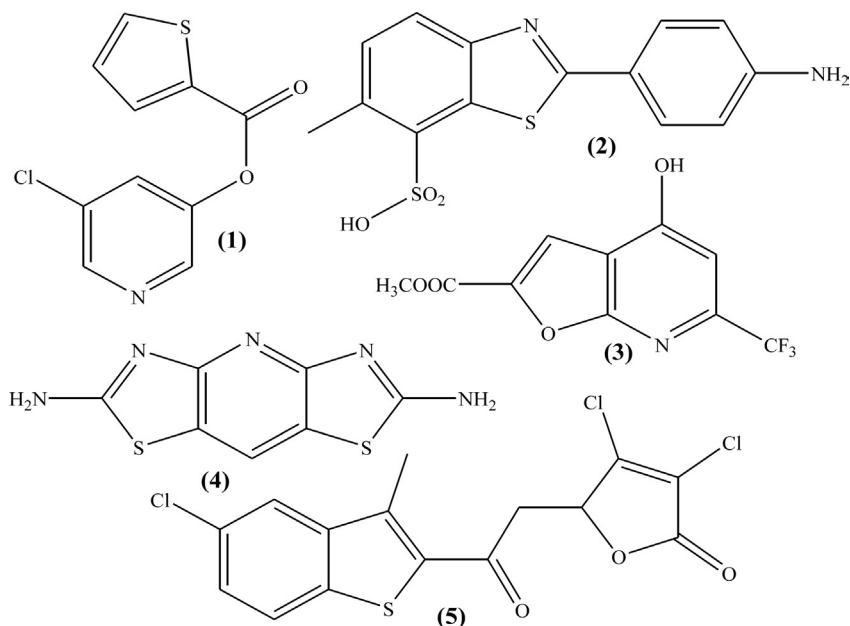
FIGURE 11.3 **SARS-CoV 3CL protease inhibitors.**

TABLE 11.3 The Biological Activity and Physicochemical Parameters of Some Small Molecule SARS-CoV 3CL[pro] Inhibitors (Fig. 11.3) for QSAR Model [Eq. (11.2)]

Compound	Obsd	Calcd	Res	Del res	Pred	PSA
1[a]	6.301	5.520	0.781	1.152	5.149	132.553
2	5.367	5.510	−0.144	−0.182	5.549	209.011
3	5.155	5.517	−0.362	−0.482	5.637	153.950
4	5.585	5.494	0.091	0.772	4.814	327.913
5	5.155	5.520	−0.366	−0.549	5.704	129.743

[a]Considered as outliers.

$N = 4$, $R = 0.984$, $R^2 = 0.969$, $R_A^2 = 0.953$, $F (1, 2) = 62.388$, $P < 0.01565$, SEE $= 0.044$, $q^2 = 0.838$, $Q = 22.364$, Outlier = Compound **1**.

This model also exhibited that the PSA of the molecule might be conducive to the enzyme inhibitory activity of the compounds. As obvious from Table 11.3, compounds **2** and **4** with a higher PSA have higher activity than compounds with the lower PSA. The sulfone and amino functions of compound **2** and the disubstituted amino acid function of compound **4** may produce higher PSA as compared to the trichloro-substituted compound **5** and the monohydroxy trifluoro substituted ester analog (compound **2**). It also suggested that the enzyme–drug interaction might be taking place in a nonhydrophobic space at the enzyme active site. Compound **1** has the lower PSA but possesses comparatively higher activity than other compounds. It may be assumed that compound **1** may behave differently. Probably, the ester function and the chloro group may have some electronic interaction with the enzyme responsible for the higher inhibitory activity. Therefore, compound **1** may be considered as an outlier.

7.1.3 Keto-Glutamine SARS-CoV 3CL[pro] Inhibitors

Jain et al. (2004) synthesized and evaluated some keto-glutamine analogs as potent SARS-CoV 3CL[pro] inhibitors (Table 11.4). For this series of compounds, the QSAR model obtained was as shown by Eq. (11.3). In this equation, "I" is an indicator parameter that was used with a value of 1 for the presence of the CONMe$_2$. For the absence of this group, its value was zero. The negative coefficient of I suggests that compounds with CONMe$_2$ function (Compounds **1–4**, Table 11.4) are less active than compounds with 3-pyrrolidinone function (Compounds **5–8**, Table 11.4). Therefore, compounds with 3-pyrrolidinone functions (Compounds **5–8**) are preferable for the higher inhibitory activity.

$$p\,IC_{50} = 5.699\,(\pm 0.139) - 1.405\,(\pm 0.197)\,I \tag{11.3}$$

$N = 8$, $R = 0.946$, $R^2 = 0.894$, $R_A^2 = 0.877$, $F (1, 6) = 50.793$, $P < 0.00038$, SEE $= 0.279$, $q^2 = 0.812$, $Q = 3.391$

TABLE 11.4 The Biological Activity and Physicochemical Parameters of Keto-Glutamine SARS-CoV 3CL^{pro} Inhibitors for QSAR Model [Eq. (11.3)]

(1–4)

(5–8)
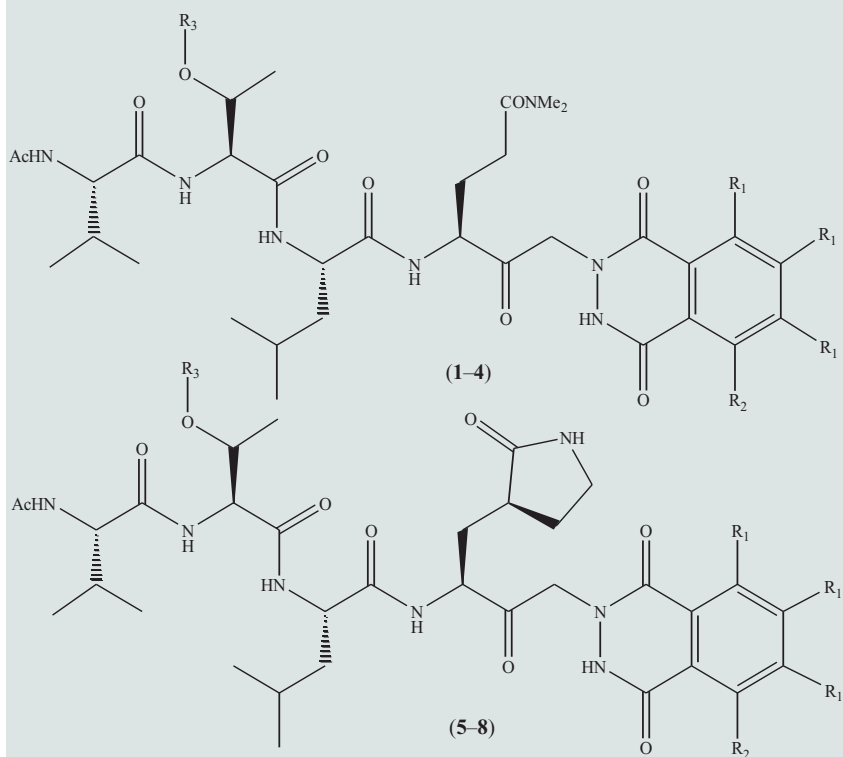
Compound	R$_1$	R$_2$	R$_3$	Obsd	Calcd	Res	Del res	Pred	I
1	H	H	Benzyl	4.194	4.294	−0.101	−0.134	4.328	1
2	H	H	H	4.553	4.294	0.259	0.345	4.208	1
3	H	NO$_2$	Benzyl	4.155	4.294	−0.139	−0.186	4.341	1
4	H	NO$_2$	H	4.276	4.294	−0.019	−0.025	4.301	1
5	H	H	Benzyl	5.569	5.699	−0.131	−0.174	5.743	0
6	H	H	H	5.538	5.699	−0.162	−0.215	5.753	0
7	H	NO$_2$	Benzyl	6.222	5.699	0.523	0.697	5.525	0
8	H	NO$_2$	H	5.469	5.699	−0.231	−0.308	5.776	0

7.1.4 Lopinavir-Like SARS- CoV 3CL^{pro} Inhibitors

Wu et al. (2004) reported some Lopinavir-like inhibitors of SARS-3CL^{pro} (Table 11.5). The model obtained was as by Eq. (11.4), where SA refers to surface area. Eq. (11.4) suggested that the increase in value of the SA may be

TABLE 11.5 Biological Activity and Physicochemical Parameters of Lopinavir-Like SARS-CoV 3CL^{pro} Inhibitors for QSAR Model [Eq. (11.4)]
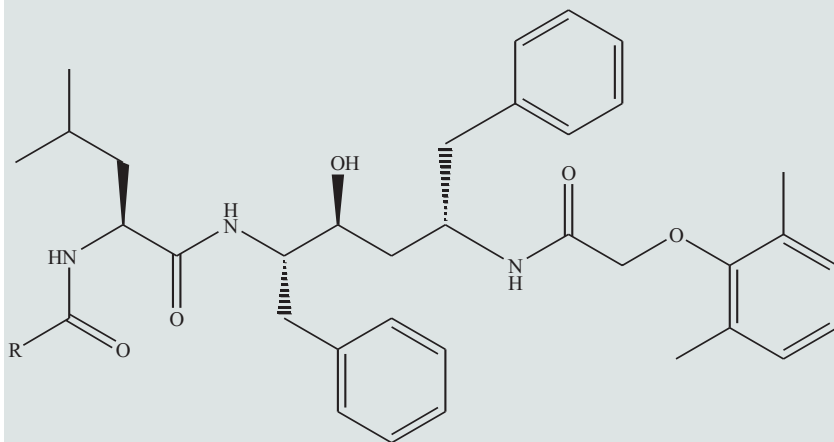
Compound	R	Obsd	Calcd	Res	Del res	Pred	SA
1	5-NO$_2$-2-furyl	4.602	4.606	−0.004	−0.006	4.608	1018.970
2[a]	β-Napthylmethyl	4.398	4.543	−0.146	−0.160	4.558	1057.910
3	m-MePh	4.602	4.589	0.013	0.016	4.587	1029.690
4	Pyridyl-2-yl-sulfanylmethyl	4.456	4.560	−0.104	−0.116	4.572	1047.550
5	Indole-2-yl	4.620	4.548	0.072	0.079	4.540	1055.240
6	2-Thioxo-4-thiazolidinone-3-ylmethyl	4.638	4.621	0.017	0.025	4.613	1010.130
7	p-CF$_3$Ph	4.602	4.555	0.047	0.052	4.550	1050.650
8[a]	p-OMePhCH=CH	4.620	4.489	0.131	0.159	4.461	1091.790
9	(CH$_2$)$_2$NHBoc	4.398	4.471	−0.073	−0.097	4.494	1102.490
10[a]	6-ClChromene-4-yl	4.602	4.506	0.096	0.110	4.492	1081.040
11	Naphthalene-2-yloxymethyl	4.398	4.447	−0.049	−0.077	4.475	1117.600

[a]Considered as outliers.

detrimental to the activity. The compounds **2**, **8**, and **10** (Table 11.5) may behave in a different fashion and, therefore, they were considered as outliers.

$$p\,IC_{50} = 6.968\,(\pm 0.617) - 0.002\,(\pm 0.001)\,SA \qquad (11.4)$$

$N = 8$, $R = 0.849$, $R^2 = 0.721$, $R_A^2 = 0.675$, $F\,(1,\,6) = 15.531$, $P < 0.00762$, SEE $= 0.059$, $q^2 = 0.618$, $Q = 14.390$, Outlier = Compounds **2**, **8**, **10**

7.1.5 Anilide-Based SARS-CoV 3CL[pro] Inhibitors

Shie et al. (2005a) reported a series of potent anilide inhibitors against SARS-3CL[pro] (Fig. 11.4; Table 11.6), for which the QSAR model obtained was as shown by Eq. (11.5). This model showed the importance of dipole moment along the X-axis (D_X), MW, PSA, and volume (Vol) for controlling the enzyme inhibition. The positive coefficient of the dipole moment along X-axis suggested that the bulky substitutions along X-axis may favor the activity. Moreover, the MW was also shown to have a positive impact on the activity, whereas PSA was shown to have the negative effect. Therefore, it may be suggested that molecules with the bigger size along with bulky substituents may be conducive to the inhibition. Moreover, the volume is found to have a parabolic relation with the enzyme inhibition. The optimum value of the volume is 6500. Compounds **1**, **7**, **9**, and **14** were considered as outliers as these molecules may work with a different mechanism(s).

$$p\,IC_{50} = 13.858\,(\pm2.004) + 0.066\,(\pm0.022)\,D_X + 0.011(\pm0.002)\,MW \\ - 0.004\,(\pm0.001)\,PSA - 0.013(\pm0.002)\,Vol - 0.000001(\pm0.000)\,Vol^2 \quad (11.5)$$

$N = 26$, $R = 0.904$, $R^2 = 0.817$, $R_A^2 = 0.771$, $F\,(5,\,20) = 17.862$, $P < 0.00000$, SEE $= 0.185$, $q^2 = 0.680$, $Q = 4.886$, $Vol_{Opt} = 6500$, Outlier $=$ Compounds **1**, **7**, **9**, **14**
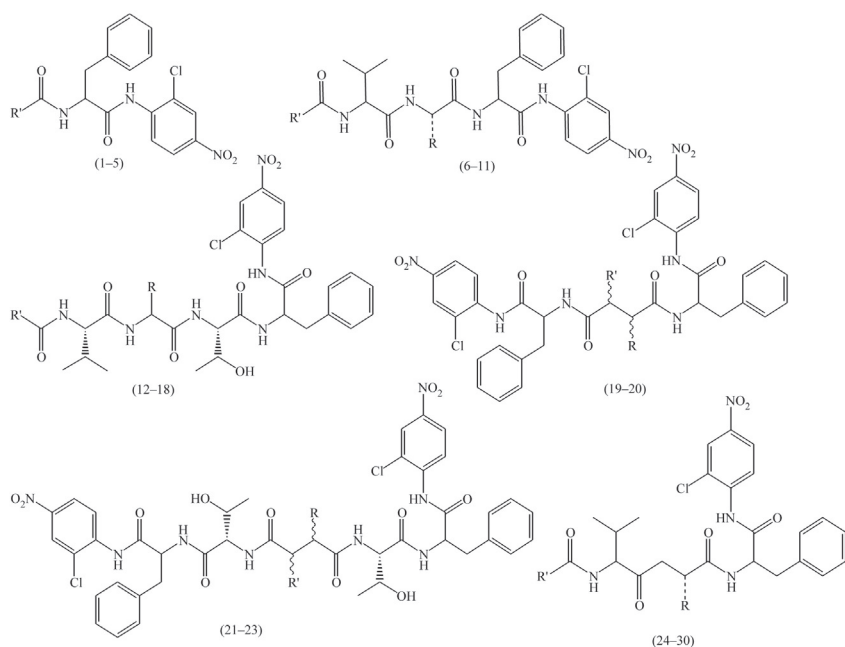
FIGURE 11.4   General structure of anilide-based SARS-CoV 3CL[pro] inhibitors.

TABLE 11.6 Biological Activity and Physicochemical Parameters of Anilide-Based SARS-CoV 3CL^{pro} Inhibitors (Fig. 11.4) for QSAR Model [Eq. (11.5)]

Compound	R	R′	Obsd	Calcd	Res	Del res	Pred	D_X	MW	PSA	Vol
1[a]	—	$Me_2NC_6H_4$	7.222	6.730	0.492	1.161	6.061	−3.032	466.917	132.531	1184.630
2	—	$C_{14}H_{29}CH(Br)$	5.523	5.533	−0.010	−0.025	5.548	−3.999	637.048	164.054	1505.220
3	—	$3,4-(NH_2)_2C_6H_3$	5.699	6.054	−0.355	−0.589	6.288	−2.424	453.878	266.781	1142.890
4	—	(Indol-3-yl)-CH=CH	5.523	5.614	−0.091	-0.109	5.632	−3.716	488.922	177.675	1290.600
5	—	(2-NH_2-1,3-thiazol-4-yl)-C(NOCH$_3$)	5.155	4.900	0.255	0.559	4.596	−4.072	502.931	304.411	1273.020
6	i-Bu	Et	5.155	5.298	−0.143	−0.155	5.310	0.087	588.095	150.968	1561.070
7[a]	i-Bu	Ph	5.398	4.970	0.428	0.492	4.906	1.527	636.138	151.962	1742.770
8	i-Bu	Morpholino	4.721	4.791	−0.070	−0.076	4.797	−0.806	645.146	167.607	1715.620
9[a]	i-Bu	Thien-2-yl	5.301	4.887	0.414	0.457	4.844	1.890	642.165	192.606	1716.130
10	$PhCH_2$	5-Me-isoxazol-3-yl	5.155	5.477	−0.322	−0.400	5.555	4.564	675.131	209.168	1697.490
11	$PhCH_2$	Thien-2-yl	5.301	5.261	0.040	0.044	5.257	1.903	676.182	191.190	1708.000
12	i-Bu	Et	5.155	4.697	0.458	0.551	4.603	−1.876	689.199	176.439	1789.010
13	i-Bu	Morpholino	4.796	4.899	−0.103	−0.118	4.914	2.387	746.250	203.573	1980.620

14[a]	PhCH$_2$	t-Bu	5.699	5.095	0.604	0.704	4.995	1.521	751.268	163.488	2001.440
15	PhCH$_2$	5-Me-isoxazol-3-yl	5.301	5.347	−0.046	−0.050	5.351	4.917	776.235	216.166	1996.140
16	PhCH$_2$	PhCH$_2$O	5.222	5.407	−0.185	−0.222	5.444	2.696	801.284	180.409	2087.700
17	4-FC$_6$H$_4$CH$_2$	Et	5.301	5.350	−0.049	−0.053	5.354	2.908	741.206	169.119	1916.260
18	4-FC$_6$H$_4$CH$_2$	Ph	5.699	5.519	0.180	0.208	5.491	2.716	789.248	173.610	2002.030
19	(S)-OH	H	5.398	5.175	0.223	0.304	5.094	7.882	737.543	291.835	1855.940
20	(R)-OH	(R)-OH	5.301	5.261	0.040	0.067	5.234	9.257	753.542	323.375	1853.190
21	H	H	5.699	5.737	−0.038	−0.050	5.749	6.265	923.751	325.291	2258.430
22	(S)-OH	H	5.699	5.764	−0.065	−0.090	5.789	7.011	939.751	353.359	2264.460
23	(R)-OH	(R)-OH	5.699	5.846	−0.147	−0.216	5.915	7.863	955.750	375.570	2288.530
24	i-Bu	Et	4.569	5.055	−0.486	−0.537	5.106	−0.653	587.107	136.197	1605.950
25	i-Bu	Ph	4.678	5.003	−0.325	−0.355	5.033	−1.172	635.150	126.423	1706.880
26	i-Bu	t-BuO	4.721	4.964	−0.243	−0.261	4.983	−0.444	631.159	143.473	1698.180
27	i-Bu	Morpholino	4.538	4.844	−0.306	−0.338	4.875	−0.935	644.158	141.182	1741.990
28	i-Bu	Thien-2-yl	4.658	4.853	−0.196	−0.210	4.868	−0.247	641.177	170.511	1703.650
29	PhCH$_2$	5-Me-isoxazol-3-yl	5.222	5.105	0.117	0.126	5.096	1.855	674.143	197.782	1725.490
30	PhCH$_2$	Thien-2-yl	4.796	4.864	−0.069	−0.082	4.878	−1.901	675.194	171.248	1727.980

[a]Considered as outliers.

7.1.6 Peptidomimetic α,β Unsaturated Esters as SARS-CoV 3CL^{pro} Inhibitors

Shie et al. (2005b) reported a series of peptidomimetic α,β unsaturated esters as promising SARS-3CL^{pro} inhibitors (Table 11.7). The QSAR model obtained for them was as shown by Eq. (11.6).

$$pIC_{50} = 14.827\,(\pm 1.418) - 0.016\,(\pm 0.002)\,MW - 0.006\,(\pm 0.001)\,PSA \quad (11.6)$$

$N = 15$, $R = 0.906$, $R^2 = 0.822$, $R_A^2 = 0.792$, $F\,(2, 12) = 27.656$, $P < 0.00003$, SEE $= 0.227$, $q^2 = 0.710$, $Q = 3.991$, Outlier $=$ Compound **8**

It was observed from Eq. (11.6) that increase in the value of both the MW, as well as the PSA may be detrimental to the activity. Thus, the model suggested that the smaller molecules with less steric bulk might favor the activity. Moreover, the enzyme-drug interaction would be more favored in non-hydrophobic space. It was observed that compounds having unsaturation at the R' position (Compounds **11–16**, Table 11.7) possess lower MW compared to the other molecules in the dataset and possess higher inhibitory activity. In compound **13,** both the phenyl rings might be accommodated in the S2 and S3 pockets. Moreover, the (dimethylamino) cinnamyl function adopts a coplanar rigid structure at the end terminal, which may help it in forming hydrogen bonding with amino acids residues Glu166, Glu189, and Glu192 at the enzyme active site. Compound **8** may behave differently and hence, this was considered as an outlier.

7.1.7 Benzotriazole Esters as SARS-CoV 3CL^{pro} Inhibitors

Wu et al. (2006) reported some benzotriazole esters as promising SARS-3CL^{pro} mechanism-based inhibitors (Table 11.8). The model obtained for this series is as shown by Eq. (11.7).

$$pK_i = 3.814\,(\pm 1.495) - 1.405\,(\pm 0.115)\,D_Y + 0.014\,(\pm 0.005)\,MW \quad (11.7)$$

$N = 11$, $R = 0.974$, $R^2 = 0.949$, $R_A^2 = 0.937$, $F\,(2, 8) = 75.154$, $P < 0.00001$, SEE $= 0.282$, $q^2 = 0.893$, $Q = 3.454$

It was observed from Eq. (11.7) that increasing value of the dipole moment along Y-axis (D_Y) may lead to a decrease in the activity, whereas increasing value of the MW may be conducive to the activity. It also suggests that compounds with the higher molecular bulk with lower steric effect may be favorable for the higher inhibitory activity. Compounds with ester functions (Compounds **1–8**, Table 11.8) is better active than compounds with acetyl function (Compounds **9–11**) as these molecules (Compounds **1–8**) possess higher bulkiness. Therefore, it may be assumed that the ester analogs impart less steric effect with the enzyme and hence, produce higher activity.

TABLE 11.7 Biological Activity and Physicochemical Parameters of Peptidomimetic α,β Unsaturated Esters as SARS-CoV 3CL^{pro}Inhibitors for QSAR Model [Eq. (11.6)]
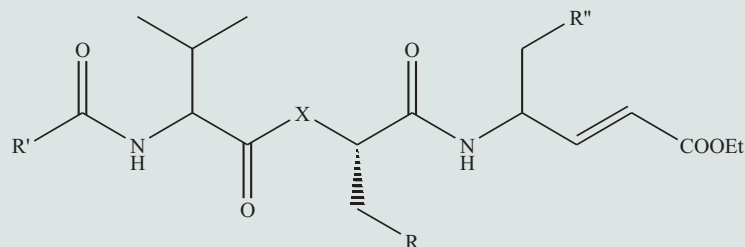
Compound	R	R′	R″	X	Obsd	Calcd	Res	Del res	Pred	MW	PSA
1	Ph	5-Me-isoxazolyl-3-yl	—	NH	4.097	4.173	−0.076	−0.125	4.222	581.660	233.331
2	Ph	PhCH$_2$O	—	NH	4.071	4.195	−0.124	−0.157	4.228	606.709	175.330
3	4-FPh	5-Me-isoxazolyl-3-yl	Ph	CH$_2$	4.409	4.563	−0.154	−0.169	4.578	591.670	150.782
4	4-FPh	PhCH$_2$O	Ph	CH$_2$	4.509	4.544	−0.036	−0.046	4.555	616.719	99.131
5	Ph	5-Me-isoxazolyl-3-yl	Ph	CH$_2$	4.886	4.815	0.072	0.077	4.809	573.679	150.790
6	Ph	PhCH$_2$O	Ph	CH$_2$	4.420	4.796	−0.376	−0.441	4.861	598.729	99.149
7	4-FPh	5-Me-isoxazolyl-3-yl	Ph	NH	4.678	4.483	0.194	0.217	4.461	592.658	161.032

(*Continued*)

TABLE 11.7 Biological Activity and Physicochemical Parameters of Peptidomimetic α,β Unsaturated Esters as SARS-CoV 3CL^proInhibitors for QSAR Model [Eq. (11.6)] (cont.)

Compound	R	R′	R″	X	Obsd	Calcd	Res	Del res	Pred	MW	PSA
8[a]	4-FPh	PhCH$_2$O	Ph	NH	4.959	4.502	0.457	0.592	4.366	617.707	103.559
9	Ph	5-Me-isoxazolyl-3-yl	Ph	NH	4.523	4.735	−0.212	−0.230	4.753	574.667	161.010
10	Ph	PhCH$_2$O	Ph	NH	4.959	4.754	0.205	0.239	4.720	599.716	103.573
11	Ph	BiPhCH=CH	Ph	NH	5.000	5.167	−0.167	−0.195	5.195	572.693	98.047
12	Ph	4-NO$_2$PhCH=CH	Ph	NH	5.301	5.054	0.247	0.317	4.984	541.594	183.426
13	Ph	4-Me$_2$NPhCH=CH	Ph	NH	6.000	5.662	0.338	0.515	5.485	539.665	92.953
14	Ph	2,4-diOMePhCH=CH	Ph	NH	5.000	5.278	−0.278	−0.326	5.326	556.649	115.705
15	Ph	3-Benzo[1,3]dioxol-5-yl-CH=CH	Ph	NH	5.155	5.398	−0.243	−0.308	5.463	540.606	131.977
16	Ph	3-Benzo[1,3]dioxol-5-yl-CH=CH	—	NH	5.000	4.847	0.153	0.203	4.797	547.599	202.480

[a]Considered as outliers.

TABLE 11.8 Biological Activity and Physicochemical Parameters of Benzotriazole Esters as SARS-CoV 3CL^{pro} Inhibitors for QSAR Model [Eq. (11.7)]

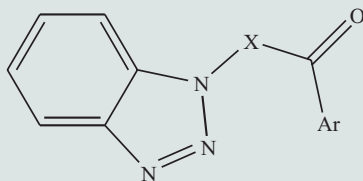| Compound	Ar	X	Obsd	Calcd	Res	Del res	Pred	D_Y	MW
1	2-NH$_2$Ph	O	7.710	7.592	0.118	0.186	7.524	−0.218	254.244
2	4-N(Me)$_2$Ph	O	7.759	7.880	−0.120	−0.138	7.897	−0.150	282.297
3	4-NHMePh	O	7.917	8.083	−0.165	−0.211	8.129	−0.431	268.271
4	4-N(Et)$_2$Ph	O	7.955	8.311	−0.356	−0.662	8.617	−0.185	310.350
5	5-Benzimidazolyl	O	7.640	7.690	−0.050	−0.056	7.696	−0.045	279.254
6	5-Indolyl	O	8.125	7.611	0.514	0.577	7.548	0.002	278.265
7	2-Indolyl	O	7.910	7.970	−0.060	−0.070	7.980	−0.254	278.265
8	5-F-2-Indolyl	O	7.860	7.595	0.265	0.320	7.540	0.188	296.256
9	4-N(Et)$_2$Ph	CH$_2$	6.000	5.782	0.218	0.437	5.563	1.597	308.378
10	4-NHMePh	CH$_2$	5.347	5.529	−0.182	−0.310	5.657	1.368	266.298
11	4-N(Me)$_2$Ph	CH$_2$	5.174	5.357	−0.183	−0.295	5.469	1.627	280.324

7.1.8   A Diverse Set of SARS-CoV 3CL^{pro} Inhibitors

Chen et al. (2006a) reported some diverse chemical entities through virtual screening, surface plasmon resonance and fluorescence resonance energy transfer based assays as promising against SARS-CoV 3CL^{pro} (Fig. 11.5; Table 11.9). The QSAR model obtained was as shown by Eq. (11.8):

$$pIC_{50} = 2.508\,(\pm 0.417) - 0.012\,(\pm 0.003)\,PSA \qquad (11.8)$$

$N = 6$, $R = 0.923$, $R^2 = 0.851$, $R_A^2 = 0.814$, $F\,(1, 4) = 22.908$, $P < 0.00874$, SEE $= 0.167$, $q^2 = 0.746$, $Q = 5.527$, Outlier = Compounds **5**, **7**

It is observed from Eq. (11.8) that increasing the value of the PSA may be detrimental to the activity. Thus it suggested that less polar molecules may have better inhibitory activity. Due to the presence of electronegative function (such as carboxyl, chloro, etc.), the molecule may have larger PSA. Compounds **5** and **7** (Table 11.9), though possess lower PSA, have higher activity and this could not be explained by this model. Thus these compounds might be supposed to involve the different mechanism of action for producing the higher activity. Therefore, these compounds are considered as outliers.
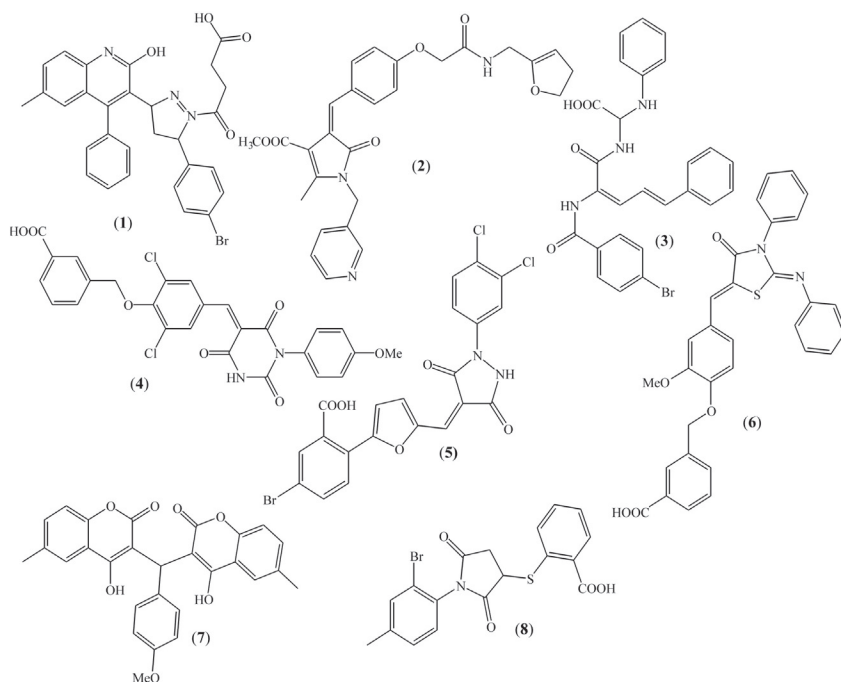

FIGURE 11.5   **Structures of diverse SARS-CoV 3CL^{pro} inhibitors.**

TABLE 11.9 Biological Activity and Physicochemical Parameters of a Diverse Set of SARS-CoV 3CL^{pro} Inhibitors (Fig. 11.5) for QSAR Model [Eq. (11.8)]

Compound	Obsd	Calcd	Res	Del res	Pred	PSA
1	4.301	4.522	−0.221	−0.258	4.559	152.625
2	4.094	4.306	−0.212	−0.318	4.413	129.832
3	4.375	4.610	−0.235	−0.269	4.644	161.878
4	5.164	5.158	0.006	0.027	5.136	219.559
5[a]	5.037	4.709	0.328	0.383	4.653	172.296
6	4.668	4.582	0.086	0.099	4.569	158.861
7[a]	5.020	4.415	0.605	0.769	4.251	141.289
8	4.250	4.607	−0.357	−0.408	4.658	161.493

[a]Considered as outliers.

7.1.9 Isatin Analogs as SARS-CoV 3CL^{pro} Inhibitors

Zhou et al. (2006) reported some isatin analogs as SARS-CoV 3CL^{pro} inhibitors (Table 11.10), for which the correlation obtained was as in Eq. (11.9):

$$pIC_{50} = -5.298 (\pm 1.846) + 0.020 (\pm 0.004) SA \qquad (11.9)$$

$N = 7$, $R = 0.929$, $R^2 = 0.862$, $R_A^2 = 0.835$, $F (1, 5) = 31.349$, $P < 0.00251$, SEE = 0.347, $q^2 = 0.688$, $Q = 2.677$, Outlier = Compound **4**

It was observed from Eq. (11.9) that increasing the SA of these molecules may impart higher inhibitory activity. Bulky substitution at the R$_1$ position, such as β-napthylmethyl (compounds **3** and **8**, Table 11.10) may impart higher SA and hence, produce higher activity. Thus substitution with –CONH$_2$ function at the R$_2$ position in place of iodo function may have a better effect (compound **8** vs. **3**, compound **6** vs. **1**, and compound **7** vs. **2**, Table 11.10). Similarly, bulky aryl function may be more favorable than the alkyl function. The larger SA may help the molecule to occupy more space in the enzyme active site to have better binding interaction as evidenced by the molecular docking analysis (Zhou et al., 2006). Compound **8** having maximum SA exhibits hydrogen bonding with His41 and Cys145 through the keto functions of the isatin moiety. Moreover, the carboxamide function at the R$_2$ position makes hydrogen bonding with Phe140 and His163. The β-napthyl moiety (Compound **8**) fits well into the hydrophobic S2 pocket whereas smaller and less bulky substituents, such as methyl (Compound **4**), n-propyl (Compound **5**), n-butyl (Compound **6**), and benzyl (Compound **7**) do not accommodate well into the S2 pocket. It is not clear why the compound **4** behaves aberrantly though possessing a comparable good SA. Therefore, compound **4** may be considered as an outlier.

TABLE 11.10 Biological Activity and Physicochemical Parameters of Isatin Analogs as SARS-CoV 3CL^{pro} Inhibitors for QSAR Model [Eq. (11.9)]
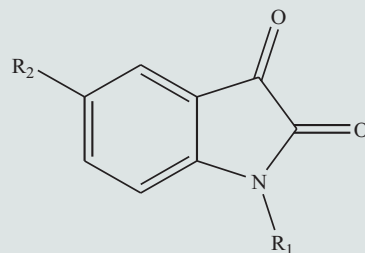
Compound	R$_1$	R$_2$	Obsd	Calcd	Res	Del res	Pred	SA
1	n-Butyl	I	4.180	4.665	−0.485	−0.564	4.745	469.003
2	Benzyl	I	4.301	4.902	−0.601	−0.686	4.987	485.295
3	β-Napthylmethyl	I	5.959	5.730	0.228	0.329	5.630	542.453
4[a]	Me	CONH$_2$	4.149	3.613	0.535	1.243	2.906	396.444
5	n-Propyl	CONH$_2$	4.602	4.421	0.181	0.223	4.379	452.138
6	n-Butyl	CONH$_2$	4.721	4.869	−0.148	−0.169	4.890	483.059
7	Benzyl	CONH$_2$	4.903	5.103	−0.199	−0.231	5.134	499.156
8	β-Napthylmethyl	CONH$_2$	6.432	5.944	0.488	0.829	5.603	557.185

[a]Considered as outliers.

7.1.10   A Diverse Set of Potent SARS-CoV 3CL^pro Inhibitors

Tsai et al. (2006) reported a series of SARS-CoV 3CL^pro inhibitors through phar-
macophore mapping and virtual screening approach (Fig. 11.6; Table 11.11).
For this, the QSAR model obtained was as shown by Eq. (11.10).

$$pIC_{50} = 3.050\,(\pm0.544) + 1.044\,(\pm0.151)\,CMR - 0.204\,(\pm0.033)\,D_Y \atop - 0.010\,(\pm0.001)\,Vol \tag{11.10}$$

$N = 24$, $R = 0.915$, $R^2 = 0.836$, $R_A^2 = 0.812$, $F\,(3, 20) = 34.080$, $P < 0.00000$,
SEE $= 0.282$, $q^2 = 0.754$, $Q = 3.245$, Outlier = Compounds **9**, **13**, **24**

It was observed from Eq. (11.10) that increasing the value of the molar re-
fractivity (CMR) and decreasing the value of the dipole moment along Y-axis
(D_Y), as well as the volume (Vol) may contribute positively to the enzyme in-
hibitory activity. It was, therefore, suggested that increasing the total molecular
bulk may increase the activity whereas bulky substituent along Y-axis may be
detrimental to the activity. Bulky substitution along Y-axis may produce some
unfavorable steric interaction with the enzyme. Therefore, the bulky molecule
with less steric effect may be favorable for the activity. Compounds **9**, **13**, and **24**
(Table 11.11) may act through different mechanism(s) of action and hence, they
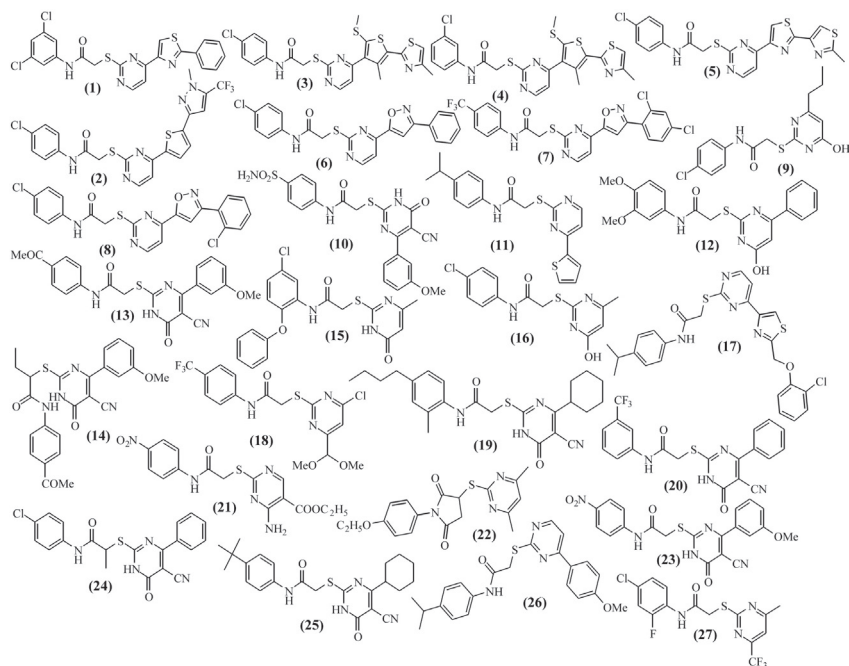were considered as outliers.

FIGURE 11.6   Structures of some potent SARS-CoV 3CL^pro inhibitors.

TABLE 11.11 Biological Activity and Physicochemical Parameters of a Diverse Set of Potent SARS-CoV 3CL^{pro} Inhibitors (Fig. 11.6) for QSAR Model [Eq. (11.10)]

| Compound	Obsd	Calcd	Res	Del res	Pred	CMR	D_Y	Vol
1	5.523	5.092	0.431	0.557	4.966	12.519	−3.187	1169.180
2	5.000	4.615	0.385	0.484	4.516	12.431	−5.072	1263.640
3	4.959	5.005	−0.046	−0.057	5.016	14.035	−2.218	1326.330
4	4.921	4.902	0.019	0.022	4.899	14.035	−2.750	1351.480
5	4.854	4.876	−0.022	−0.026	4.880	12.090	−4.583	1180.750
6	4.824	4.491	0.333	0.355	4.469	11.433	−3.308	1132.790
7	4.824	4.455	0.369	0.411	4.413	12.434	−3.499	1251.610
8	4.824	4.812	0.012	0.014	4.810	11.924	−3.530	1148.570
9[a]	4.523	3.698	0.825	0.948	3.575	8.952	−2.453	948.018
10	4.398	4.131	0.267	0.283	4.114	11.976	−0.619	1182.810
11	4.398	4.313	0.085	0.091	4.307	10.628	−3.433	1070.780
12	4.347	4.220	0.127	0.135	4.212	10.814	−3.237	1099.490
13[a]	4.222	3.362	0.860	1.193	3.029	11.698	2.871	1180.190
14	4.222	4.050	0.172	0.226	3.996	12.626	1.981	1209.220
15	4.000	4.371	−0.371	−0.469	4.469	10.749	−0.795	1019.780
16	3.699	3.794	−0.095	−0.124	3.823	8.024	−2.450	833.212
17	3.699	4.193	−0.494	−0.699	4.398	14.036	−1.711	1424.160
18	3.699	3.986	−0.287	−0.331	4.030	9.615	−3.899	1013.380
19	3.699	3.759	−0.060	−0.073	3.772	12.531	−0.188	1284.230
20	3.699	3.998	−0.299	−0.315	4.014	10.628	−2.143	1085.260
21	3.602	3.703	−0.101	−0.112	3.714	9.476	−2.069	996.643
22	3.523	3.808	−0.285	−0.327	3.850	9.710	−3.228	1033.240
23	3.523	3.557	−0.034	−0.040	3.563	11.346	1.299	1149.300
24[a]	3.523	4.283	−0.760	−0.871	4.394	11.073	−0.759	1066.380
25	3.456	4.031	−0.575	−0.625	4.081	12.067	0.024	1192.450
26	3.398	3.887	−0.489	−0.539	3.937	11.435	−1.858	1182.620
27	3.301	3.264	0.037	0.047	3.255	8.397	−0.405	901.161

[a]Considered as outliers.
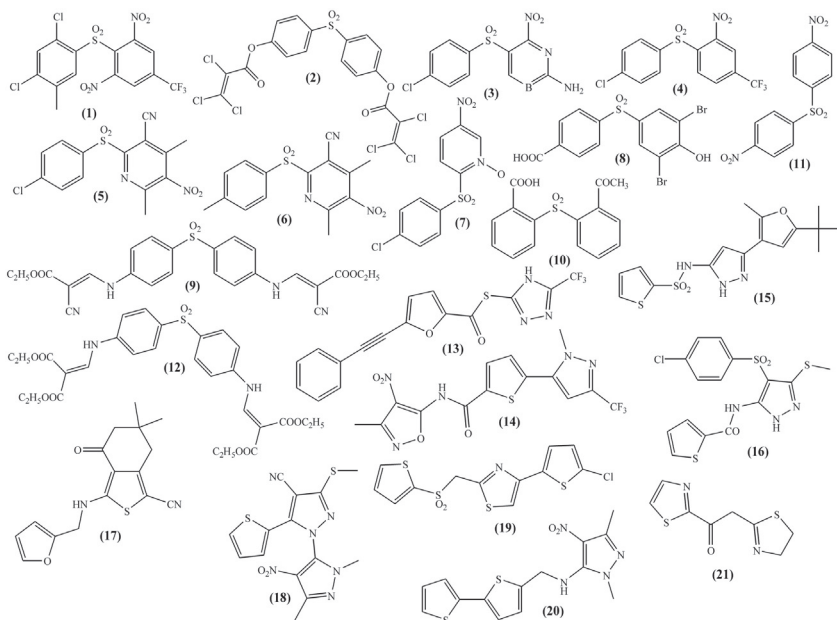
FIGURE 11.7 Structures of nonpeptide SARS-CoVM^{pro} inhibitors.

7.1.11 A Series of Nonpeptide SARS-CoV 3CL^{pro} Inhibitors

Lu et al. (2006) reported a series of nonpeptide SARS-CoV M^{pro} inhibitors (Fig. 11.7; Table 11.12) through structure-based drug design approach, for which the QSAR model obtained was as shown by Eq. (11.11). It was observed from this equation that the increase in the value of the SA and the polar volume (Pol Vol) may be conducive to the activity, whereas the increasing in the value of volume and dipole moment along X-axis (D_X) might be detrimental to the activity. Thus it could be suggested that bulky substitutions along X-axis might produce unfavorable steric hindrance that may lower the activity. Moreover, this model also revealed that compounds having higher polar volume may favor the activity compared to compounds with lower polar volume. In compound **1** (Table 11.12), one of the nitro groups is closer to the imidazole function of His41 and thus there may be some electrostatic interaction between them leading to better activity. Moreover, the phenyl ring may form π–π interactions with His237 at the enzyme active site leading to potent activity. Compounds **1** and **8** (Table 11.12) might act in a different manner and hence, they were considered as outliers.

$$pIC_{50} = 2.664\,(\pm 0.339) + 0.020\,(\pm 0.003)\,SA - 0.010\,(\pm 0.002)\,Vol$$
$$- 0.075\,(\pm 0.015)\,D_X + 0.003\,(\pm 0.001)\,Pol\,Vol$$

(11.11)

$N = 19$, $R = 0.911$, $R^2 = 0.830$, $R_A^2 = 0.781$, $F\,(1, 14) = 17.089$, $P < 0.00003$, SEE $= 0.178$, $q^2 = 0.605$, $Q = 5.118$, Outlier $=$ Compounds **1, 8**

TABLE 11.12 Biological Activity and Physicochemical Parameters of a Series of Nonpeptide SARS-CoV 3CL[pro] Inhibitors (Fig. 11.7) for QSAR Model [Eq. (11.11)]

Compound	Obsd	Calcd	Res	Del res	Pred	D_X	Pol Vol	SA	Vol
1[a]	6.523	4.965	1.558	1.879	4.644	−1.109	177.492	547.807	939.699
2	6.046	5.466	0.579	0.931	5.115	−1.905	182.783	733.597	1184.370
3	5.222	5.057	0.165	0.212	5.010	−0.568	251.310	497.859	803.261
4	4.921	5.232	−0.311	−0.389	5.310	−4.454	158.771	509.445	843.770
5	4.886	4.955	−0.069	−0.073	4.960	0.390	216.773	526.936	873.061
6	4.886	5.053	−0.167	−0.180	5.066	−0.772	211.376	534.514	881.205
7	4.824	4.559	0.265	0.366	4.458	7.202	245.339	483.718	773.796
8[a]	4.796	5.293	−0.497	−0.851	5.647	0.780	299.398	829.728	1389.050
9	4.796	5.013	−0.217	−0.235	5.031	−0.547	171.214	524.341	865.596
10	4.796	4.991	−0.196	−0.242	5.038	−1.866	136.667	477.650	800.051
11	4.602	4.655	−0.053	−0.072	4.674	6.493	261.992	497.278	787.197
12	4.495	4.811	−0.316	−1.040	5.534	2.675	283.177	773.777	1382.880
13	5.523	5.228	0.295	0.340	5.183	−0.933	175.089	612.441	988.794
14	5.301	5.179	0.122	0.141	5.160	−1.175	255.605	614.602	1017.590
15	5.000	5.216	−0.216	−0.247	5.247	−2.424	233.334	638.284	1077.980
16	4.824	5.028	−0.204	−0.294	5.118	−2.348	289.728	543.817	943.419
17	4.796	4.945	−0.149	−0.176	4.972	0.299	141.590	526.835	873.189
18	4.745	4.559	0.186	0.334	4.410	5.607	371.972	528.119	903.617
19	4.745	4.905	−0.161	−0.207	4.952	3.748	158.165	534.331	834.408
20	4.699	4.788	−0.089	−0.111	4.810	4.862	190.284	564.125	911.548
21	4.398	4.921	−0.523	−0.711	5.109	−0.151	98.696	388.069	601.894

[a]Considered as outliers.

7.1.12 Quercetin-3-β-Galactoside SARS-CoV 3CL^{pro} Inhibitors

Chen et al. (2006b) reported some quercetin-3-β-galactoside and its analogs as promising SARS-CoV 3CL^{pro} inhibitors (Table 11.13), for which the QSAR model obtained was as in Eq. (11.12):

$$pIC_{50} = 6.112\,(\pm 0.057) - 0.005\,(\pm 0.0002)\,PSA \qquad (11.12)$$

$N = 4$, $R = 0.999$, $R^2 = 0.998$, $R_A^2 = 0.996$, $F\,(1,\,2) = 842.36$, $P < 0.00119$, SEE = 0.008, $q^2 = 0.984$, $Q = 124.875$, Outlier = Compound **4**

It was observed from Eq. (11.12) that decreasing the value of the PSA would have the positive effect on the biological activity. It meant that less polar molecules would be preferred to the high polar molecules. Due to the presence of a number of hydroxyl groups, these molecules may interact with the enzyme as hydrogen bond acceptors. The molecular modeling study revealed that the side chain of Gln189 forms four hydrogen bonds with compound **5** (Table 11.13), whereas two hydrogen bonding interactions are observed with the nitrogen atom of Glu166. It was, however, observed that compound **4** having the highest PSA value due to the presence of two galactose rings was less active. Probably, compound **4** might behave in an aberrant fashion and hence, it was considered as an outlier.

7.1.13 Phthalhydrazide Ketones as Potent SARS-CoV 3CL^{pro} Inhibitors

Zhang et al. (2007) synthesized and evaluated some phthalhydrazide ketones (Table 11.14) and heteroatomic ester as potential SARS-3CL^{pro} inhibitors. The QSAR model developed for this set of compounds was as shown by Eq. (11.13):

$$pIC_{50} = 8.108\,(\pm 0.131) - 0.009\,(\pm 0.001)\,PolVol \qquad (11.13)$$

$N = 6$, $R = 0.970$, $R^2 = 0.942$, $R_A^2 = 0.927$, $F\,(1,\,4) = 64.539$, $P < 0.00130$, SEE = 0.072, $q^2 = 0.739$, $Q = 13.472$, Outlier = Compounds **2**, **7**

Eq. (11.13) suggested that high polar volume of the compound would not favor the activity. A molecular modeling study had revealed that the halopyridine moiety of the compounds was well accommodated in the S1 binding pocket where it could have van der Waals interactions. Moreover, it was observed that the halogen atom does not interact with the enzyme and is directed toward the solvent exposed area. The furyl group of compound **3** is located near the catalytic Cys145 residue where it can have hydrophobic interaction. Compounds **2** and **7** being a misfit in the correlation were excluded.

7.1.14 Some Peptidomimetic SARS-CoV 3CL^{pro} Inhibitors

Ghosh et al. (2007) reported some peptidomimetic SARS-CoV 3CL^{pro} inhibitors (Table 11.15), for which a QSAR model obtained was as:

$$pIC_{50} = 5.009\,(\pm 0.174) - 0.504\,(\pm 0.067)\,D_z \qquad (11.14)$$

TABLE 11.13 Biological Activity and Physicochemical Parameters of Quercetin-3-β-Galactoside SARS-CoV 3CL^pro Inhibitors for QSAR Model [Eq. (11.12)]
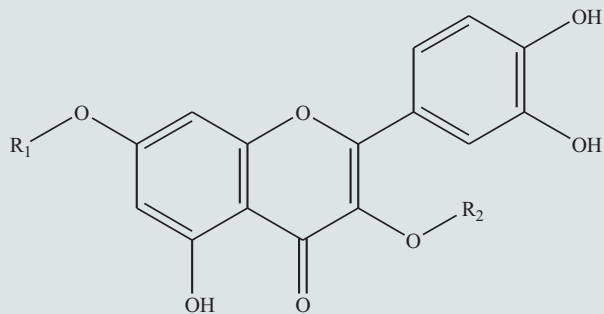
Compound	R_1	R_2	Obsd	Calcd	Res	Del res	Pred	PSA
1	H	L-Fucose	4.617	4.568	0.049	0.099	4.518	306.747
2	H	D-Arabinose	4.500	4.486	0.014	0.019	4.481	333.869
3	H	D-Glucose	4.311	4.378	−0.067	−0.084	4.395	369.951
4[a]	D-Galactose	D-Galactose	4.211	4.166	0.045	0.236	3.975	440.138
5	H	D-Galactose	4.369	4.410	−0.041	−0.052	4.420	359.227

[a]Considered as outliers.

TABLE 11.14 Biological Activity and Physicochemical Parameters of Phthalhydrazide Ketones as Potent SARS-CoV 3CL^{pro} Inhibitors for QSAR Model [Eq. (11.13)]
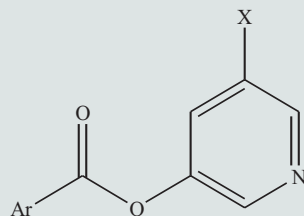
Compound	Ar	X	Obsd	Calcd	Res	Del res	Pred	Pol Vol
1	2-Furyl	Cl	7.222	7.134	0.088	0.115	7.106	93.111
2[a]	Benzofuran-2-yl	Cl	6.770	7.086	−0.317	−0.388	7.158	99.866
3	2-Furyl	Br	7.301	7.144	0.157	0.211	7.090	91.748
4	2-Indolyl	Cl	7.187	6.993	0.194	0.222	6.965	113.106
5	2-Benzothiophenyl	Cl	7.022	6.889	0.133	0.157	6.866	127.948
6	Thiazole-4-yl	Cl	6.569	6.562	0.006	0.031	6.537	174.454
7[a]	3-OMePh	Cl	6.469	6.962	−0.493	−0.564	7.032	117.647
8	5-(4-ClPh)-Furan-2-yl	Cl	7.201	6.969	0.231	0.264	6.936	116.549

[a]Considered as outliers.

TABLE 11.15 Biological Activity and Physicochemical Parameters of Some Peptidomimetic SARS-CoV 3CL^pro Inhibitors for QSAR Model [Eq. (11.14)]
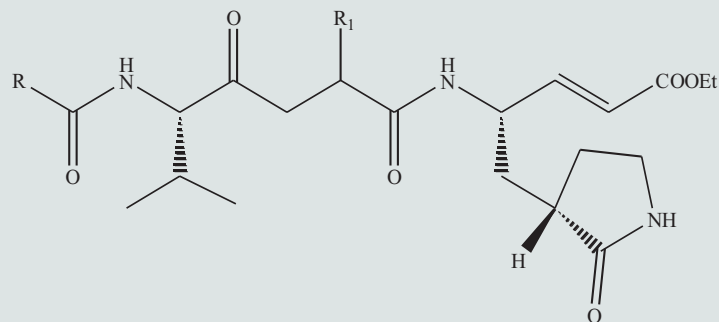
Compound	R	R$_1$	Obsd	Calcd	Res	Del res	Pred	D$_Z$
1	5-Me-isoxazolyl-3-yl	Benzyl	3.060	3.334	−0.273	−0.359	3.419	3.323
2	5-Me-isoxazolyl-3-yl	CH$_2$CH=C(Me)$_2$	3.097	3.365	−0.268	−0.348	3.444	3.260
3	CH(CH$_2$OH)NHBoc	CH$_2$CH=C(Me)$_2$	4.097	4.062	0.035	0.041	4.055	1.879
4	CH(CH$_2$OH)NHBoc	i-Butyl	5.000	5.049	−0.049	−0.106	5.106	−0.080
5	CH(CH$_2$OH)NHBoc	Benzyl	4.824	4.786	0.038	0.061	4.763	0.442
6	5-Me-isoxazolyl-3-yl	Benzyl	3.523	3.334	0.189	0.249	3.274	3.323
7	5-Me-isoxazolyl-3-yl	i-Butyl	3.699	3.371	0.328	0.424	3.275	3.249

$N = 7$, $R = 0.959$, $R^2 = 0.919$, $R_A^2 = 0.903$, F (1, 5) = 56.603, $P < 0.00066$, SEE = 0.243, $q^2 = 0.860$, $Q = 3.947$

It was observed from Eq. (11.14) that increasing the value of the dipole moment along Z-axis (D_Z) will lead to decrease the enzyme inhibitory activity. It thus suggested that the bulky substituent along Z-axis will not be conducive to the activity. The long chain linear aminobutoxy derivatives (Compounds **4** and **5**, Table 11.15) are better than the isoxazole analogs (Compounds **1**, **2**, **6**, and **7**, Table 11.15) as the isoxazole moiety may produce more bulkiness that may impart unfavorable steric effect with the enzyme.

7.1.15 Arylmethylene Ketones and Fluorinated Methylene Ketones as SARS-CoV 3CL^pro Inhibitors

Zhang et al. (2008) reported some arylmethylene ketones and fluorinated methylene ketones as SARS-CoV 3CL^pro inhibitors (Table 11.16). The QSAR model for them was as shown by Eq. (11.15), where the indicator variable "I" stands for a value of unity for the ester group. A positive coefficient of it suggested that the ester group may be favorable for imparting the higher inhibitory activity. Compounds bearing ester functions (Compounds **2–4**, Table 11.16) are highly active compared to the nonester derivatives (Compounds **5–8**, Table 11.16). Compounds **5–7** are found to be oriented from S1 to S4 pocket and the furan oxygen atom forms hydrogen bonds with the amino function of Glu166. Moreover, it is observed that compound **1** though having ester function, may behave in an aberrant fashion. Therefore, it was considered as an outlier.

$$pIC_{50} = 4.452\,(\pm 0.133) + 2.789\,(\pm 0.203)\,I \qquad (11.15)$$

$N = 7$, $R = 0.987$, $R^2 = 0.974$, $R_A^2 = 0.969$, F (1, 5) = 188.18, $P < 0.00004$, SEE = 0.266, $q^2 = 0.954$, $Q = 3.711$, Outlier = Compound **1**

7.1.16 Chloropyridine Esters as Potent SARS-CoV 3CL^pro Inhibitors

The QSAR model obtained for a series of chloropyridine esters reported by Niu et al. (2008) as potent SARS-CoV 3CL^pro inhibitors (Table 11.17) was as shown by Eq. (11.16), which suggested that increasing the molar refractivity and decreasing the total dipole moment may favor 3CL protease inhibitory activity

$$pIC_{50} = 3.460\,(\pm 0.429) + 0.470\,(\pm 0.063)\,CMR - 0.067\,(\pm 0.019)\,D_{Tot} \qquad (11.16)$$

$N = 10$, $R = 0.945$, $R^2 = 0.892$, $R_A^2 = 0.861$, F (2, 7) = 29.024, $P < 0.00041$, SEE = 0.148, $q^2 = 0.778$, $Q = 6.385$, Outlier = Compound **5**, **6**.

This also suggested that the smaller molecules with less steric effect may be conducive to the inhibitory activity. The α-naphthyl (Compound **11**, Table 11.17) and the 2-oxochromene function (Compound **12**, Table 11.17) at Ar position yield less dipole moment and better molar refractivity compared to the nitrophenyl (Compounds **9** and **10**), the chlorophenyl (Compound **8**) or the

TABLE 11.16 Biological Activity and Physicochemical Parameters of Arylmethylene Ketones and Fluorinated Methylene Ketones as SARS-CoV 3CL[pro] Inhibitors for QSAR Model [Eq. (11.15)]
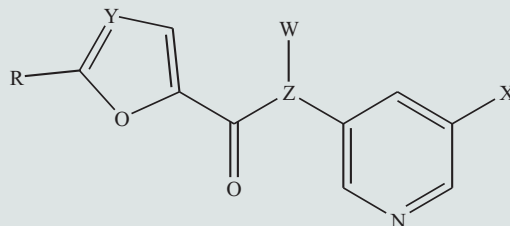
Compound	R	X	Y	Z	W	Obsd	Calcd	Res	Del res	Pred	I
1[a]	H	H	CH	O	—	5.102	6.706	−1.604	−2.139	7.241	1
2	H	Br	CH	O	—	7.301	6.706	0.595	0.793	6.508	1
3	H	Cl	CH	O	—	7.222	6.706	0.515	0.687	6.535	1
4	4-ClPh	Cl	CH	O	—	7.201	6.706	0.494	0.659	6.542	1
5	4-ClPh	Br	CH	CH$_2$	—	4.886	4.452	0.434	0.579	4.307	0
6	4-ClPh	Br	CH	CH	F	4.553	4.452	0.101	0.134	4.418	0
7	4-ClPh	Br	CH	C	F,F	4.244	4.452	−0.208	−0.277	4.521	0
8	4-ClPh	Br	N	CH$_2$	—	4.125	4.452	−0.327	−0.436	4.561	0

[a]Considered as outliers.

TABLE 11.17 Biological Activity and Physicochemical Parameters of Chloropyridine Esters as Potent SARS-CoV 3CL^{pro} Inhibitors for QSAR Model [Eq. (11.16)]

(1–5)   (6–12)
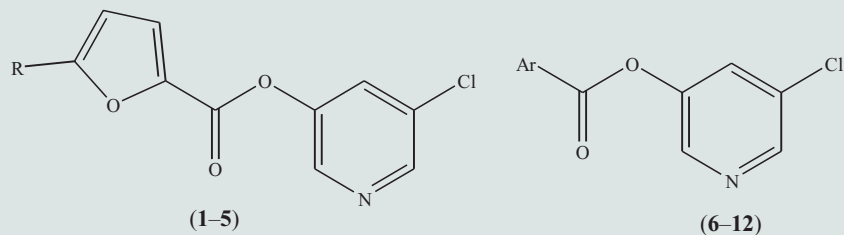
Compound	R	Ar	Obsd	Calcd	Res	Del res	Pred	CMR	D_{Tot}
1	4-ClPh	—	7.201	7.087	0.114	0.156	7.045	8.349	3.682
2	4-NO$_2$Ph	—	7.222	7.022	0.200	0.252	6.970	8.469	5.001
3	2-NO$_2$,4-ClPh	—	6.914	6.789	0.125	0.184	6.730	8.961	10.027
4	2-NO$_2$Ph	—	6.682	6.594	0.088	0.130	6.552	8.469	10.059
5[a]	3-NO$_2$Ph	—	6.301	6.727	−0.426	−0.534	6.835	8.469	8.490
6[a]	—	4-Pyr	6.785	6.378	0.407	0.568	6.217	5.922	0.861
7	—	3-Pyr	6.157	6.348	−0.191	−0.266	6.423	5.922	1.216
8	—	4-ClPh	6.363	6.633	−0.270	−0.331	6.693	6.624	1.092
9	—	2-NO$_2$Ph	6.478	6.260	0.217	0.305	6.172	6.744	6.047
10	—	3-NO$_2$Ph	6.165	6.371	−0.206	−0.252	6.417	6.744	4.736
11	—	α-Napthyl	6.907	7.022	−0.115	−0.157	7.064	7.821	2.014
12	—	2-Oxo-chromene	6.967	6.909	0.058	0.071	6.896	7.607	2.361

[a]Considered as outliers.

pyridyl analog (Compound **7**) and thus compounds **11** and **12** are more potent than compounds **7–10**. Furyl derivatives (Compounds **1–4**) are better inhibitors as compared to the other aryl ester analogs (Compounds **7–12**) as they have higher molar refractivity despite having comparatively moderate bulky *p*-chlorophenyl or the *p*-nitrophenyl groups at R position. A slight reduction in the activity is noticed for the disubstituted aryl function (Compound **3**) and the alteration of the nitro function at the 2nd position of the phenyl ring (Compound **4**) in contrast to the 4th position (Compound **2**), which increases the bulkiness or total bulk, and reduces the activity slightly. It is observed from the molecular modeling study that increasing the length of the side chain may increase the interaction between S2 and S4 pocket and the inhibitor that can be reflected by the QSAR model. Compound **5** possesses the higher molar refractivity while compound **6** possesses the lowest value of total dipole moment but it is not reflected in their activity. Probably, these compounds behave differently from other compounds in the dataset and hence were outliers.

7.1.17 Cinanserin Analogs as Promising SARS-CoV 3CL^{pro} Inhibitors

Yang et al. (2008) reported some cinanserin analogs as SARS-CoV 3CL^{pro} inhibitors (Table 11.18), for which the QSAR model obtained was as shown by Eq. (11.17). This equation clearly exhibited that high molecular volume will not be favorable to the activity. Thus compounds having aryl (Compound **4**), the heteroaryl (Compounds **6**, **7**), or the long chain amide function (Compounds **1**, **2**) at Y position have the lower activity than compounds having at this position the unsaturation (Compounds **8**, **9**) or the ester function (Compound **5**). Compound **8** enters into the deep S1 pocket and has hydrophobic interactions. However, compound **3** has the lowest volume but it does not show the highest activity. Probably, this compound (Compound **3**) may behave in a different manner with the enzyme and hence it is considered as an outlier.

$$p\text{IC}_{50} = 24.586\,(\pm 3.262) - 0.020\,(\pm 0.003)\,\text{Vol} \qquad (11.17)$$

$N = 8$, $R = 0.931$, $R^2 = 0.867$, $R_A^2 = 0.845$, $F\,(1,\,6) = 39.280$, $P < 0.00077$, SEE $= 0.347$, $q^2 = 0.686$, $Q = 2.683$, Outlier = Compound **3**

7.1.18 Trifluoromethyl, Benzothiazolyl, and Thiazolyl Ketone Compounds as Promising SARS-CoV 3CL^{pro} Inhibitors

The QSAR model derived for some trifluoromethyl, benzothiazolyl, and thiazolyl ketone compounds with peptide side chain reported by Regnier et al. (2009) as promising SARS-CoV 3CL^{pro} inhibitors (Table 11.19) was as shown by Eq. (11.18)

$$pK_i = 6.096\,(\pm 0.893) - 0.027\,(\pm 0.008)\,\text{Pol Vol} + 0.0001\,(\pm 0.000)\,\text{Pol Vol}^2 \;(11.18)$$

$N = 15$, $R = 0.856$, $R^2 = 0.732$, $R_A^2 = 0.687$, $F\,(2,\,12) = 16.394$, $P < 0.00037$, SEE $= 0.375$, $q^2 = 0.536$, $Q = 2.283$, Pol Vol$_{opt} = 135$.

TABLE 11.18 Biological Activity and Physicochemical Parameters of Cinanserin Analogs as Promising SARS-CoV 3CL[pro] Inhibitors for QSAR Model [Eq. (11.17)]
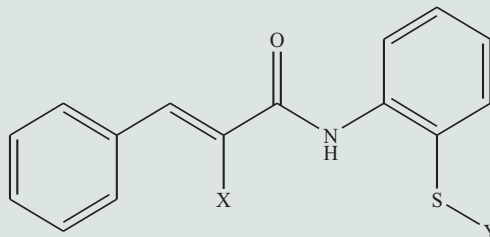
Compound	X	Y	Obsd	Calcd	Res	Del res	Pred	Vol
1	H	$(CH_2)_3N(Me)_2$	3.491	3.964	−0.473	−0.542	4.033	1020.630
2	CN	$(CH_2)_3N(Me)_2$	3.903	3.771	0.132	0.158	3.745	1034.690
3[a]	H	$CH_2C≡CH$	4.706	5.450	−0.745	−1.488	6.194	912.242
4	H	Benzyl	3.686	3.477	0.209	0.280	3.406	1056.120
5	H	$(CH_2)_2COOMe$	4.870	4.741	0.128	0.157	4.713	963.919
6	H	2-Pyridylmethyl	3.533	3.638	−0.104	−0.130	3.663	1044.400
7	H	3-Pyridylmethyl	3.457	3.663	−0.206	−0.254	3.711	1042.560
8	H	COCH=CHPh	5.975	5.019	0.955	1.318	4.657	943.645
9	CN	COC(CN)=CHPh	4.360	4.257	0.103	0.116	4.244	999.248

[a]Considered as outliers.

TABLE 11.19 Biological Activity and Physicochemical Parameters of Trifluoromethyl, Benzothiazolyl, and Thiazolyl Ketone Compounds as Promising SARS-CoV 3CL^{pro} Inhibitors for QSAR Model [Eq. (11.18)]
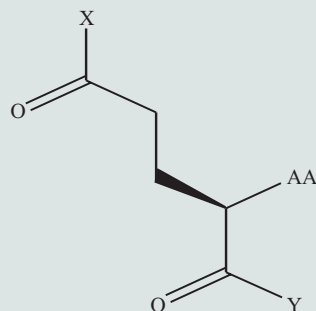
Compound	AA	X	Y	Obsd	Calcd	Res	Del res	Pred	Pol Vol
1	Cbz-Val-Leu-NH	OH	CF$_3$	3.936	3.959	−0.023	−0.026	3.961	416.522
2	Cbz-Ala-Val-Leu-NH	NH$_2$	CF$_3$	3.870	3.939	−0.069	−0.078	3.947	415.318
3	Cbz-Val-Leu-NH	N(Et)$_2$	CF$_3$	3.440	3.882	−0.442	−0.499	3.939	411.755
4	Cbz-Val-Leu-NH	Morpholine	CF$_3$	4.678	4.267	0.411	0.455	4.223	434.513
5	Cbz-Val-Leu-NH	N(Me)Benzyl	CF$_3$	4.467	3.779	0.688	0.795	3.672	405.044
6	Cbz-Ala-Val-Leu-NH	N(Et)$_2$	CF$_3$	3.527	3.426	0.101	0.135	3.393	379.365
7	Cbz-Leu-NH	N(Et)$_2$	CF$_3$	3.234	3.469	−0.235	−0.324	3.558	133.810
8	Cbz-Val-Leu-NH	Morpholine	Thiazole-2-yl	3.321	3.520	−0.200	−0.253	3.574	386.735
9	Cbz-Val-Leu-NH	N(Et)$_2$	Thiazole-2-yl	3.951	4.131	−0.180	−0.199	4.150	426.813
10	Cbz-Val-Leu-NH	2-Oxo-pyrrolidin-3-yl	Thiazole-2-yl	5.658	5.214	0.443	0.862	4.795	480.804
11	Cbz-Val-Leu-NH	N(Et)$_2$	Thiazole-2-yl	4.345	4.787	−0.442	−0.576	4.921	461.239
12	Cbz-Leu-NH	N(Et)$_2$	Thiazole-2-yl	3.335	3.316	0.020	0.026	3.310	146.432
13	Cbz-Val-NH	N(Et)$_2$	Thiazole-2-yl	3.212	3.415	−0.203	−0.273	3.485	138.098
14	Cbz-Val-Leu-NH	N(Et)$_2$	Benzohiazole-2-yl	4.307	4.604	−0.297	−0.355	4.662	452.238
15	Cbz-Val-NH	N(Et)$_2$	Benzohiazole-2-yl	3.799	3.370	0.429	0.567	3.232	141.781

Eq. (11.18) showed that the enzyme inhibitory activity was correlated with the polar volume of the molecules through a parabolic relation. It, therefore, suggests that the activity would decrease upto an optimum value of polar volume (Pol Vol$_{opt}$ = 135) and beyond that will start increasing. Compound with the 2-oxo-pyrrolidin-3-yl function (Compound **10**, Table 11.19) possesses the higher polar volume and hence, possess the maximum inhibition. Comparing the activity of this compound with those of compounds **8**, **10–13**, it may be suggested that the 2-oxo-pyrrolidin-3-yl function in compound **10** is favorable than the diethylamino function in compounds **11–13** and morpholino function in compound **8** at the X position. Moreover, the benzothiazole-2-yl function in compounds **14**, **15** is favorable than the thiazole function in compounds **8**, **12**, **13**. The bulky group, such as the morpholino in compound **4** and the benzyl-methylamino function in compound **5** are favorable than the smaller substituents, such as the hydroxyl in compound **1**, the amino group in compound **2**, and the diethylamino group in compounds **3**, **6**, and **7** at X position. Comparing compound **14** with **15**, it may be inferred that the bulky amino acid moiety (compound **14**) is favorable than smaller amino acid functions (Compound **15**), as bulky functions may produce the higher polar volume. The molecular modeling study revealed that the benzyloxycarbonyl moiety of compound **10** did not make any hydrophobic interaction rather had hydrogen bonding interactions with Glu166 through its adjacent amino function.

7.1.19 Pyrazolone Analogs as Promising SARS-CoV 3CL^{pro} Inhibitors

Ramajayam et al. (2010) reported some pyrazolone analogs as promising SARS-CoV 3CL^{pro} inhibitors (Table 11.20), for which the QSAR model obtained was as:

$$pIC_{50} = 9.292\,(\pm 0.347) - 0.281(\pm 0.074)\,C\log P \tag{11.19}$$

N = 7, R = 0.862, R^2 = 0.744, R_A^2 = 0.692, F (1, 5) = 14.512, P < 0.01251, SEE = 0.119, q^2 = 0.529, Q = 7.244, Outlier = Compounds **1**, **5**

Eq. (11.19) thus suggested that increasing value of the hydrophobicity of these molecules may be detrimental to the activity. Compounds with the smaller halogen substitution, such as fluorine at R position (Compound **8**, Table 11.20) are better than compounds with the bigger halogen substituents, such as the chloro (Compounds **2** and **6**, Table 11.20). Further, a dihalo substituted compound, such as compound **7** was shown to be less active as compared to mono-halo-substituted analogs (Compounds **2**, **6**, and **8**). The cyano (Compound **4**) and the nitro (Compound **9**) substitutions also produced the higher activity as compared to the methoxy substitution (Compound **3**). The docking study suggested that the N1-phenyl group was located near to the S1' pocket. One of the oxygen atoms of the nitro group forms a hydrogen bond with Gly143. The keto function of the pyrazolone ring was also found to form another hydrogen bond

TABLE 11.20 Biological Activity and Physicochemical Parameters of Pyrazolone Analogs as Promising SARS-CoV 3CL[pro] Inhibitors for QSAR Model [Eq. (11.19)]
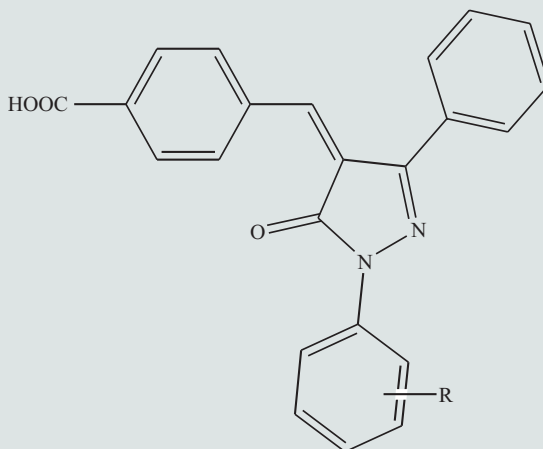
Compound	R	Obsd	Calcd	Res	Del res	Pred	C Log P
1[a]	H	7.745	7.998	−0.254	−0.297	8.042	4.380
2	4-Cl	7.857	7.760	0.097	0.115	7.742	5.093
3	4-OMe	7.921	8.025	−0.105	−0.125	8.046	4.299
4	4-CN	8.260	8.188	0.072	0.113	8.147	3.813
5[a]	4-OCF$_3$	7.377	7.655	−0.278	−0.377	7.754	5.408
6	3-Cl	7.967	7.760	0.207	0.245	7.722	5.093
7	3,4-diCl	7.614	7.562	0.052	0.089	7.526	5.686
8	4-F	8.167	7.951	0.217	0.247	7.920	4.523
9	3-NO$_2$	8.076	8.084	−0.008	−0.011	8.087	4.123

[a]Considered as outliers.

with Glu166. The C-3 phenyl ring was found to be well-accommodated in the S2 pocket. The benzylidene ring without any carboxyl functions lost the activity. Therefore, it may be assumed that hydrogen bonding interaction is more important than the hydrophobic interaction. The oxygen atom of the carboxyl group forms a hydrogen bond with Gln192. Therefore, apart from S2 pocket, none of the aryl functions has exhibited hydrophobic interactions, whereas three hydrogen bonding interactions were observed. Compounds **1** and **5** considered as outliers.
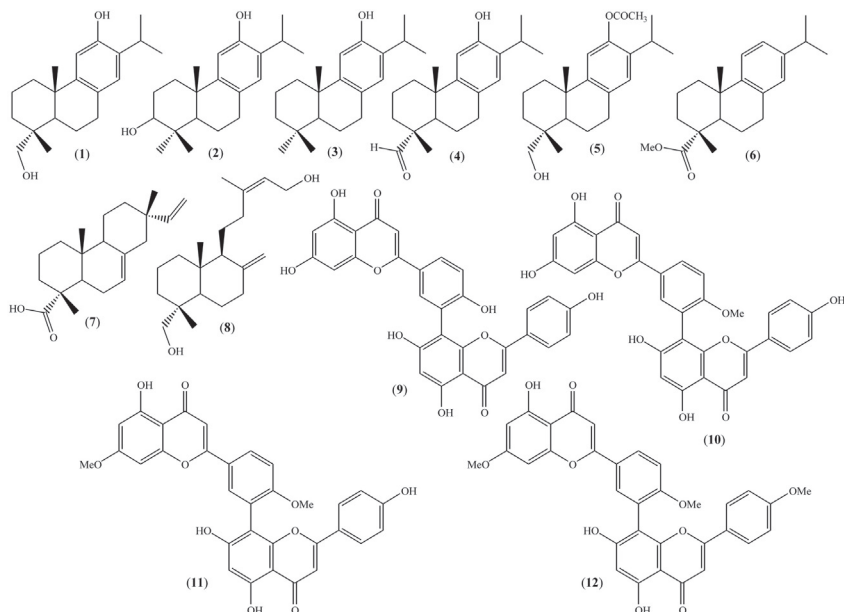
FIGURE 11.8 **General structure of some biflavonoid analogs.**

7.1.20 *Biflavonoids as Potential SARS-CoV 3CL^{pro} Inhibitors*

Ryu et al. (2010) reported a series of biflavonoids (Fig. 11.8; Table 11.21) from *Torreya nucifera* having potential SARS-CoV 3CL^{pro} inhibitory activity. The QSAR model obtained for them was as shown by Eq. (11.20). It was observed from Eq. (11.20) that the increasing value of the dipole moment along *X*-axis may be conducive to the activity. Thus, the bulky substitution at X-axis of these molecules may be favorable for activity. Compounds **10–12** (Table 11.21) possess higher dipole moment due to much bulky aryl groups as compared to the compounds **1–2**, **4–8** and, therefore, have higher activity. Compounds **3** and **9** exhibited the aberrant behavior and thus were considered as outliers.

$$pIC_{50} = 3.833(\pm 0.037) + 0.212(\pm 0.026)\, D_X \qquad (11.20)$$

$N = 10$, $R = 0.946$, $R^2 = 0.895$, $R_A^2 = 0.882$, $F(1, 8) = 68.528$, $P < 0.00003$, SEE $= 0.114$, $q^2 = 0.805$, $Q = 8.298$, Outlier = Compounds **3**, **9**

7.1.21 *A Series of Some Promising SARS-CoV 3CL^{pro} Inhibitors*

Nguyen et al. (2011) reported some promising SARS-CoV 3CL^{pro} inhibitors through virtual screening (Fig. 11.9; Table 11.22). The QSAR model obtained for these compounds was as shown by Eq. (11.21), which exhibited that the activity is well correlated with the hydrophobicity of the molecules. The docking

TABLE 11.21 Biological Activity and Physicochemical Parameters of Biflavonoids as Potential SARS-CoV 3CL^{pro} Inhibitors (Fig. 11.8) for QSAR Model [Eq. (11.20)]

| Compound	Obsd	Calcd	Res	Del res	Pred	D_X
1	3.656	3.749	−0.093	−0.108	3.764	−0.708
2	3.632	3.811	−0.179	−0.204	3.835	−0.460
3[a]	4.305	3.843	0.461	0.518	3.786	−0.333
4	3.787	3.920	−0.133	−0.146	3.934	−0.028
5	3.890	4.018	−0.129	−0.140	4.030	0.364
6	3.684	3.498	0.187	0.261	3.423	−1.708
7	3.547	3.783	−0.235	−0.270	3.818	−0.573
8	3.861	3.933	−0.072	−0.079	3.940	0.024
9[a]	5.081	4.462	0.619	0.777	4.303	2.129
10	4.141	4.223	−0.082	−0.092	4.233	1.179
11	4.495	4.581	−0.087	−0.121	4.615	2.603
12	4.416	4.672	−0.257	−0.398	4.814	2.965

[a]Considered as outliers.
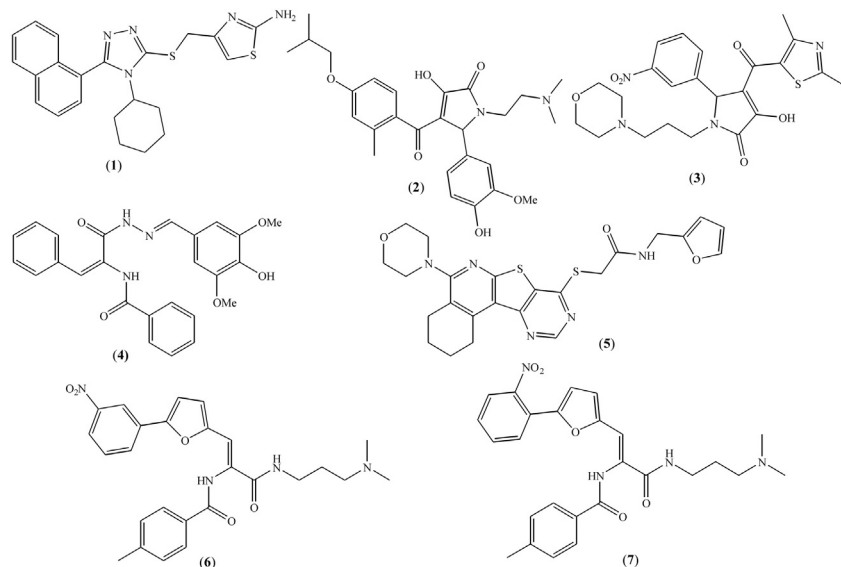
FIGURE 11.9 General structure of some potent SARS-CoV 3CL^{pro} inhibitors.

TABLE 11.22 Biological Activity and Physicochemical Parameters of a Series of Some Promising SARS-CoV 3CL[pro] Inhibitors (Fig. 11.9) for QSAR Model [Eq. (11.21)]

Compound	Obsd	Calcd	Res	Del res	Pred	C Log P
1	7.234	7.235	−0.001	−0.002	7.235	4.707
2[a]	7.202	7.283	−0.081	−0.108	7.310	5.049
3	6.994	7.016	−0.022	−0.060	7.054	3.135
4[a]	7.113	7.286	−0.173	−0.233	7.346	5.069
5	7.042	7.079	−0.037	−0.057	7.099	3.587
6	7.414	7.242	0.172	0.208	7.206	4.752
7	7.383	7.242	0.142	0.171	7.212	4.752

[a]Considered as outliers.

study had revealed that compound **7** (Table 11.22) had good hydrophobic interactions with His41, Phe140, Leu141, Cys145, His163, Glu166, Gly170, and His172 apart from a number of hydrogen bonding interactions (the nitro group with Gly143, methacrylamide group with Phe140, one of the oxygen atoms of the nitro group with Cys145). The nitrophenyl group was found to be the most crucial moiety to enter into the S1 pocket for imparting potent inhibition. Compounds **2** and **4** though possessed a higher value of hydrophobicity but less activity than expected, hence, they were considered as outliers.

$$pIC_{50} = 6.238(\pm 0.213) + 0.233(\pm 0.050)C \log P \qquad (11.21)$$

$N = 5$, $R = 0.937$, $R^2 = 0.878$, $R_A^2 = 0.837$, $F (1, 3) = 21.594$, $P < 0.01879$, SEE = 0.077, $q^2 = 0.703$, $Q = 12.169$, Outlier = Compounds **2**, **4**

7.1.22 Peptidomimetic SARS-CoV 3CL[pro] Inhibitors

Some peptidomimetic SARS-CoV 3CL[pro] inhibitors (Table 11.23) were synthesized and evaluated by Akaji et al. (2011) and the QSAR model obtained for this [Eq. (11.22)] indicated that the activity is controlled by a single indicator parameter "I" used for an imidazolyl-4-yl methyl substituent at the R_1 position. The positive coefficient of this indicated that such a substituent would conducive to the activity. The reason of this may be that this substituent might have better steric fitting in the S1 pocket of the enzyme formed by Phe140, Leu141, and Glu166. Compounds **4** and **8** (Table 11.23) were considered as outliers.

$$pIC_{50} = 4.319(\pm 0.168) + 2.409(\pm 0.213)I \qquad (11.22)$$

$N = 8$, $R = 0.977$, $R^2 = 0.955$, $R_A^2 = 0.948$, $F (1, 6) = 128.20$, $P < 0.00003$, SEE = 0.291, $q^2 = 0.929$, $Q = 3.397$, Outlier = Compounds **4**, **8**

TABLE 11.23 Biological Activity and Physicochemical Parameters of Peptidomimetic SARS-CoV 3CL[pro] Inhibitors for QSAR Model [Eq. (11.22)]
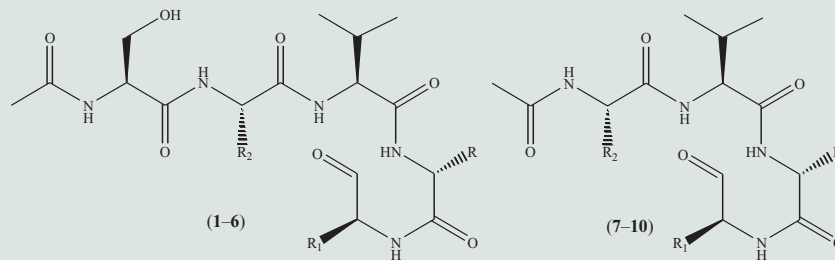
Compound	R	R_1	R_2	Obsd	Calcd	Res	Del res	Pred	I
1	i-Butyl	$(CH_2)_2CONMe_2$	Me	4.432	4.319	0.112	0.169	4.263	0
2	i-Butyl	c-Hexylmethyl	Me	4.208	4.319	−0.112	−0.168	4.375	0
3	i-Butyl	2-Thiophenylmethyl	Me	4.319	4.319	−0.001	−0.001	4.320	0
4[a]	i-Butyl	Imidazole-4-ylmethyl	Me	5.244	6.127	−0.882	−1.030	6.274	1
5	Benzyl	Imidazole-4-ylmethyl	Me	6.409	6.127	0.282	0.329	6.080	1
6	c-Hexylmethyl	Imidazole-4-ylmethyl	Me	7.187	6.127	1.061	1.237	5.950	1
7	c-Hexylmethyl	Imidazole-4-ylmethyl	Me	6.569	6.127	0.442	0.516	6.053	1
8[a]	c-Hexylmethyl	Imidazole-4-ylmethyl	CH_2CONH_2	4.000	6.127	−2.127	−2.481	6.481	1
9	c-Hexylmethyl	Imidazole-4-ylmethyl	CH_2OH	6.469	6.127	0.342	0.399	6.070	1
10	c-Hexylmethyl	Imidazole-4-ylmethyl	CH(OH)Me	7.009	6.127	0.882	1.029	5.980	1

[a]Considered as outliers

7.1.23 Flavonoids as SARS-CoV 3CL^{pro} Inhibitors

Nguyen et al. (2012) reported some flavonoids from *Pichia pastoris* (Fig. 11.10; Table 11.24) having SARS-CoV 3CL^{pro} inhibitory activity. For these compounds, the inhibition activity was shown to be correlated with the PSA of the molecule [Eq. (11.23)], suggesting that highly polar molecules may have better activity. Substituents like hydroxy might give better PSA, leading to better
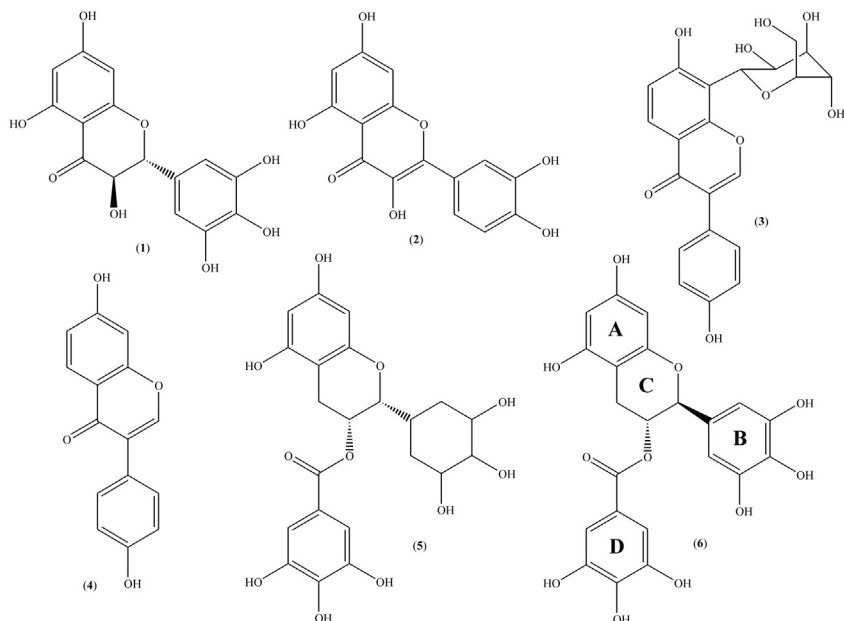
FIGURE 11.10 General structure of some flavonoids as SARS-CoV 3CL^{pro} inhibitors.

TABLE 11.24 Biological Activity and Physicochemical Parameters of Flavonoids as SARS-CoV 3CL^{pro} Inhibitors (Fig. 11.10) for QSAR Model [Eq. (11.23)]

Compound	Obsd	Calcd	Res	Del res	Pred	PSA
1[a]	3.439	3.873	−0.435	−0.525	3.964	314.921
2	4.137	3.794	0.343	0.412	3.725	290.968
3	3.419	3.644	−0.225	−0.291	3.710	245.862
4	3.455	3.320	0.134	0.392	3.062	148.364
5	4.137	4.052	0.085	0.117	4.020	368.594
6	4.328	4.230	0.097	0.195	4.133	422.452

[a]Considered as outliers.

activity and also such substituents might form the hydrogen bonds. A molecular docking study showed that the galloyl group forms hydrogen bonds with Leu141, Gly143, Ser144, and His163 at the enzyme active site.

$$pIC_{50} = 2.859\,(\pm0.339) + 0.004\,(\pm0.001)\,PSA \qquad (11.23)$$

$N = 5$, $R = 0.880$, $R^2 = 0.774$, $R_A^2 = 0.699$, $F\,(1,\,3) = 10.292$, $P < 0.04903$, SEE = 0.233, $q^2 = 0.556$, $Q = 3.777$, Outlier = Compound **1**

Compounds without any B ring (Compounds **3** and **4**) are less active. Compound **1** with no 2, 3 double bond in the C ring is less active than the compound **2** though possessing the higher PSA. Compound **1** was found to act as an outlier. It was also observed that the rigid aryl substitution with the hydroxyl group (Compound **6**) was better than the flexible cycloalkyl substitution with the hydroxyl group (Compound **5**).

7.1.24 Dipeptidyl Aldehydes and α-Keto Amides as Promising SARS-CoV 3CL^pro Inhibitors

Mandadapu et al. (2013b) reported some dipeptidyl aldehydes and α-keto amides as potent norovirus 3CL^pro inhibitors (Table 11.25). The QSAR model obtained for these compounds was as shown by Eq. (11.24) that again exhibited that the hydrophobicity of the compounds may be beneficial to SARS-CoV 3CL^pro inhibitory activity of the compounds. Compounds with cyclohexylmethyl group appeared to be more potent than other compounds. This might be due to the bulkiness of this group providing the higher C log P value and due to its better fitting in the active site of the enzyme. Compounds **1** and **7,** however, showed aberrant behaviors and thus were considered as outliers.

$$pIC_{50} = 4.890\,(\pm0.129) + 0.553\,(\pm0.085)\,C\log P \qquad (11.24)$$

$N = 8$, $R = 0.936$, $R^2 = 0.876$, $R_A^2 = 0.855$, $F\,(1,\,6) = 42.329$, $P < 0.00063$, SEE = 0.164, $q^2 = 0.781$, $Q = 5.707$, Outlier = Compounds **1**, **7**

7.1.25 A Series of Dipeptide-Type SARS CoV 3CL^pro Inhibitors

Thanigaimalai et al. (2013a) reported a series of dipeptide-type SARS-CoV 3CL^pro inhibitors (Table 11.26), for which the QSAR model obtained was as shown by Eq. (11.25).

$$pK_i = -67.682\,(\pm\,23.859) - 0.082\,(\pm0.014)\,SA + 0.145\,(\pm0.034)\,Vol \\ -\,0.00001\,(\pm0.000)\,Vol^2 \qquad (11.25)$$

$N = 17$, $R = 0.865$, $R^2 = 0.749$, $R_A^2 = 0.691$, $F\,(3,\,13) = 12.899$, $P < 0.00034$, SEE = 0.557, $q^2 = 0.548$, $Q = 1.553$, $Vol_{opt} = 7250$, Outlier = Compound **14**

TABLE 11.25 Biological Activity and Physicochemical Parameters of Dipeptidyl Aldehydes and α-Keto Amides as Promising SARS-CoV 3CL^{pro} Inhibitors for QSAR Model [Eq. (11.24)]
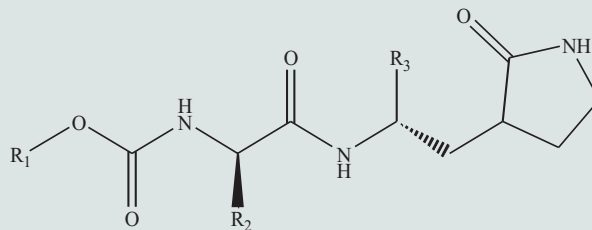
Compound	R$_1$	R$_2$	R$_3$	Obsd	Calcd	Res	Del res	Pred	C Log P
1[a]	Benzyl	i-But	CHO	6.222	5.632	0.590	0.666	5.556	1.075
2	Benzyl	n-Pr	CHO	5.215	5.435	−0.221	−0.278	5.493	0.676
3	Benzyl	i-But	CHO	5.347	5.696	−0.349	−0.389	5.736	1.205
4	Benzyl	(c-Hex)methyl	CHO	6.301	6.220	0.081	0.122	6.179	2.268
5	Benzyl	Benzyl	CHO	5.292	5.613	−0.320	−0.364	5.657	1.036
6	4-FBenzyl	i-But	CHO	5.745	5.703	0.042	0.047	5.698	1.218
7[a]	m-FBenzyl	i-But	CHO	6.155	5.703	0.452	0.504	5.651	1.218
8	2-Phenethyl	i-But	CHO	5.721	5.826	−0.105	−0.117	5.838	1.468
9	(2-c-Hex)ethyl	i-But	CHO	6.222	6.359	−0.137	-0.274	6.496	2.550
10	Benzyl	i-But	C(OH)(SO$_3$Na) CONHc-Pr	5.276	5.309	−0.033	−0.047	5.323	0.419

[a]Considered as outliers.

TABLE 11.26 Biological Activity and Physicochemical Parameters of a Series of Dipeptide-Type SARS CoV 3CL^pro Inhibitors for QSAR Model [Eq. (11.25)]
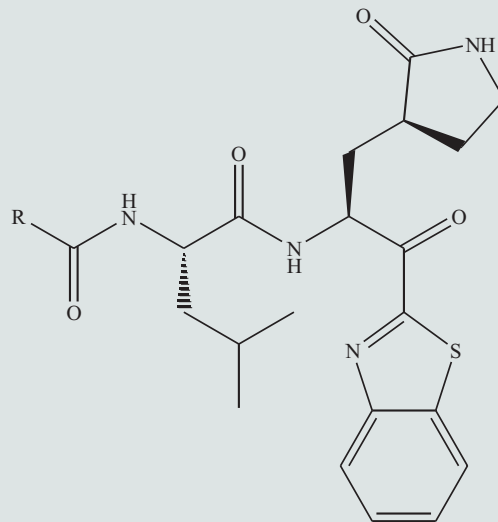
Compound	R	Obsd	Calcd	Res	Del res	Pred	SA	Vol
1	5-Oxo-pyrrolidin-2-yl	5.569	5.978	−0.410	−0.712	6.280	729.379	1329.150
2	2-Pyrrolyl	5.770	5.306	0.464	1.066	4.704	727.381	1313.560

3	2-Indolyl	7.187	7.437	−0.250	−0.294	7.481	795.312	1463.480
4	5-OMe-Indole-2-yl	7.174	6.483	0.691	0.761	6.413	840.460	1523.020
5	5-OH-Indole-2-yl	6.796	7.262	−0.466	−0.524	7.320	810.363	1486.140
6	5-Cl-Indole-2-yl	7.553	7.276	0.277	0.310	7.243	818.124	1500.870
7	6-OMe-Indole-2-yl	6.481	6.843	−0.362	−0.392	6.874	836.137	1524.160
8	4-OMe-Indole-2-yl	8.201	7.584	0.616	0.718	7.482	834.821	1541.680
9	4-O-i-Pr-Indole-2-yl	7.319	7.720	−0.402	−0.535	7.853	865.057	1612.100
10	4-O-i-But-Indole-2-yl	7.523	7.143	0.380	0.914	6.608	901.604	1687.260
11	4-OH-Indole-2-yl	7.585	7.337	0.248	0.284	7.302	804.247	1476.920
12	3-Me,5-OMe- Indole-2-yl	5.174	5.199	−0.025	−0.040	5.213	894.897	1601.640
13	3-Et,5-OMe- Indole-2-yl	5.125	5.626	−0.501	-0.818	5.943	913.184	1661.880
14[a]	Benzimidazole-2-yl	7.658	6.210	1.447	1.648	6.010	832.069	1499.850
15	Benzthiazole-2-yl	6.097	6.343	−0.246	−0.275	6.372	830.805	1500.860
16	2,3-dihydroindole-2-yl	6.921	6.510	0.410	0.451	6.470	842.313	1527.410
17	Benzofuran-2-yl	4.854	5.812	−0.958	−1.187	6.041	834.923	1495.060
18	Indole-3-yl	6.167	7.082	−0.915	−1.012	7.180	811.144	1483.120

[a]Considered as outlier.

It was suggested from Eq. (11.25) that decreasing value of the SA may be conducive to the enzyme inhibition. However, the volume of the molecules was found to exhibit a parabolic relation with the enzyme inhibitory activity. It, therefore, suggested that increase in volume may be responsible for enhancing the activity only up to an optimum value of 7250. Beyond this value, the activity would decrease. Thus it indicated that molecules with limited bulk or with substituents with limited bulk might be favorable to the activity. Thus indole derivatives with less bulky substitution (Compounds **3–11**, Table 11.26) resulted in higher activity than those with a greater bulk (Compounds **12, 13**). Compared to the indole analogs, the oxopyrrolidine (Compound **1**), the pyrrole (Compound **2**), the benzothiazole (Compound **15**), and the benzofuran (Compound **17**) analogs were comparatively less active. However, it could not be explained by the model why benzimidazole analog (Compound **14**) had higher activity as compared to the benzothiazole (Compound **15**) and benzofuran analogs (Compound **17**). Probably, this compound may behave differently as compared to the other compounds in the dataset. Therefore, this compound is considered as an outlier.

7.1.26 A Series of Novel Dipeptide-Type SARS-CoV 3CL ^{pro} Inhibitors

In the subsequent study, Thanigaimalai et al. (2013b) reported a series of dipeptide-type SARS-CoV 3CL protease inhibitors (Table 11.27) whose activity was shown to be controlled by the molar refractivity (CMR) and the polar volume (Pol Vol) of the compounds [Eq. (11.26)]. Since the correlation was quadratic with respect to both CMR and Pol Vol, it suggested that compounds with limited bulk and polarity may have a better binding affinity. Several compounds, however, were treated as outliers.

$$pK_i = -177.032\,(\pm 33.763) + 18.238\,(\pm 3.699)\,CMR - 0.598\,(\pm 0.124)\,CMR^2$$
$$+0.334\,(\pm 0.077)\,Pol\,Vol - 0.001\,(\pm 0.000)\,Pol\,Vol^2 \qquad (11.26)$$

$N = 19$, $R = 0.874$, $R^2 = 0.764$, $R_A^2 = 0.697$, $F\,(4,\,14) = 11.331$, $P < 0.00026$, SEE = 0.275, $q^2 = 0.577$, $Q = 3.178$, $CMR_{Opt} = 15.249$, Pol Vol$_{opt}$ = 167, Outlier = Compounds **1, 6, 7, 15, 21, 24, 25**

7.1.27 A Series of N-(Benzo [1,2,3]Triazol-1-yl)-N-(Benzyl) Acetamido) Phenyl) Carboxamides as SARS-CoV 3CL^{pro} Inhibitors

Turlington et al. (2013) reported a series of *N*-(benzo [1,2,3]triazol-1-yl)-*N*-(benzyl)acetamido) phenyl) carboxamides as promising SARS-CoV 3CL^{pro} inhibitors (Table 11.28). The QSAR model obtained for these compounds [Eq. (11.27)] suggested that highly hydrophobic ($C \log P > 4.1$) molecule with high molar refractivity but the less MW will be conducive to the activity. With the

TABLE 11.27 Biological Activity and Physicochemical Parameters of a Series of Novel Dipeptide-Type SARS-CoV 3CL [pro] Inhibitors for QSAR Model [Eq. (11.26)]
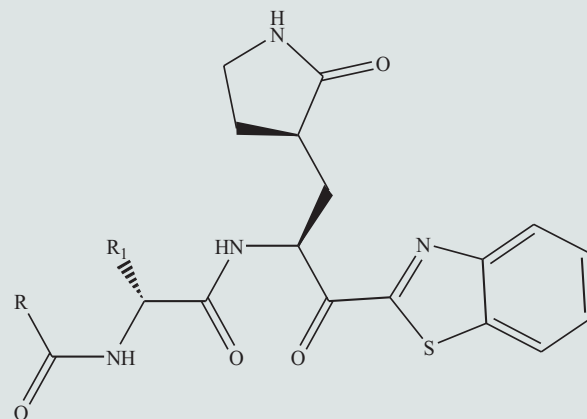
Compound	R	R_1	Obsd	Calcd	Res	Del res	Pred	CMR	Pol Vol
1[a]	i-But	i-But	5.229	4.658	0.571	1.189	4.040	13.395	246.218
2	O-t-But	i-But	4.638	4.998	−0.359	−0.645	5.284	13.548	277.670
3	OBnz	i-But	6.337	5.834	0.503	0.559	5.778	14.667	249.660
4	OBnz	n-But	5.796	5.921	−0.125	−0.147	5.943	14.667	283.458
5	OBnz	i-Pr	5.767	5.501	0.266	0.308	5.459	14.204	242.641
6[b]	OBnz	Sec-But	4.538	5.851	−1.313	−1.454	5.992	14.667	251.687
7[a]	OBnz	$(CH_2)_2SMe$	5.027	5.035	−0.008	−0.058	5.085	15.010	348.627

(*Continued*)

TABLE 11.27 Biological Activity and Physicochemical Parameters of a Series of Novel Dipeptide-Type SARS-CoV 3CL ^{pro} Inhibitors for QSAR Model [Eq. (11.26)] (*cont.*)

Compound	R	R_1	Obsd	Calcd	Res	Del res	Pred	CMR	Pol Vol
8	OBnz	Bnz	5.921	5.826	0.095	0.104	5.817	15.787	260.830
9	Bnz	i-But	5.495	5.688	−0.193	−0.223	5.717	14.514	241.735
10	4-OMe-Bnz	i-But	6.377	6.019	0.358	0.397	5.980	15.131	266.950
11	4-OMe-Phenethyl	i-But	6.215	5.928	0.287	0.312	5.903	15.595	282.725
12	3-Pyridylethyl	i-But	5.131	5.657	−0.527	−0.726	5.857	14.767	231.621
13	PhCH=CH	i-But	6.161	5.743	0.418	0.575	5.587	15.257	234.084
14	4-OMe-PhCH=CH	i-But	6.155	5.774	0.380	0.418	5.737	15.874	260.311
15[a]	3,4-diOMe-PhCH=CH	i-But	5.886	5.205	0.681	0.951	4.935	16.491	294.794
16	Phenoxymethyl	i-But	6.252	5.930	0.322	0.364	5.888	14.667	267.498
17	4-OMe-Phenoxymethyl	i-But	5.807	5.881	−0.074	−0.084	5.891	15.284	301.759
18	4-OH-Phenoxymethyl	i-But	5.076	5.790	−0.715	−0.853	5.929	14.821	307.175
19	3-NMe$_2$-Phenoxymethyl	i-But	6.076	5.739	0.337	0.366	5.709	15.964	281.487
20	4-OMe-PhNHCH$_2$	i-But	5.495	5.822	−0.327	−0.365	5.859	15.500	303.153
21[a]	3-OMe-PhNHCH$_2$	i-But	6.409	5.779	0.630	0.708	5.701	15.500	307.108
22	2-OMe-PhNHCH$_2$	i-But	6.481	5.918	0.564	0.621	5.860	15.500	291.600
23	OBnz	i-But	6.180	5.874	0.307	0.330	5.850	15.745	269.597
24[a]	OBnz	i-But	4.432	5.560	−1.128	−1.299	5.731	16.209	275.135
25[a]	OBnz	i-But	4.284	5.416	−1.132	−1.405	5.689	16.362	276.355
26	OBnz	i-But	5.602	5.417	0.185	0.230	5.372	16.362	274.643

[a]Considered as outlier.

TABLE 11.28 Biological Activity and Physicochemical Parameters of a Series of *N*-(benzo[1,2,3]triazol-1-yl)-*N*-(benzyl) acetamido) phenyl) carboxamides as SARS-CoV 3CL^{pro} Inhibitors for QSAR Model [Eq. (11.27)]
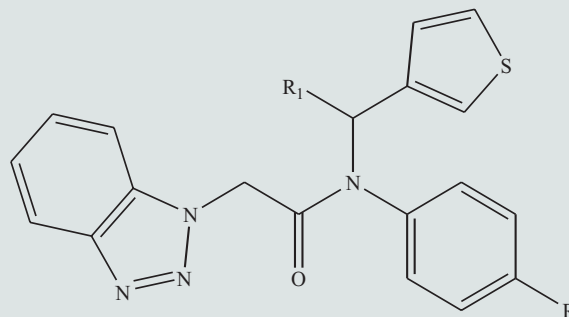
Compound	R	R$_1$	Obsd	Calcd	Res	Del res	Pred	C Log P	CMR	MW
1	NHCOMe	CONH-*t*-But	5.112	5.374	−0.262	−0.326	5.439	3.135	14.067	504.604
2	NHSO$_2$Me	CONH-*t*-But	4.597	4.665	−0.068	−0.117	4.714	2.925	14.440	540.658
3	NHCOEt	CONH-*t*-But	5.161	5.034	0.127	0.142	5.019	3.664	14.530	518.630
4	NHCO-*i*-Pr	CONH-*t*-But	5.387	5.030	0.357	0.421	4.966	3.973	14.994	532.657
5[a]	NHCO-*t*-But	CONH-*t*-But	4.648	5.151	−0.504	−0.641	5.289	4.372	15.458	546.684
6	NHCO-*c*-Pr	CONH-*t*-But	5.041	4.993	0.048	0.055	4.986	3.719	14.857	530.641
7	NHCO-*c*-But	CONH-*t*-But	5.420	4.943	0.477	0.575	4.845	4.048	15.281	544.668
8	NHCO-5-(Isoxazole)	CONH-*t*-But	4.585	4.440	0.145	0.190	4.395	3.410	15.117	557.624
9	NHCOEt	H	5.538	5.400	0.138	0.163	5.374	3.267	11.807	419.499

(*Continued*)

TABLE 11.28 Biological Activity and Physicochemical Parameters of a Series of *N*-(benzo[1,2,3]triazol-1-yl)-*N*-(benzyl) acetamido) phenyl) carboxamides as SARS-CoV 3CL^{pro} Inhibitors for QSAR Model [Eq. (11.27)] (*cont.*)

Compound	R	R$_1$	Obsd	Calcd	Res	Del res	Pred	C Log P	CMR	MW
10	NHCO-*i*-Pr	H	5.444	5.256	0.188	0.212	5.231	3.576	12.271	433.526
11	NHCO-*t*-But	H	4.876	5.198	−0.322	−0.364	5.240	3.975	12.735	447.553
12	NHCO(CH$_2$)$_2$OMe	H	5.469	5.563	−0.094	−0.133	5.602	2.862	12.424	449.525
13	NHCO-*c*-Pr	H	5.387	5.334	0.053	0.061	5.326	3.322	12.133	431.510
14	NHCO-*c*-But	H	5.092	5.136	−0.044	−0.050	5.141	3.651	12.557	445.537
15[a]	NHCO-*c*-Hex	H	4.656	5.432	−0.776	−0.857	5.512	4.769	13.485	473.590
16	NHCOO-*i*-but	H	4.987	4.862	0.125	0.179	4.808	4.645	12.888	463.552
17	NHMe	H	5.678	5.770	−0.093	−0.131	5.809	3.218	10.844	377.463
18	NHBnz	H	5.824	6.029	−0.205	−0.277	6.101	4.666	13.355	453.559
19	Ph	H	7.292	7.037	0.255	0.595	6.697	5.607	12.522	424.517
20	3-Pyridyl	H	6.013	5.549	0.465	0.527	5.486	4.672	12.680	440.520
21	2-OMe-3-Pyridyl	H	6.155	6.115	0.040	0.066	6.089	5.520	13.297	470.546
22	4-Pyridyl	H	5.699	5.549	0.150	0.171	5.528	4.672	12.680	440.520
23	2-OMe-Pyrimidin-5-yl	H	4.903	5.104	−0.201	−0.296	5.199	5.011	13.086	471.534

[a]Considered as outlier.

adjustment of such parameters, compounds **19–22** of Table 11.28 were found to have higher activity.

$$pIC_{50} = 12.976\,(\pm1.456) - 4.268\,(\pm0.773)\text{CLogP} + 0.520\,(\pm0.089)\,C\,\text{Log}\,P^2$$
$$+1.681\,(\pm0.279)\text{CMR} - 0.045\,(\pm0.007)\text{MW} \tag{11.27}$$

$N = 21$, $R = 0.941$, $R^2 = 0.885$, $R_A^2 = 0.857$, $F\,(4,\,16) = 30.898$, $P < 0.00000$, SEE $= 0.228$, $q^2 = 0.799$, $Q = 4.127$, $C\,\log P_{\text{Opt}} = 4.104$, Outlier $=$ Compounds **5**, **15**

7.1.28   Tripeptidyl Transition State Norwalk Virus 3C-Like Protease Inhibitors

A QSAR model obtained [Eq. (11.28)] for some tripeptidyl transition state Norwalk virus 3C-like protease inhibitors (Table 11.29) reported by Prior et al. (2013) suggested that the PSA of the molecules will control their activity and that a –CHO group at their X-position, for which an indicator parameter "I" was used, will have an added advantage. While the PSA may affect the activity due to a polar interaction of the molecule, the –CHO group might be involved in some hydrogen bond interactions with some residue of the active site.

$$pIC_{50} = 1.825\,(\pm0.582) + 0.023\,(\pm0.003)\text{PSA} + 1.614\,(\pm0.189)\,I \tag{11.28}$$

$N = 8$, $R = 0.972$, $R^2 = 0.944$, $R_A^2 = 0.921$, $F\,(2,\,5) = 42.078$, $P < 0.00074$, SEE $= 0.236$, $q^2 = 0.742$, $Q = 4.119$

7.1.29   5-Sulfonyl Isatin Derivatives as Promising SARS-CoV 3CL^{pro} Inhibitors

Liu et al. (2014) reported a series of 5-sulfonyl isatin derivatives as potent SARS-CoV 3CL protease inhibitors (Table 11.30), for which the QSAR model was as shown by Eq. (11.29).

$$pIC_{50} = 9.333\,(\pm1.030) + 0.376\,(\pm0.079)\,C\,\text{Log}\,P - 3.002\,(\pm0.537)\,D_{\text{Tot}}$$
$$+0.379\,(\pm0.064)\,D_{\text{Tot}}^2 - 1.047\,(\pm0.244)\,I \tag{11.29}$$

$N = 21$, $R = 0.894$, $R^2 = 0.800$, $R_A^2 = 0.750$, $F\,(4,\,16) = 15.999$, $P < 0.00002$, SEE $= 0.307$, $q^2 = 0.655$, $Q = 2.912$, $D_{\text{Tot (opt)}} = 3.960$, Outlier $=$ Compounds **5**, **8**, **16**, **18**

It was observed from Eq. (11.29) that increasing value of hydrophobicity may be favorable for the activity and that the moderate dipole moment of the compound will also be conducive to the inhibition of the enzyme. However, a negative value of the indicator variable "I", which was used with a value of 1 for compounds having a β-napthylmethyl function at R$_1$-position, indicated

TABLE 11.29 Biological Activity and Physicochemical Parameters of Tripeptidyl Transition State Norwalk Virus 3C-like Protease Inhibitors for QSAR Model [Eq. (11.28)]
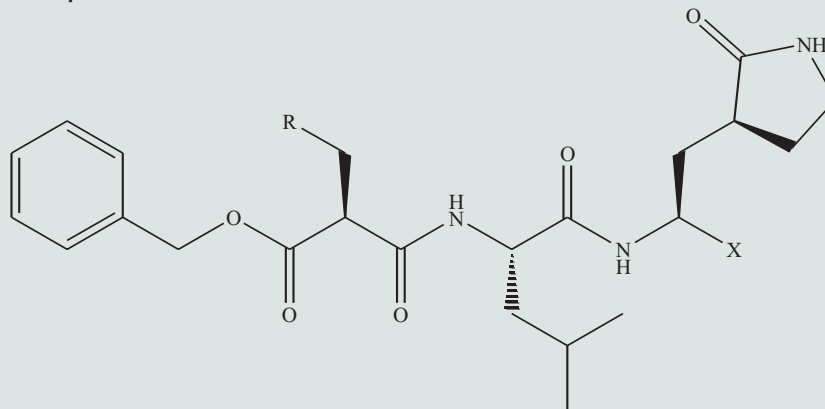
Compound	R	X	Obsd	Calcd	Res	Del res	Pred	PSA	I
1	Ph	CHO	6.678	6.898	−0.220	−0.284	6.962	153.457	1
2	(S)-α-Napthyl	CHO	6.854	6.789	0.065	0.082	6.772	148.629	1
3	(R)-α-Napthyl	CHO	6.155	5.822	0.333	0.647	5.508	105.728	1
4	(S)-β-Napthyl	CHO	6.824	6.898	−0.074	−0.096	6.920	153.477	1
5	(S)-Biph	CHO	6.745	6.848	−0.103	−0.131	6.876	151.233	1
6	(S)-α-Napthyl	COONH-i-Pr	5.585	5.656	−0.071	−0.107	5.692	169.965	0
7	(S)-α-Napthyl	CH(OH)SO₃Na	6.620	6.372	0.248	0.641	5.979	201.709	0
8	(S)-α-Napthyl	CH(OH)P(O)(OEt)₂	4.450	4.627	−0.177	−0.569	5.019	124.302	0

TABLE 11.30 Biological Activity and Physicochemical Parameters of 5-Sulfonyl Isatin Derivatives as Promising SARS-CoV 3CL^{pro} Inhibitors for QSAR Model [Eq. (11.29)]
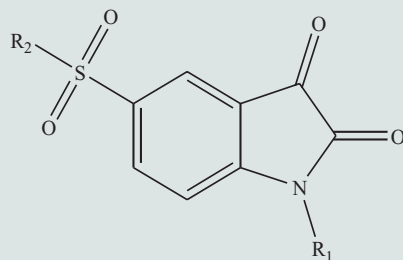
Compound	R$_1$	R$_2$	Obsd	Calcd	Res	Del res	Pred	C Log P	D$_{Tot}$	I
1	H	4-Me-Piperazine	4.115	4.836	−0.721	−0.829	4.944	0.530	5.641	0
2	H	3-ClBnz-Piperazine	4.499	4.860	−0.361	−0.402	4.901	2.252	2.880	0
3	H	3,4,5-triOMeBnz-Piperazine	4.494	4.836	−0.342	−0.380	4.874	1.552	5.150	0
4	H	4-Phenethyl-piperazine	4.457	4.917	−0.460	−0.519	4.976	2.508	2.909	0
5[a]	H	(Furan-2-carbonyl)-piperazine	4.997	5.301	−0.304	−0.982	5.979	0.311	1.277	0
6	H	2-Pyridyl-(4-piperazine)	4.290	4.445	−0.156	−0.182	4.472	1.013	3.230	0
7	H	Piperidine	5.352	5.164	0.187	0.217	5.135	1.216	5.866	0
8[a]	H	Morpholine	4.898	4.519	0.379	0.463	4.435	-0.031	5.346	0
9	H	4-Me-Piperidine	5.928	5.282	0.646	0.752	5.176	1.735	5.839	0
10	H	2-Me-Piperidine	5.648	5.294	0.354	0.413	5.235	1.735	5.857	0

TABLE 11.30 Biological Activity and Physicochemical Parameters of 5-Sulfonyl Isatin Derivatives as Promising SARS-CoV 3CL[pro] Inhibitors for QSAR Model [Eq. (11.29)] *(cont.)*

Compound	R_1	R_2	Obsd	Calcd	Res	Del res	Pred	C Log P	D_{Tot}	I
11	H	3,5-diMe-Piperidine	5.367	5.409	−0.042	−0.051	5.417	2.254	5.827	0
12	Me	4-Me-Piperazine	4.927	4.724	0.203	0.251	4.676	0.585	2.191	0
13	Bnz	4-Me-Piperazine	4.173	4.768	−0.595	−0.690	4.862	2.353	3.395	0
14	β-NapthylCH$_2$	4-Me-Piperazine	4.081	4.758	−0.677	−0.834	4.915	3.527	5.326	1
15	β-NapthylCH$_2$	4-Phenethyl-piperazine	4.858	4.922	−0.064	−0.084	4.942	5.505	3.322	1
16[a]	β-NapthylCH$_2$	2-Pyridyl-(4-piperazine)	5.258	4.520	0.738	0.933	4.325	4.010	3.398	1
17	β-NapthylCH$_2$	Piperidine	4.854	4.929	−0.075	−0.095	4.949	4.213	2.309	1
18[a]	Me	Morpholine	5.004	4.147	0.857	1.167	3.837	0.024	3.492	0
19	Bnz	Morpholine	4.858	4.989	−0.131	−0.145	5.004	1.792	5.334	0
20	β-NapthylCH$_2$	Morpholine	4.399	4.617	−0.218	−0.282	4.681	2.966	5.337	1
21	Bnz	4-Me-Piperazine	5.983	5.392	0.591	0.752	5.231	3.558	2.403	0
22	β-NapthylCH$_2$	4-Me-Piperazine	5.772	5.660	0.112	0.181	5.592	4.732	6.204	1
23	Me	4-Me-Piperazine	4.749	4.900	−0.151	−0.167	4.916	1.790	2.466	0
24	Bnz	3,5-diMe-Piperidine	5.550	5.504	0.046	0.064	5.485	4.077	2.452	0
25	β-NapthylCH$_2$	3,5-diMe-Piperidine	5.328	5.144	0.184	0.234	5.094	5.251	2.424	1

[a]Considered as outlier.

that such a substituent would not be preferred, probably such a substituent might create steric hindrance in the interaction of the compounds with the receptor.

7.1.30 Some Substituted Pyrazoles and Substituted Pyrimidines as SARS-CoV 3CL^{pro} Inhibitors

Mohamed et al. (2015) recently reported some substituted pyrazoles and substituted pyrimidines as promising SARS-CoV 3CL^{pro} inhibitors (Fig. 11.11; Table 11.31). The QSAR model [Eq. (11.30)] obtained for these compounds simply suggested that highly polar fraction of the molecule with the high value of its X-component of dipole moment (D_X) will not be conducive to the activity.

$$pIC_{50} = 6.437\,(\pm 0.052) - 0.162\,(\pm 0.036)\,D_X \qquad (11.30)$$

$N = 8$, $R = 0.881$, $R^2 = 0.776$, $R_A^2 = 0.739$, F (1, 6) = 20.776, $P < 0.00386$, SEE = 0.139, $q^2 = 0.657$, $Q = 6.338$, Outlier = Compounds **1**, **2**, **5**, **12**

7.1.31 Dipeptidyl Norovirus 3CL^{pro} Inhibitors

Galasiti et al. (2015) recently reported a series of dipeptidyl norovirus 3CL^{pro} inhibitors having potent inhibitory activity (Table 11.32). The QSAR model obtained for these inhibitors was as shown by Eq. (11.31). This equation simply suggested that while the z-component of the dipole moment will be favorable to the activity, its moderate PSA will have an adverse effect.
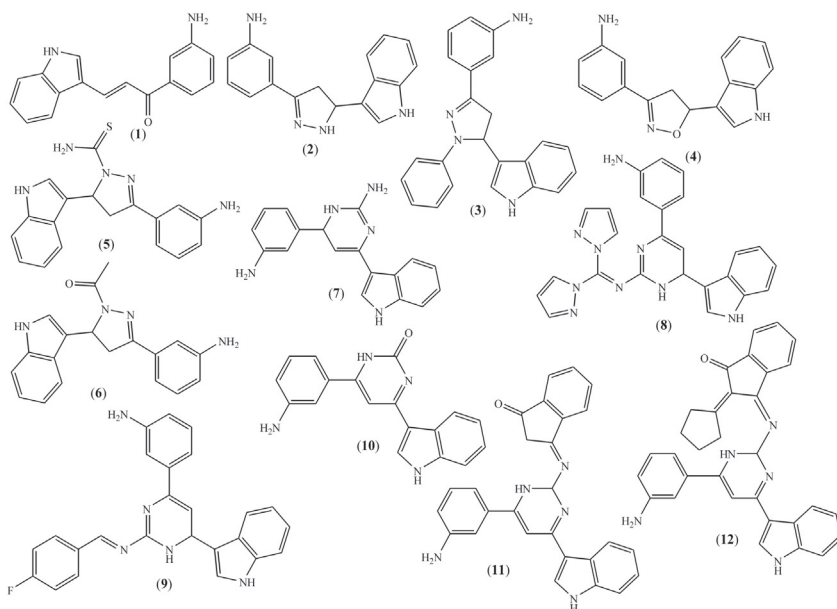

FIGURE 11.11 General structure of substituted pyrazoles and substituted pyrimidines.

TABLE 11.31 Biological Activity and Physicochemical Parameters of Some Substituted Pyrazoles and Substituted Pyrimidines as SARS-CoV 3CL^pro Inhibitors (Fig. 11.8) for QSAR Model [Eq. (11.30)]

Compound	Obsd	Calcd	Res	Del res	Pred	D_X
1[a]	6.009	6.357	−0.348	−0.382	6.391	0.582
2[a]	6.745	6.320	0.425	0.475	6.269	0.928
3	6.229	6.232	−0.003	−0.004	6.233	1.757
4	6.155	6.344	−0.189	−0.208	6.363	0.704
5[a]	6.161	6.628	−0.467	−0.672	6.833	−1.977
6	6.244	6.365	−0.121	−0.132	6.376	0.504
7	6.420	6.468	−0.048	−0.054	6.474	−0.470
8	6.347	6.383	−0.036	−0.040	6.386	0.333
9	6.018	6.120	−0.103	−0.169	6.187	2.811
10	6.854	6.650	0.203	0.313	6.541	−2.190
11	6.638	6.398	0.240	0.262	6.376	0.189
12[a]	6.921	6.475	0.446	0.501	6.420	−0.533

[a]Considered as outliers.

$$pIC_{50} = 19.197\,(\pm 2.508) + 0.105\,(\pm 0.036)\,D_Z + 0.002\,(\pm 0.001)\,D_Z^2 \\ -0.165\,(\pm 0.032)\,PSA + 0.001\,(\pm 0.000)\,PSA^2 \quad (11.31)$$

$N = 23$, $R = 0.870$, $R^2 = 0.757$, $R_A^2 = 0.703$, $F\,(4, 18) = 14.036$, $P < 0.00002$, SEE = 0.269, $q^2 = 0.636$, $Q = 3.234$, $D_{Zopt} = -26.25$, $PSA_{opt} = 82.5$, Outlier = Compounds **3**, **5**, **14**

7.1.32 Peptidomimetic Bat Coronavirus HKU4 3CL^pro Inhibitors

St. John et al. (2015) reported a series of peptidomimetic bat coronavirus HKU4 3CL^pro inhibitors (Table 11.33), for which the QSAR model obtained [Eq. (11.32)] suggested that molecules should have an optimum lipophilicity value for imparting the higher activity.

$$pIC_{50} = 3.401\,(\pm 0.540) + 1.030\,(\pm 0.290)\,C\,Log\,P - 0.108\,(\pm 0.037)\,C\,Log\,P^2 \\ + 0.074\,(\pm 0.012)\,D_X + 0.014\,(\pm 0.002)\,PSA - 0.009\,(\pm 0.002)\,Pol\,Vol \quad (11.32)$$

$N = 38$, $R = 0.907$, $R^2 = 0.822$, $R_A^2 = 0.795$, $F\,(5, 32) = 29.620$, $P < 0.00000$, SEE = 0.238, $q^2 = 0.745$, $Q = 3.811$, $C\,Log\,P_{opt} = 4.769$, Outlier = Compounds **20–22**, **25**, **35**.

The activity may be further supported by the X-component of the dipole moment and the PSA of the molecule. Notwithstanding, the high polar volume of the molecule will be delirious to the activity.

TABLE 11.32 Biological Activity and Physicochemical Parameters of Dipeptidyl Norovirus 3CL^{pro} Inhibitors for QSAR Model [Eq. (11.31)]
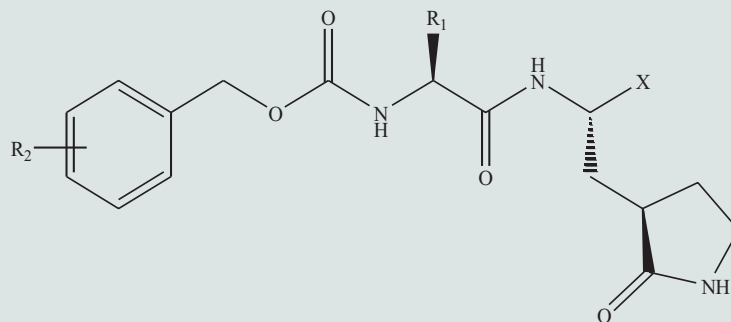
Compound	R$_1$	R$_2$	X	Obsd	Calcd	Res	Del res	Pred	D$_Z$	PSA
1	(c-Hex)CH$_2$	o-Cl	CHO	6.097	6.381	−0.284	−0.326	6.423	−1.786	121.901
2	(c-Hex)CH$_2$	o-Cl	CH(OH)SO$_3$Na	6.155	6.524	−0.369	−0.449	6.604	−64.476	152.366
3[a]	(c-Hex)CH$_2$	m-Cl	CHO	7.000	6.260	0.740	0.834	6.166	−2.721	121.894
4	(c-Hex)CH$_2$	m-Cl	CH(OH)SO$_3$Na	7.000	6.678	0.322	0.401	6.599	−65.412	152.335
5[a]	(c-Hex)CH$_2$	m-Cl	COCONH-c-Pr	6.602	5.767	0.835	1.068	5.534	−1.938	184.498
6	c-Hex	m-Cl	CHO	5.292	5.547	−0.255	−0.289	5.582	−2.687	144.957
7	i-Butyl	m-Cl	CHO	6.046	5.995	0.050	0.061	5.985	0.903	147.129
8	i-Butyl	m-Cl	COCONH-c-Pr	5.260	5.496	−0.237	−0.275	5.534	−2.592	148.775
9	(c-Hex)CH$_2$	p-Cl	CHO	6.149	6.122	0.027	0.030	6.119	−3.833	121.895

(Continued)

TABLE 11.32 Biological Activity and Physicochemical Parameters of Dipeptidyl Norovirus 3CL^{pro} Inhibitors for QSAR Model [Eq. (11.31)] (*cont.*)

Compound	R$_1$	R$_2$	X	Obsd	Calcd	Res	Del res	Pred	D$_Z$	PSA
10	(*c*-Hex)CH$_2$	*o*-F	CHO	6.046	6.474	−0.428	−0.509	6.554	−1.085	121.894
11	(*c*-Hex)CH$_2$	*m*-F	CHO	5.921	6.277	−0.356	−0.402	6.323	−2.592	121.894
12	(*c*-Hex)CH$_2$	*m*-F	COCONH-*c*-Pr	5.456	5.635	−0.179	−0.198	5.654	−2.663	140.867
13	(*c*-Hex)CH$_2$	*m*-Br	CHO	6.523	6.258	0.265	0.299	6.224	−2.739	121.893
14^a	(*c*-Hex)CH$_2$	*m*-Br	CH(OH)P(O)(OEt)$_2$	5.187	5.648	−0.461	−0.556	5.743	−5.135	130.026
15	(*c*-Hex)CH$_2$	*m*-Br	CH(OH)SO$_3$Na	6.824	6.681	0.143	0.178	6.646	−65.428	152.344
16	(*c*-Hex)CH$_2$	*m*-Br	COCONH-*c*-Pr	5.824	5.616	0.208	0.231	5.592	−2.809	140.890
17	(*c*-Hex)CH$_2$	*m*-I	CHO	6.456	6.258	0.198	0.223	6.233	−2.740	121.891
18	(*c*-Hex)CH$_2$	*m*-I	CH(OH)SO$_3$Na	6.824	6.681	0.143	0.178	6.645	−65.428	152.355
19	(*c*-Hex)CH$_2$	*m*-OMe	CHO	5.854	5.560	0.294	0.343	5.511	−4.235	136.191
20	(*c*-Hex)CH$_2$	*m*-NHBoc	CHO	5.347	5.720	−0.373	−0.457	5.803	−0.205	161.925
21	(*c*-Hex)CH$_2$	*m*-NO$_2$	CHO	6.222	6.569	−0.347	−1.243	7.465	−4.328	212.100
22	*i*-Butyl	H	CHO	6.222	6.125	0.097	0.129	6.093	1.790	147.121
23	*i*-Butyl	H	CH(OH)SO$_3$Na	6.097	6.023	0.073	0.190	5.907	−55.699	199.888
24	*i*-Butyl	H	COCONH-*c*-Pr	5.469	5.552	−0.083	−0.095	5.564	−2.016	150.177
25	(*c*-Hex)CH$_2$	H	CHO	6.523	6.245	0.278	0.314	6.209	−2.848	121.888
26	(*c*-Hex)CH$_2$	H	CH(OH)SO$_3$Na	6.398	6.698	−0.300	−0.376	6.774	−65.535	152.353

^{a}Considered as outliers.

TABLE 11.33 Biological Activity and Physicochemical Parameters of Peptidomimetic Bat Coronavirus HKU4 3CL^{pro} Inhibitors for QSAR Model [Eq. (11.32)]
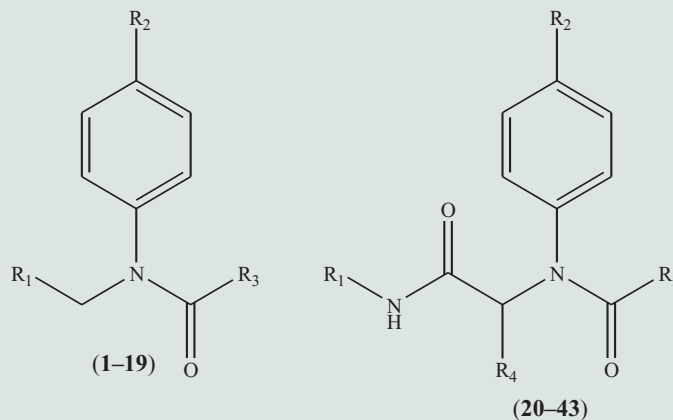
Compound	R$_1$	R$_2$	R$_3$	R$_4$	Obsd	Calcd	Res	Del res	Pred	C Log P	D$_X$	PSA	Pol Vol
1	3-Thienyl	NHCO-(3-thienyl)	(2-Benzotriazolyl)methyl	—	6.481	6.327	0.154	0.195	6.286	4.065	6.553	237.419	302.836
2	3-Thienyl	NHCOPh	(2-Benzotriazolyl)methyl	—	6.387	5.987	0.400	0.451	5.936	4.227	6.409	194.671	291.571
3	3-Thienyl	NHCO-c-but	(2-Benzotriazolyl)methyl	—	5.921	5.657	0.264	0.280	5.641	3.651	3.217	187.416	288.775
4	3-Thienyl	NHCO-c-Pent	(2-Benzotriazolyl)methyl	—	5.921	6.005	−0.084	−0.097	6.018	4.769	6.487	179.306	266.098
5	3-Thienyl	4-Pyr	(2-Benzotriazolyl)methyl	—	5.824	5.854	−0.030	−0.034	5.857	3.474	4.957	220.355	317.406
6	3-Thienyl	NHCO-i-Pr	(2-Benzotriazolyl)methyl	—	5.796	5.580	0.216	0.232	5.564	3.576	−1.272	184.840	252.498

(Continued)

TABLE 11.33 Biological Activity and Physicochemical Parameters of Peptidomimetic Bat Coronavirus HKU4 3CL[pro] Inhibitors for QSAR Model [Eq. (11.32)] (*cont.*)

Compound	R_1	R_2	R_3	R_4	Obsd	Calcd	Res	Del res	Pred	C Log P	D_X	PSA	Pol Vol
7	3-Thienyl	(2-OMe-Pyr)-3-yl	(2-Benzotriazolyl)methyl	—	5.770	6.032	−0.263	−0.303	6.073	4.210	7.061	211.031	316.028
8	3-Thienyl	NHCO-c-Pr	(2-Benzotriazolyl)methyl	—	5.721	5.432	0.289	0.304	5.417	3.322	−1.281	191.518	274.817
9	3-Thienyl	(2-OMe-Pyr)-5-yl	(2-Benzotriazolyl)methyl	—	5.699	5.698	0.001	0.001	5.698	3.624	4.380	233.228	364.577
10	3-Thienyl	NHCOCF₃	(2-Benzotriazolyl)methyl	—	5.658	5.718	−0.060	−0.077	5.734	3.847	−3.437	195.593	237.299
11	3-Thienyl	3-Pyr	(2-Benzotriazolyl)methyl	—	5.620	5.885	-0.265	−0.298	5.918	3.474	5.735	220.889	320.479
12	3-Thienyl	NHCOO-i-butyl	(2-Benzotriazolyl)methyl	—	5.553	5.581	-0.028	−0.032	5.585	4.645	−2.550	186.127	263.229
13	3-Thienyl	NHCOEt	(2-Benzotriazolyl)methyl	—	5.509	5.467	0.041	0.044	5.465	3.267	−1.330	185.781	256.440
14	3-Thienyl	NHCOCH₂OMe	(2-Benzotriazolyl)methyl	—	5.509	5.151	0.358	0.412	5.097	2.532	−0.411	207.442	297.225
15	3-Thienyl	NHCO(CH₂)₂OMe	(2-Benzotriazolyl)methyl	—	5.432	5.243	0.189	0.206	5.226	2.862	−2.343	196.610	274.182
16	3-Thienyl	NHMe	(2-Benzotriazolyl)methyl	—	5.319	5.329	−0.011	−0.011	5.330	3.218	−2.694	156.296	216.523
17	3-Thienyl	NHCH₂Ph	(2-Benzotriazolyl)methyl	—	5.276	5.440	−0.165	−0.181	5.457	4.666	−2.698	155.649	236.128
18	3-Thienyl	NHCO-t-butyl	(2-Benzotriazolyl)methyl	—	5.056	5.180	−0.124	−0.135	5.190	3.975	−3.963	155.121	259.023
19	3-Thienyl	NHCO-i-Pr	(1,2,3-Triazole)1-yl	—	4.796	4.709	0.087	0.130	4.666	1.982	−1.272	165.375	238.400
20[a]	t-Butyl	t-Butyl	(1-Me-imidazole)-4-yl	3-Pyr	5.886	4.965	0.921	1.120	4.766	3.604	−0.676	71.113	178.314
21[a]	Benzyl	NHCO-i-Pr	(2-Benzotriazolyl)methyl	3-FPh	5.824	5.112	0.712	0.818	5.006	5.114	−3.858	123.131	220.187
22[a]	t-Butyl	NHCOMe	(2-Benzotriazolyl)methyl	3-Thienyl	5.745	4.926	0.819	0.913	4.832	3.135	−4.596	175.901	290.678
23	t-Butyl	2-CNPh	2-Furyl	3-Pyr	5.658	5.407	0.251	0.281	5.377	4.147	−1.284	93.556	152.746

| 24	t-Butyl	t-Butyl	(2-Indolyl)methyl	3-Pyr	5.658	5.256	0.402	0.488	5.169	5.466	−0.015	67.832	132.826
25[a]	t-Butyl	NHCO-c-Pr	(2-Benzotriazolyl)methyl	3-Thienyl	5.569	5.142	0.427	0.486	5.082	3.719	−1.920	189.368	330.556
26	Benzyl	NHCO-c-butyl	(2-Benzotriazolyl)methyl	3-FPh	5.469	5.463	0.005	0.007	5.461	5.189	6.476	138.478	281.050
27	t-Butyl	OCH$_2$F	(2-Indolyl)methyl	3-Pyr	5.409	5.452	−0.043	−0.050	5.459	3.732	0.712	84.008	137.546
28	t-Butyl	NHCOPh	(2-Benzotriazolyl)methyl	3-Thienyl	5.377	5.268	0.108	0.138	5.239	4.624	2.529	170.484	336.095
29	t-Butyl	i-Pr	(2-Benzotriazolyl)methyl	3-Pyr	5.161	5.406	−0.245	−0.286	5.447	5.067	−0.043	67.838	120.946
30	Benzyl	NHCO-c-Pr	(2-Benzotriazolyl)methyl	3-FPh	5.155	5.449	−0.294	−0.318	5.473	4.860	−1.115	156.448	248.714
31	t-Butyl	t-butyl	(2-Oxazo-5-yl)methyl	3-Pyr	5.066	5.048	0.018	0.020	5.045	3.155	−0.616	83.224	161.469
32	t-Butyl	t-butyl	(2-Imidazo-4-yl)methyl	3-Pyr	5.032	5.386	−0.354	−0.393	5.424	3.305	1.332	110.996	177.477
33	t-Butyl	Me	2-Furyl	3-Pyr	5.022	5.203	−0.181	−0.227	5.249	3.949	0.627	47.293	125.546
34	t-Butyl	t-Butyl	(2-Imidazo-4-yl)methyl	3-Pyr	4.955	5.192	−0.238	−0.262	5.217	3.305	−1.670	99.248	162.438
35[a]	t-Butyl	NHCO(2-benzotria)	(2-Benzotriazolyl)methyl	3-Thienyl	4.833	5.512	−0.680	−0.751	5.584	3.410	1.015	237.356	360.408
36	t-Butyl	t-Butyl	(2-Imidazo-4-yl)methyl	2-Pyrim-5-yl	4.812	4.817	−0.004	−0.005	4.817	2.348	−2.326	122.867	182.158
37	t-Butyl	NHCO-i-Pr	(2-Benzotriazolyl)methyl	3-Thienyl	4.764	5.072	−0.307	−0.345	5.110	3.973	−4.585	159.577	277.847
38	t-Butyl	NHCOEt	(2-Benzotriazolyl)methyl	3-Thienyl	4.738	5.013	−0.276	−0.310	5.048	3.664	−4.603	165.613	286.848
39	t-Butyl	NHCOMe	(2-Benzotriazolyl)methyl	3-FPh	4.728	5.072	−0.344	−0.371	5.099	3.632	−3.646	123.951	218.588
40	t-Butyl	NH$_2$	(2-Benzotriazolyl)methyl	3-Thienyl	4.658	5.036	−0.379	−0.417	5.075	2.889	−3.545	194.693	295.576
41	t-Butyl	t-butyl	2-Furyl	3-Pyr	4.449	4.699	−0.251	−0.524	4.972	6.149	−1.580	35.972	119.956
42	t-Butyl	NHCO-i-Pr	(2-Benzimidazolyl)methyl	3-Thienyl	4.281	4.940	−0.658	−0.770	5.052	4.161	−3.325	125.993	261.488
43	t-Butyl	t-Butyl	(2-Oxazo-5-yl)methyl	2-Pyrim-5-yl	4.255	4.634	−0.379	−0.497	4.752	2.198	−1.272	106.846	180.953

[a]Considered as outliers.

7.1.33 Substituted Furan Analogs as Promising SARS CoV 3C^pro Inhibitors

Kumar et al. (2016) recently reported a series of substituted furan analogs as promising SARS-CoV 3C^pro inhibitors (Table 11.34). The QSAR model obtained for these compounds was as shown by Eq. (11.33)

$$pIC_{50} = 4.555\,(\pm 0.067) + 0.522\,(\pm 0.141)\,I_1 + 0.597\,(\pm 0.141)\,I_2 \qquad (11.33)$$

$N = 11$, $R = 0.874$, $R^2 = 0.763$, $R_A^2 = 0.704$, $F\,(2, 8) = 12.907$, $P < 0.00313$, SEE $= 0.176$, $q^2 = 0.536$, $Q = 4.966$, Outlier = Compound **6.**

TABLE 11.34 Biological Activity and Physicochemical Parameters of Substituted Furan Analogs as Promising SARS CoV 3C^pro Inhibitors for QSAR Model [Eq. (11.33)]
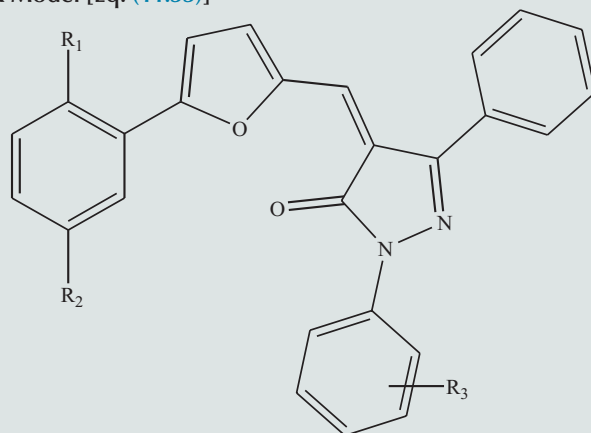
Compound	R_1	R_2	R_3	Obsd	Calcd	Res	Del res	Pred	I_1	I_2
1	COOH	Cl	3-COOH	4.350	4.634	−0.285	−0.325	4.675	0	0
2	COOH	Cl	H	4.785	4.634	0.151	0.172	4.613	0	0
3	COOH	Cl	4-F	4.695	4.634	0.060	0.069	4.626	0	0
4	COOH	Cl	4-i-Pr	5.222	5.077	0.145	0.290	4.932	1	0
5	COOH	Cl	4-t-But	5.237	5.151	0.086	0.171	5.066	0	1
6[a]	H	H	3-COOH	5.194	4.634	0.559	0.639	4.555	0	0
7	COOH	H	H	4.385	4.634	−0.249	−0.285	4.670	0	0
8	COOH	H	4-F	4.426	4.634	−0.208	−0.238	4.664	0	0
9	COOH	H	4-i-Pr	4.932	5.077	−0.145	−0.290	5.222	1	0
10	COOH	H	4-t-But	5.066	5.151	−0.086	−0.171	5.237	0	1
11	COOH	H	4-CN	4.728	4.634	0.094	0.107	4.621	0	0
12	COOH	H	4-OMe	4.513	4.634	−0.122	−0.139	4.652	0	0

[a]Considered as outlier.

Where the activity is shown to be correlated with two indicator variables, I_1 and I_2. I_1 and I_2, with a value of 1 each, indicate the presence of the *i*-propyl and the *t*-butyl moiety at R_3-position, respectively. The positive coefficients of both these parameters suggested that the *i*-propyl and the *t*-butyl functions at R_3-position will be favorable for inhibitory activity. Compound **6** behaved aberrantly and therefore it was considered as an outlier. It may be observed that the *t*-butyl substitution at R_3-position in compounds **5** and **10** gave better activity than the *i*-butyl substitution at the same position in compounds **4** and **9**.

7.2 QSAR Model Development on Human Rhinovirus 3C^{pro} Inhibitors

7.2.1 A Series of Michael Acceptor Type HRV 3C^{pro} Inhibitors

Dragovich et al. (1998a) reported a series of Michael acceptor type potent HRV 3C^{pro} inhibitors (Fig. 11.12; Table 11.35), for which the QSAR model [Eq. (11.34)] exhibited that the positive effect on the activity of the compounds will be produced by the Z-component of the dipole moment and the SA of the compounds till it attains an optimum value. These two properties indicate the same kind of electronic interactions of the molecule with the receptor.

$$pEC_{50} = -56.622(\pm19.902) + 0.423(\pm0.117)D_Z + 0.102(\pm0.021)D_Z^2$$
$$+ 0.134(\pm0.041)SA - 0.0001(\pm0.00002)SA^2 - 0.018(\pm0.004)PolVol$$
(11.34)

$N = 33$, $R = 0.841$, $R^2 = 0.708$, $R_A^2 = 0.654$, $F(5, 27) = 13.087$, $P < 0.00000$, SEE = 0.411, $q^2 = 0.584$, $Q = 2.046$, $D_{Zopt} = -2.074$, $SA_{opt} = 670$, Outlier = Compounds **4**, **9**, **11**, **15**, **16**, **18**, **21**, **23**, **30**, **34**
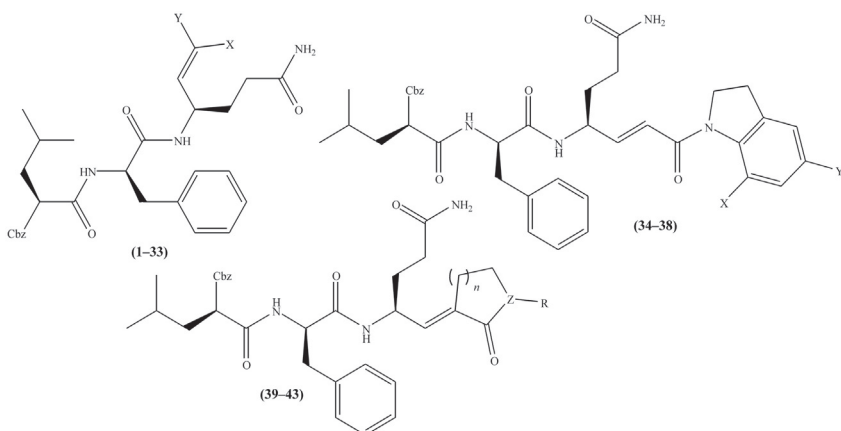

FIGURE 11.12 General structure of Michael acceptor type HRV 3C^{pro} inhibitors.

TABLE 11.35 Biological Activity and Physicochemical Parameters of a Series of Michael Acceptor Type HRV 3C^{pro} Inhibitors (Fig. 11.12) for QSAR Model [Eq. (11.34)]

Compound	X	Y	X	Y	Z	n	R	Obsd	Calcd	Res	Del res	Pred	D_Z	SA	Pol Vol
1	COOMe	H	—	—	—	—	—	5.886	5.268	0.618	0.699	5.187	0.447	892.098	240.514
2	H	COOMe	—	—	—	—	—	5.495	5.269	0.226	0.258	5.237	0.501	889.632	239.189
3	COOEt	H	—	—	—	—	—	6.268	5.819	0.449	0.599	5.668	1.733	919.558	252.873
4	COOEt	Me	—	—	—	—	—	5.523	5.922	−0.399	−0.523	6.046	1.697	925.084	241.339
5[a]	COO-c-Pent	H	—	—	—	—	—	6.252	5.258	0.994	1.075	5.177	−0.640	995.992	259.677
6	COO-c-Hex	H	—	—	—	—	—	5.444	5.322	0.122	0.136	5.308	−0.610	1019.220	240.828
7	COOBnz	H	—	—	—	—	—	5.495	5.206	0.288	0.313	5.182	−0.667	1004.590	263.005
8	COOCH$_2$-t-But	H	—	—	—	—	—	6.301	5.633	0.668	0.757	5.544	0.277	972.403	237.458
9[a]	CONME$_2$	H	—	—	—	—	—	4.252	5.764	−1.512	−1.750	6.002	0.314	932.597	206.888
10	COPyrrolidine	H	—	—	—	—	—	4.658	5.090	−0.432	−0.457	5.114	−2.650	983.638	266.905
11[a]	CON(Me)Ph	H	—	—	—	—	—	3.801	4.981	−1.180	−1.258	5.059	−2.564	1025.570	263.713
12	COTetrahydroquinoline	H	—	—	—	—	—	3.900	4.573	−0.673	−0.749	4.649	−2.685	1058.120	288.062
13	COIndoline	H	—	—	—	—	—	4.796	4.564	0.232	0.255	4.541	−2.671	1048.840	299.918
14	CON(Me)OMe	H	—	—	—	—	—	5.398	5.246	0.152	0.160	5.238	−1.033	944.039	248.567
15	CON(Me)OH	H	—	—	—	—	—	4.377	5.268	−0.892	−0.980	5.357	0.311	915.220	260.579
16	COIsoxazolidine	H	—	—	—	—	—	4.347	5.246	−0.899	−1.000	5.346	−4.621	971.546	280.447
17	CO[1,2]Oxazinan	H	—	—	—	—	—	4.796	4.997	−0.201	−0.213	5.009	−4.087	989.697	298.674
18	COPyrrole	H	—	—	—	—	—	5.854	4.952	0.901	0.964	4.890	−2.527	967.760	284.960
19	COIndole	H	—	—	—	—	—	5.745	4.837	0.907	0.959	4.786	−2.454	1032.130	277.918

No.															
20[a]	COMe	H	—	—	—	—	—	5.699	5.118	0.581	0.773	4.926	0.619	870.192	236.384
21	CO-t-Butyl	H	—	—	—	—	—	5.770	5.811	−0.042	−0.049	5.819	0.326	945.814	208.111
22	COPh	H	—	—	—	—	—	5.398	5.160	0.238	0.255	5.143	−2.434	985.661	256.507
23	4-OMeCOPh	H	—	—	—	—	—	4.658	5.147	−0.489	−0.582	5.240	−2.980	1030.290	240.131
24	4-NO₂COPh	H	—	—	—	—	—	4.495	4.660	−0.165	−0.183	4.678	−4.312	1025.260	333.702
25[a]	4-CNCOPh	H	—	—	—	—	—	4.301	4.714	−0.413	−0.457	4.758	−2.116	1021.670	302.664
26[a]	CO-2-(1,3-Benzodioxole)	H	—	—	—	—	—	5.495	4.830	0.665	0.706	4.789	−2.247	1034.870	276.486
27	CO-2-Furyl	H	—	—	—	—	—	5.620	5.317	0.303	0.320	5.300	−0.875	962.609	248.127
28	SO₂Ph	H	—	—	—	—	—	3.699	4.439	−0.740	−1.075	4.774	−3.287	1005.240	355.178
29	CN	H	—	—	—	—	—	4.745	4.971	−0.226	−0.326	5.070	0.503	865.270	244.002
30	C=NOMe	H	—	—	—	—	—	4.000	5.161	−1.161	−1.226	5.226	−0.997	932.010	253.879
31	2-Oxopyrrolidine	H	—	—	—	—	—	6.051	5.354	0.697	0.799	5.252	−5.150	982.770	283.742
32	2-Oxooxazolidine	H	—	—	—	—	—	5.796	5.369	0.427	0.514	5.282	−6.068	968.853	321.802
33	3-Me-2-oxo-imidazolidine	H	—	—	—	—	—	5.301	4.939	0.362	0.410	4.891	−5.335	1007.300	340.586
34	—	—	H	NO₂	—	—	—	4.770	5.228	−0.458	−1.727	6.496	−8.144	1088.210	380.953
35	—	—	H	F	—	—	—	4.959	4.645	0.314	0.347	4.612	−3.694	1058.160	289.980
36	—	—	Cl	H	—	—	—	4.252	4.490	-0.238	−0.266	4.518	−3.307	1060.860	301.647
37	—	—	H	Cl	—	—	—	5.252	4.531	0.721	0.859	4.393	−3.370	1071.540	282.633
38	—	—	H	Br	—	—	—	4.328	4.455	−0.127	−0.159	4.486	−3.179	1077.580	281.707
39	—	—	—	—	O	1	—	5.284	4.876	0.408	0.509	4.775	−4.057	907.495	280.430
40[a]	—	—	—	—	O	2	—	4.796	5.025	−0.229	−0.260	5.056	−3.775	930.567	273.891
41	—	—	—	—	N	1	COMe	6.149	5.364	0.785	0.912	5.236	−5.619	969.035	301.375
42[a]	—	—	—	—	N	1	COOMe	4.553	4.685	−0.132	−0.156	4.709	−3.719	990.921	333.132
43	—	—	—	—	N	1	OMe	4.745	5.195	−0.450	−0.506	5.250	−5.047	954.961	298.399

aConsidered as outlier.

7.2.2 A Series of Peptide-Derived HRV 3C^{pro} Inhibitors

Dragovich et al. (1998b) reported a series of peptide-derived potent HRV 3C^{pro} inhibitors (Table 11.36), the QSAR model [Eq. (11.35)] suggested that the activity would be primarily controlled by the hydrophobicity of the molecule. The polar volume and the total dipole moment of the compounds would also help to increase the activity of the compounds. "I" is an indicator parameter indicating the presence of i-butyl moiety at R_3 position. Its negative coefficient suggested that i-butyl function is not favorable at R_3-position. This might be creating some steric problem.

$$pEC_{50} = 5.030\,(\pm 0.717) + 0.549\,(\pm 0.060)\,C\,\text{Log }P - 0.076\,(\pm 0.032)\,D_Y$$
$$+ 0.160\,(\pm 0.042)\,D_{\text{Tot}} - 0.007\,(\pm 0.001)\,\text{MW} \tag{11.35}$$
$$+ 0.008\,(\pm 0.001)\,\text{Pol Vol} - 0.869\,(\pm 0.109)\,\text{I}$$

$N = 64$, $R = 0.858$, $R^2 = 0.736$, $R_A^2 = 0.708$, $F\,(6, 57) = 26.421$, $P < 0.00000$, SEE = 0.361, $q^2 = 0.648$, $Q = 2.377$, Outlier = Compounds **5**, **9**, **11**, **20**, **25**, **26**, **40**, **42**, **51**, **60**, **69**, **71**, **73**, **77**

7.2.3 Ketomethylene Containing Peptide-Based HRV 3C^{pro} Inhibitors

Dragovich et al. (1999a) reported some ketomethylene group containing peptide-based HRV 3C^{pro} inhibitors (Table 11.37). The QSAR model obtained for them was as shown by Eq. (11.36):

$$pEC_{50} = 6.795\,(\pm 0.154) - 0.154\,(\pm 0.036)\,D_Y - 0.434\,(\pm 0.190)\,I_1$$
$$+ 0.601\,(\pm 0.196)\,I_2 \tag{11.36}$$

$N = 14$, $R = 0.927$, $R^2 = 0.859$, $R_A^2 = 0.816$, $F\,(3, 10) = 20.273$, $P < 0.00014$, SEE = 0.266, $q^2 = 0.727$, $Q = 3.485$

It is observed from Eq. (11.36) that decreasing value of the dipole moment along Y-axis may increase the activity. This model also showed the importance of two indicator variables, I_1 and I_2, each of which was used with a value of unity i-butyl and the i-propyl substituent at R_2 position, respectively. The negative coefficient of I_1 suggested that i-butyl group will not be conducive to the activity, while the positive coefficient of I_2 suggested that i-propyl group would be favorable to the activity. These facts are observed from the i-butyl substituted compounds **1–3** and **5–7** and the i-propyl substituted compounds **4**, **8–11**.

7.2.4 Peptide-Based HRV 3C^{pro} Inhibitors

Dragovich et al. (1999b) reported some HRV 3C^{pro} inhibitors (Table 11.38). The QSAR model is shown in Eq. (11.37) obtained for them suggested that the high polarity of the compound in the X-direction will be detrimental to the inhibition potency of the compound. The simple structure–activity relationship study of

TABLE 11.36 Biological Activity and Physicochemical Parameters of a Series of Peptide-Derived HRV 3C^{pro} Inhibitors for QSAR Model [Eq. (11.35)]
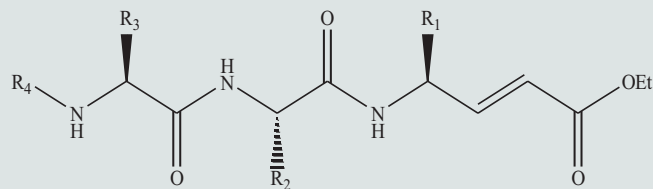
Compound	R$_1$	R$_2$	R$_3$	R$_4$	Obsd	Calcd	Res	Del res	Pred	C Log P	D$_Y$	D$_{Tot}$	MW	Pol Vol	I
1	(CH$_2$)$_2$CONH$_2$	Bnz	i-But	Cbz	6.268	5.643	0.625	0.644	5.623	4.402	−0.526	2.710	594.698	413.706	1
2	(CH$_2$)$_2$CONHTr	Bnz	i-But	Cbz	4.000	4.542	−0.542	−1.136	5.136	6.581	−1.113	1.932	825.002	330.906	1
3	(CH$_2$)$_2$CONHMe	Bnz	i-But	Cbz	5.252	5.273	−0.021	−0.023	5.275	4.582	2.135	2.543	608.725	398.617	1
4	(CH$_2$)$_2$CONMe$_2$	Bnz	i-But	Cbz	5.398	5.323	0.075	0.083	5.315	4.954	2.531	3.027	622.752	389.226	1
5[a]	(CH$_2$)$_2$COOH	Bnz	i-But	Cbz	4.854	5.724	−0.870	−0.933	5.787	5.138	−2.225	2.775	595.683	337.877	1
6	(CH$_2$)$_2$COMe	Bnz	i-But	Cbz	5.796	5.550	0.246	0.266	5.530	5.278	−0.507	2.894	593.710	318.394	1
7	(CH$_2$)$_2$SOMe	Bnz	i-But	Cbz	5.796	5.602	0.194	0.204	5.592	4.342	−2.187	3.447	613.765	387.787	1
8	CH$_2$NHCOMe	Bnz	i-But	Cbz	5.658	5.155	0.502	0.564	5.094	4.379	5.417	7.240	594.698	313.448	1
9[a]	CH$_2$NHCONH$_2$	Bnz	i-But	Cbz	4.495	5.681	−1.186	−1.274	5.769	4.015	−0.559	2.258	595.687	465.089	1
10	CH$_2$OCONH$_2$	Bnz	i-But	Cbz	5.796	5.587	0.209	0.229	5.567	4.459	−0.530	0.909	596.671	446.942	1
11[a]	(CH$_2$)$_2$CONH$_2$	H	i-But	Cbz	3.851	5.073	−1.222	−1.323	5.174	2.675	2.269	5.487	504.576	315.571	1
12	(CH$_2$)$_2$CONH$_2$	Me	i-But	Cbz	4.699	5.020	−0.321	−0.357	5.056	2.984	−0.004	4.193	518.602	291.439	1

(Continued)

TABLE 11.36 Biological Activity and Physicochemical Parameters of a Series of Peptide-Derived HRV 3C^{pro} Inhibitors for QSAR Model [Eq. (11.35)] (*cont.*)

Compound	R$_1$	R$_2$	R$_3$	R$_4$	Obsd	Calcd	Res	Del res	Pred	C Log P	D$_Y$	D$_{Tot}$	MW	Pol Vol	I
13	(CH$_2$)$_2$CONH$_2$	Et	*i*-But	Cbz	5.222	5.181	0.041	0.044	5.178	3.513	0.010	4.173	532.629	295.871	1
14	(CH$_2$)$_2$CONH$_2$	*n*-Pr	*i*-But	Cbz	5.301	5.517	−0.216	−0.233	5.534	4.042	2.612	3.991	546.656	381.286	1
15	(CH$_2$)$_2$CONH$_2$	*i*-But	*i*-But	Cbz	5.268	5.452	−0.184	−0.199	5.467	4.441	−0.030	4.239	560.682	301.966	1
16	(CH$_2$)$_2$CONH$_2$	CH$_2$SMe	*i*-But	Cbz	5.051	5.422	−0.371	−0.399	5.449	3.513	−0.768	5.152	564.694	342.413	1
17	(CH$_2$)$_2$CONH$_2$	CH$_2$SEt	*i*-But	Cbz	5.000	5.564	−0.564	−0.606	5.606	4.042	−0.744	5.171	578.721	342.413	1
18	(CH$_2$)$_2$CONH$_2$	CH$_2$C-Hex	*i*-But	Cbz	5.721	5.933	−0.212	−0.230	5.951	5.634	0.021	2.242	600.746	394.126	1
19	(CH$_2$)$_2$CONH$_2$	4-FBnz	*i*-But	Cbz	5.745	5.543	0.201	0.209	5.536	4.545	−2.108	2.393	612.689	386.902	1
20^a	(CH$_2$)$_2$CONH$_2$	4-MeBnz	*i*-But	Cbz	6.745	5.717	1.028	1.071	5.673	4.901	−2.119	2.623	608.725	378.323	1
21	(CH$_2$)$_2$CONH$_2$	4-OHBnz	*i*-But	Cbz	5.276	5.308	−0.032	−0.033	5.309	3.735	−1.100	2.275	610.698	428.516	1
22	(CH$_2$)$_2$CONH$_2$	4-OAcBnz	*i*-But	Cbz	4.959	4.819	0.139	0.153	4.806	3.751	4.402	6.233	652.735	384.882	1
23	(CH$_2$)$_2$CONH$_2$	4-OMeBnz	*i*-But	Cbz	5.770	5.303	0.467	0.545	5.224	4.321	6.526	8.296	624.725	375.690	1
24	(CH$_2$)$_2$CONH$_2$	4-OPO$_3$H$_2$Bnz	*i*-But	Cbz	4.854	4.636	0.218	0.322	4.532	2.397	6.797	9.078	691.686	481.642	1
25^a	(CH$_2$)$_2$CONH$_2$	4-CH$_2$OHBnz	*i*-But	Cbz	6.260	5.157	1.103	1.197	5.062	3.364	−2.137	3.570	624.725	398.350	1
26^a	(CH$_2$)$_2$CONH$_2$	4-CH$_2$OMeBnz	*i*-But	Cbz	4.409	5.260	−0.851	−0.882	5.291	4.200	0.299	3.964	638.751	397.994	1
27	(CH$_2$)$_2$CONH$_2$	4-(CH$_2$)$_2$OHBnz	*i*-But	Cbz	5.456	5.026	0.430	0.463	4.993	3.593	−2.114	2.115	638.751	410.287	1
28	(CH$_2$)$_2$CONH$_2$	4-CNBnz	*i*-But	Cbz	5.252	5.483	−0.232	−0.244	5.496	3.835	−2.202	2.611	619.708	436.415	1
29	(CH$_2$)$_2$CONH$_2$	CH$_2$-2-Imidazol	*i*-But	Cbz	4.569	4.524	0.045	0.049	4.519	2.001	5.302	7.567	584.664	371.088	1

|															
30	(CH$_2$)$_2$CONH$_2$	CH$_2$-2-(N-Melmid)	i-But	Cbz	5.000	4.958	0.042	0.047	4.953	2.017	−0.320	3.569	598.691	471.960	1
31	(CH$_2$)$_2$CONH$_2$	CH$_2$-2-Thienyl	i-But	Cbz	6.252	5.770	0.481	0.542	5.710	4.048	−0.074	2.329	600.726	491.708	1
32	(CH$_2$)$_2$CONH$_2$	CH(R-OH)Me	i-But	Cbz	4.252	4.698	−0.446	−0.499	4.750	2.437	−0.602	3.575	548.629	320.804	1
33	(CH$_2$)$_2$CONH$_2$	Bnz	H	Cbz	5.252	5.644	−0.392	−0.451	5.703	2.636	6.383	7.818	538.592	342.483	0
34	(CH$_2$)$_2$CONH$_2$	Bnz	Me	Cbz	5.699	5.673	0.026	0.030	5.669	2.945	6.386	7.863	552.619	338.858	0
35	(CH$_2$)$_2$CONH$_2$	Bnz	i-Pr	Cbz	6.420	6.292	0.128	0.137	6.283	3.873	−0.517	2.730	580.672	422.592	0
36	(CH$_2$)$_2$CONH$_2$	Bnz	CH(S-Me)Et	Cbz	6.102	6.405	−0.303	−0.326	6.429	4.402	−0.561	2.688	594.698	417.655	0
37	(CH$_2$)$_2$CONH$_2$	Bnz	t-But	Cbz	6.495	6.325	0.170	0.182	6.313	4.272	−0.577	2.633	594.698	414.693	0
38	(CH$_2$)$_2$CONH$_2$	Bnz	(CH$_2$)$_2$SMe	Cbz	5.854	6.212	−0.358	−0.401	6.255	3.093	−0.565	3.842	612.737	483.809	0
39	(CH$_2$)$_2$CONH$_2$	Bnz	CH$_2$SMe	Cbz	6.745	6.005	0.740	0.798	5.946	3.329	−0.522	1.569	598.710	467.024	0
40[a]	(CH$_2$)$_2$CONH$_2$	Bnz	CH(R-Me)S-i-Pr	Cbz	5.000	5.942	−0.942	−1.017	6.017	4.476	−1.336	1.448	640.790	402.437	0
41	(CH$_2$)$_2$CONH$_2$	Bnz	c-Hex	Cbz	6.000	6.254	−0.254	−0.277	6.277	5.066	0.233	2.017	620.736	398.422	0
42	(CH$_2$)$_2$CONH$_2$	Bnz	CH$_2$c-Hex	Cbz	5.921	6.531	−0.610	−0.681	6.602	5.595	0.242	2.071	634.762	422.208	0
43	(CH$_2$)$_2$CONH$_2$	Bnz	Bnz	Cbz	6.252	6.009	0.243	0.256	5.996	4.363	0.637	2.656	628.715	412.373	0
44	(CH$_2$)$_2$CONH$_2$	Bnz	CH$_2$SPh	Cbz	6.921	5.975	0.946	1.048	5.873	4.975	0.134	0.894	660.780	432.119	0
45	(CH$_2$)$_2$CONH$_2$	Bnz	CH$_2$SBnz	Cbz	6.699	6.057	0.642	0.711	5.988	5.252	0.595	1.560	674.806	432.894	0
46	(CH$_2$)$_2$CONH$_2$	Bnz	Phenethyl	Cbz	6.602	6.088	0.514	0.552	6.050	4.892	0.147	2.107	642.741	406.351	0
47	(CH$_2$)$_2$CONH$_2$	Bnz	CH$_2$OH	Cbz	5.745	5.409	0.336	0.373	5.371	1.944	5.520	7.889	568.618	377.703	0
48	(CH$_2$)$_2$CONH$_2$	Bnz	CH(R-OH)Me	Cbz	5.745	5.382	0.363	0.393	5.352	2.253	5.016	6.785	582.645	384.249	0
49	(CH$_2$)$_2$CONH$_2$	Bnz	CMe$_2$OH	Cbz	6.180	5.584	0.596	0.631	5.550	2.652	0.924	3.276	596.671	424.567	0
50	(CH$_2$)$_2$CONH$_2$	Bnz	CMe$_2$CH$_2$OH	Cbz	5.886	5.452	0.434	0.468	5.418	2.285	0.346	3.352	610.698	436.415	0

TABLE 11.36 Biological Activity and Physicochemical Parameters of a Series of Peptide-Derived HRV 3C^{pro} Inhibitors for QSAR Model [Eq. (11.35)] (*cont.*)

Compound	R_1	R_2	R_3	R_4	Obsd	Calcd	Res	Del res	Pred	C Log P	D_Y	D_{Tot}	MW	Pol Vol	I
51[a]	$(CH_2)_2CONH_2$	Bnz	$(CH_2)_4NH_2$	Cbz	3.688	5.803	−2.115	−2.293	5.981	2.645	−0.448	2.678	609.713	473.406	0
52	$(CH_2)_2CONH_2$	Bnz	$(CH_2)_2Morphol$	Cbz	5.292	5.349	−0.056	−0.063	5.356	2.418	−0.519	2.657	651.750	460.861	0
53	$(CH_2)_2CONH_2$	Bnz	$(CH_2)_3Morphol$	Cbz	5.149	5.564	−0.415	−0.465	5.613	2.947	−1.018	2.732	665.776	463.920	0
54	$(CH_2)_2CONH_2$	Bnz	CH_2COOH	Cbz	5.620	5.486	0.134	0.153	5.467	2.366	4.934	8.528	596.628	365.901	0
55	$(CH_2)_2CONH_2$	Bnz	$(CH_2)_2COOH$	Cbz	5.260	5.101	0.158	0.199	5.061	2.057	8.211	10.633	610.655	341.532	0
56	$(CH_2)_2CONH_2$	Bnz	CH_2CONMe_2	Cbz	5.229	5.213	0.016	0.018	5.211	2.309	−0.516	0.519	623.697	464.062	0
57	$(CH_2)_2CONH_2$	Bnz	i-But	2-MeCbz	6.000	5.732	0.268	0.279	5.721	5.049	0.227	3.329	608.725	391.567	1
58	$(CH_2)_2CONH_2$	Bnz	i-But	2-ClCbz	6.201	5.874	0.327	0.345	5.855	5.313	−1.058	3.636	629.144	391.664	1
59	$(CH_2)_2CONH_2$	Bnz	i-But	$COOCH_2$ (4-Pyr)	4.252	4.818	−0.566	−0.614	4.866	3.103	0.604	2.039	595.687	407.187	1
60[b]	$(CH_2)_2CONH_2$	Bnz	i-But	COOMe	5.886	5.071	0.815	0.881	5.006	2.243	−1.063	3.298	518.602	366.847	1
61	$(CH_2)_2CONH_2$	Bnz	i-But	COO-c-Hex	5.119	5.702	−0.583	−0.601	5.720	4.274	−0.617	3.216	586.720	410.790	1
62	$(CH_2)_2CONH_2$	Bnz	i-But	COO-t-But	5.347	5.683	−0.336	−0.359	5.706	3.480	−0.904	4.859	560.682	393.366	1
63	$(CH_2)_2CONH_2$	Bnz	i-But	COSMe	5.959	5.787	0.172	0.188	5.770	3.236	−1.830	4.270	534.668	398.801	1

|															
64	$(CH_2)_2CONH_2$	Bnz	*i*-But	COSEt	6.337	6.009	0.328	0.364	5.974	3.765	−1.847	4.246	548.695	414.000	1
65	$(CH_2)_2CONH_2$	Bnz	*i*-But	COS-c-Pent	6.745	6.060	0.685	0.737	6.007	4.708	−1.713	3.770	588.759	410.214	1
66	$(CH_2)_2CONH_2$	Bnz	*i*-But	COSBnz	6.569	5.908	0.661	0.693	5.876	4.940	−1.782	2.960	610.764	410.261	1
67	$(CH_2)_2CONH_2$	Bnz	*i*-But	CO-2-Napthyl	6.000	5.632	0.368	0.410	5.590	4.898	−3.035	3.347	614.731	336.399	1
68	$(CH_2)_2CONH_2$	Bnz	*i*-But	COPh	5.284	5.551	−0.267	−0.275	5.559	3.724	−0.370	3.364	564.673	401.162	1
69[a]	$(CH_2)_2CONH_2$	Bnz	*i*-But	COPhOPh	5.284	6.351	−1.067	−1.295	6.579	5.822	−0.349	4.902	656.768	452.361	1
70	$(CH_2)_2CONH_2$	Bnz	*i*-But	COMe	4.854	4.855	−0.001	−0.001	4.855	2.073	0.390	3.421	502.603	342.891	1
71[a]	$(CH_2)_2CONH_2$	Bnz	*i*-But	CO-*i*-Pr	6.000	5.185	0.815	0.854	5.146	2.911	0.267	3.332	530.656	369.905	1
72	$(CH_2)_2CONH_2$	Bnz	*i*-But	CO-*t*-But	5.745	5.312	0.433	0.448	5.296	3.310	0.354	3.399	544.683	377.655	1
73[a]	$(CH_2)_2CONH_2$	Bnz	*i*-But	CO-c-Pent	6.222	5.281	0.941	0.975	5.247	3.545	0.062	2.830	556.694	377.076	1
74	$(CH_2)_2CONH_2$	Bnz	*i*-But	$COCH_2OH$	4.523	4.666	−0.143	−0.164	4.687	1.913	1.111	2.402	518.602	379.856	1
75	$(CH_2)_2CONH_2$	Bnz	*i*-But	$CO(CH_2)_2OH$	4.721	4.816	−0.095	−0.102	4.824	1.746	1.759	4.449	532.629	398.315	1
76	$(CH_2)_2CONH_2$	Bnz	*i*-But	CON(Me)Bnz	5.252	5.496	−0.244	−0.254	5.506	4.072	0.071	2.815	607.740	438.202	1
77[a]	$(CH_2)_2CONH_2$	Bnz	*i*-But	Ac-L-Val	4.201	5.106	−0.906	−0.998	5.198	3.802	4.372	4.664	574.709	374.435	1
78	$(CH_2)_2CONH_2$	Bnz	*i*-But	Ac-L-Ala	4.699	5.077	−0.378	−0.397	5.096	2.874	2.249	4.207	546.656	385.237	1

[a]Considered as outlier.

TABLE 11.37 Biological Activity and Physicochemical Parameters of Ktomethylene Containing Peptide-Based HRV 3C^{pro} Inhibitors for QSAR Model [Eq. (11.36)]
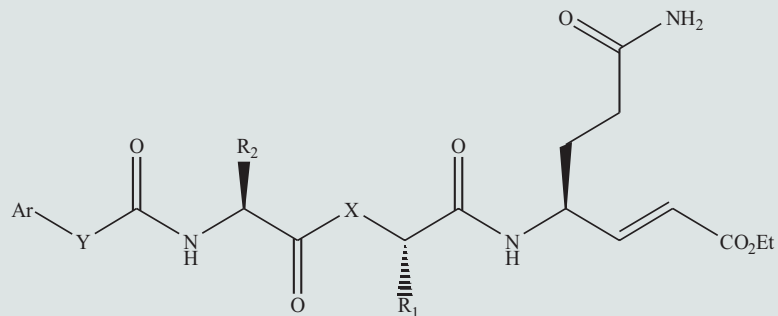
Compound	Ar	Y	X	R$_1$	R$_2$	Obsd	Calcd	Res	Del res	Pred	D$_Y$	I$_1$	I$_2$
1	Bnz	O	NH	Bnz	i-But	6.268	6.245	0.023	0.029	6.238	0.755	1	0
2	Bnz	O	CH$_2$	Bnz	i-But	6.444	6.207	0.237	0.307	6.137	1.002	1	0
3	Bnz	S	CH$_2$	Bnz	i-But	6.167	6.284	−0.117	−0.146	6.313	0.498	1	0

4	Bnz	S	CH$_2$	Bnz	i-Pr	6.721	7.317	−0.596	−0.778	7.499	0.508	0	1
5	c-Pent	S	CH$_2$	Bnz	i-But	6.721	6.827	−0.106	−0.141	6.863	−3.025	1	0
6	c-Pent	S	CH$_2$	4F-Bnz	i-But	6.553	6.536	0.016	0.020	6.533	−1.139	1	0
7	c-Pent	S	CH$_2$	4-MeBnz	i-But	6.796	6.850	−0.054	−0.073	6.869	−3.172	1	0
8	c-Pent	S	CH$_2$	Bnz	i-Pr	7.699	7.861	−0.162	−0.226	7.925	−3.021	0	1
9	c-Pent	S	CH$_2$	4F-Bnz	i-Pr	7.699	7.570	0.129	0.162	7.537	−1.130	0	1
10	c-Pent	S	CH$_2$	4-MeBnz	i-Pr	8.222	7.883	0.338	0.480	7.742	−3.168	0	1
11	c-Pent	S	CH$_2$	4-CF$_3$Bnz	i-Pr	7.301	7.011	0.290	0.485	6.816	2.495	0	1
12	c-Pent	S	CH$_2$	4F-Bnz	Bnz	6.319	6.445	−0.126	−0.227	6.545	2.268	0	0
13	c-Pent	S	CH$_2$	4-MeBnz	Bnz	6.854	6.759	0.095	0.143	6.710	0.233	0	0
14	c-Pent	S	CH$_2$	Bnz	t-But	7.301	7.270	0.031	0.060	7.241	−3.084	0	0

TABLE 11.38 Biological Activity and Physicochemical Parameters of Peptide-Based HRV 3C^{pro} Inhibitors for QSAR Model [Eq. (11.37)]
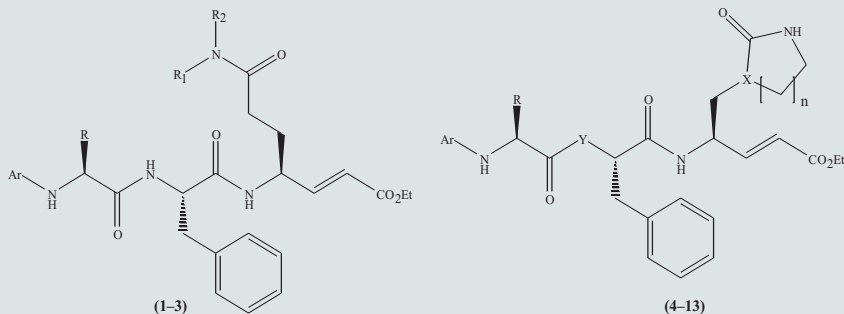
Compound	Ar	Ar$_1$	R	R$_1$	R$_2$	n	X	Y	Obsd	Calcd	Res	Del res	Pred	D_X
1[a]	Cbz	Bnz	i-But	H	H	—	—	—	6.268	4.694	1.573	2.178	4.090	2.748
2	Cbz	Bnz	i-But	Me	H	—	—	—	3.125	4.926	−1.801	−2.359	5.484	2.545
3	Cbz	Bnz	i-But	Me	Me	—	—	—	4.222	4.419	−0.197	−0.296	4.517	2.988
4	Cbz	Bnz	i-But	—	—	1	(S)-CH	NH	7.000	7.112	−0.112	−0.122	7.122	0.640
5	Cbz	Bnz	i-But	—	—	2	(S)-CH	NH	7.523	8.286	−0.763	−0.922	8.445	−0.383
6	Cbz	Bnz	i-But	—	—	1	(R)-CH	NH	5.796	7.112	−1.316	−1.432	7.228	0.640
7	Cbz	Bnz	i-But	—	—	1	N	NH	6.222	6.177	0.045	0.050	6.172	1.456
8	Cbz	Bnz	i-Pr	—	—	1	(S)-CH	NH	7.523	7.128	0.395	0.430	7.093	0.627
9	5-Me-isoxazole-3-CO	4F-Bnz	i-Pr	—	—	1	(S)-CH	NH	8.000	7.938	0.062	0.071	7.929	−0.079
10	5-Me-isoxazole-3-CO	4F-Bnz	i-Pr	—	—	2	(S)-CH	NH	7.699	6.937	0.762	0.826	6.873	0.793
11	5-Me-isoxazole-3-CO	4F-Bnz	i-Pr	—	—	1	(S)-CH	CH$_2$	8.301	8.522	−0.221	−0.278	8.579	−0.589
12	5-Me-isoxazole-3-CO	4F-Bnz	i-Pr	—	—	2	(S)-CH	CH$_2$	9.000	7.510	1.490	1.651	7.349	0.293
13	5-Me-isoxazole-3-CO	4F-Bnz	t-But	—	—	1	(S)-CH	NH	8.000	7.915	0.085	0.098	7.902	−0.059

[a]Considered as outlier.

these compounds had suggested that (S)-conformation of the compound had better activity than (R)-conformation.

$$pEC_{50} = 7.890\,(\pm 0.309) - 1.383\,(\pm 0.239)\,D_X \qquad (11.37)$$

$N = 12$, $R = 0.877$, $R^2 = 0.769$, $R_A^2 = 0.746$, $F\,(1,\,10) = 33.377$, $P < 0.00018$, SEE = 0.876, $q^2 = 0.652$, $Q = 1.001$, Outlier = Compound **1**

Dragovich et al. (1999c) had also reported some tripeptidyl N-methyl amino acids as HRV 3C^{pro} inhibitors (Table 11.39), for which the QSAR model obtained [Eq. (11.38)] had suggested that the activity will be totally governed by the total dipole moment of the compound. This indicated the strong electronic interaction between the molecule and the receptor.

$$pEC_{50} = 6.094\,(\pm 0.122) + 0.075\,(\pm 0.019)\,D_{\text{Tot}} \qquad (11.38)$$

$N = 8$, $R = 0.852$, $R^2 = 0.726$, $R_A^2 = 0.680$, $F\,(1,\,6) = 15.869$, $P < 0.00725$, SEE = 0.173, $q^2 = 0.537$, $Q = 4.925$, Outlier = Compounds **7**, **10**

However, for some ketone containing tripeptidyl HRV 3C^{pro} inhibitors (Table 11.40) reported by Dragovich et al. (2000), the QSAR model [Eq. (11.39)] exhibited the importance of only Z-component of the dipole moment of the compound. In the Z-direction, the polarity of the compound may be more favorable for electronic interaction with the receptor.

$$pK_i = 3.662\,(\pm 0.583) + 2.862\,(\pm 0.713)\,D_Z \qquad (11.39)$$

$N = 6$, $R = 0.895$, $R^2 = 0.801$, $R_A^2 = 0.751$, $F\,(1,\,4) = 16.096$, $P < 0.01597$, SEE = 0.490, $q^2 = 0.594$, $Q = 1.827$, Outlier = Compounds **5**, **7**

7.2.5 Depsipeptidyl HRV 3C^{pro} Inhibitors

Webber et al. (2001) reported some depsipeptidyl HRV 3C^{pro} inhibitors (Table 11.41), for which the QSAR model obtained was as is shown by Eq. (11.40). This model suggested that in this case, the polar volume of the molecule will not be conducive to the activity.

$$pEC_{50} = 18.601\,(\pm 2.905) - 0.029\,(\pm 0.008)\,\text{Pol Vol} \qquad (11.40)$$

$N = 7$, $R = 0.866$, $R^2 = 0.750$, $R_A^2 = 0.700$, $F\,(1,\,5) = 15.030$, $P < 0.01168$, SEE = 0.499, $q^2 = 0.533$, $Q = 1.735$, Outlier = Compounds **2**, **6**

7.2.6 2-Pyridone Containing Peptidomimetics as HRV 3C^{pro} Inhibitors

For some 2-pyridone containing peptidomimetics as promising HRV 3C^{pro} inhibitors (Table 11.42) reported by Dragovich et al. (2002), the QSAR model [Eq. (11.41)] had, however, suggested that the SA of the molecule will be favorable to the activity, probably because of dispersion interaction between the active surface of the molecule and that of the receptor. However, a very high

TABLE 11.39 Biological Activity and Physicochemical Parameters of Some Tripeptidyl *N*-methyl Amino Acids for QSAR Model [Eq. (11.38)]
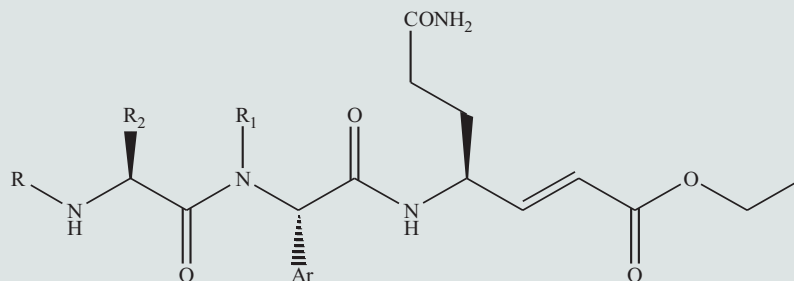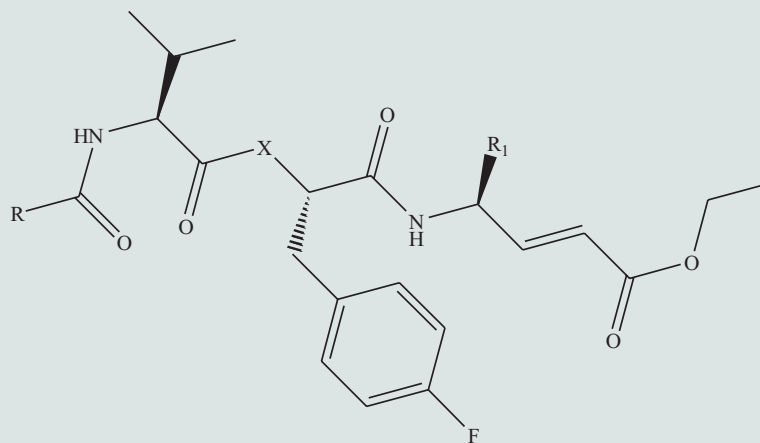

Compound	R	R_1	R_2	Ar	Obsd	Calcd	Res	Del res	Pred	D_{Tot}
1	NHCBz	H	*i*-But	Bnz	6.268	6.165	0.103	0.160	6.108	1.102
2	NHCBz	Me	*i*-But	Bnz	6.000	6.187	−0.187	−0.272	6.272	1.542
3	CO-S-*c*-Pent	Me	*i*-But	Bnz	6.495	6.351	0.144	0.163	6.331	4.724
4	CO-S-*c*-Pent	Me	*i*-Pr	Bnz	6.721	6.353	0.368	0.418	6.303	4.759
5	CO-S-*c*-Pent	Me	CH₂SPh	Bnz	6.268	6.331	−0.064	−0.073	6.341	4.336
6	5-Methyl-isoxazole-3-carbonyl	Me	*i*-But	Bnz	6.854	6.547	0.307	0.364	6.490	8.521
7[a]	5-Methyl-isoxazole-3-carbonyl	Me	*i*-But	4-FBnz	6.398	6.594	−0.197	−0.249	6.647	9.449
8	5-Methyl-isoxazole-3-carbonyl	Me	CH₂(1-Napthyl)	4-FBnz	6.699	6.592	0.107	0.135	6.564	9.400
9	5-Methyl-isoxazole-3-carbonyl	Me	CH₂(2-Napthyl)	4-FBnz	6.796	6.641	0.155	0.214	6.581	10.349
10[a]	5-Methyl-isoxazole-3-carbonyl	Me	CH₂(4-Imidazole)	4-FBnz	5.745	6.482	−0.737	−0.831	6.575	7.262

[a]Considered as outlier.

TABLE 11.40 Biological Activity and Physicochemical Parameters of Some Ketone Containing Tripeptidyl HRV 3C^{pro} Inhibitors for QSAR Model [Eq. (11.39)]
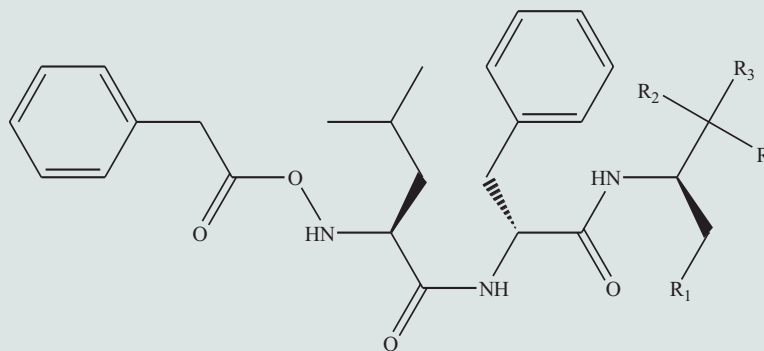
Compound	R	R$_1$	R$_2$	R$_3$	Obsd	Calcd	Res	Del res	Pred	D$_Z$
1	Benzothiazol-2-yl	NHCOMe	=O		5.770	5.512	0.257	0.321	5.449	0.645
2	Benzothiazol-2-yl	CH$_2$CONH$_2$	=O		5.456	5.458	−0.002	−0.003	5.459	0.596
3	Benzothiazol-2-yl	2-Oxo-pyrrolidin-3-yl	=O		7.187	6.227	0.960	1.266	5.921	1.287
4	Benzothiazol-2-yl	2-Oxo-pyrrolidin-3-yl	OH	H	4.469	5.225	−0.756	−1.245	5.714	0.386
5[a]	Thiazol-2-yl	2-Oxo-pyrrolidin-3-yl	=O		6.155	6.350	−0.195	−0.290	6.445	1.399
6	2-Pyridyl	2-Oxo-pyrrolidin-3-yl	=O		6.770	5.742	1.028	1.182	5.588	0.851
7[a]	Benzothiophen-2-yl	2-Oxo-pyrrolidin-3-yl	=O		5.328	6.387	−1.059	−1.639	6.966	1.431
8	Ph	2-Oxo-pyrrolidin-3-yl	=O		5.495	5.727	−0.232	−0.268	5.763	0.838

[a]Considered as outlier.

TABLE 11.41 Biological Activity and Physicochemical Parameters of Depsipeptidyl HRV 3C^{pro} Inhibitors for QSAR Model [Eq. (11.40)]

Compound	R	R$_1$	X	Obsd	Calcd	Res	Del res	Pred	Pol Vol
1	S-c-pent	(CH$_2$)$_2$CONH$_2$	O	6.000	6.466	−0.466	−0.692	6.692	426.668
2^a	S-c-pent	(CH$_2$)$_2$CONH$_2$	NH	6.721	6.244	0.477	0.894	5.827	438.416
3	S-c-pent	(CH$_2$)$_2$CONH$_2$	CH$_2$	7.699	7.329	0.370	0.418	7.281	380.864
4	5-Methyl-isoxazole	(CH$_2$)$_2$CONH$_2$	O	7.000	7.360	−0.360	−0.407	7.407	379.172
5	5-Methyl-isoxazole	(CH$_2$)$_2$CONH$_2$	NH	6.377	7.042	−0.665	−0.762	7.138	396.070
6^a	5-Methyl-isoxazole	(CH$_2$)$_2$CONH$_2$	CH$_2$	7.000	7.773	−0.773	−0.974	7.974	357.284
7	5-Methyl-isoxazole	5-(2-Oxo-pyrrolidin-3-yl)	O	8.155	7.516	0.639	0.739	7.416	370.905
8	5-Methyl-isoxazole	5-(2-Oxo-pyrrolidin-3-yl)	NH	8.000	7.379	0.621	0.703	7.297	378.176
9	5-Methyl-isoxazole	5-(2-Oxo-pyrrolidin-3-yl)	CH$_2$	8.301	8.144	0.157	0.258	8.043	337.594

^{a}Considered as outlier.

TABLE 11.42 Biological Activity and Physicochemical Parameters of 2-Pyridone Containing Peptidomimetics as HRV 3C^{pro} Inhibitors for QSAR Model [Eq. (11.41)]
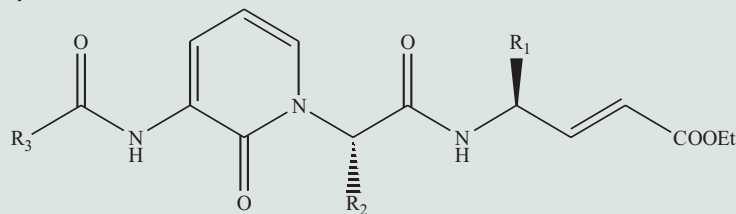
Compound	R$_1$	R$_2$	R$_3$	Obsd	Calcd	Res	Del res	Pred	SA
1	(CH$_2$)$_2$CONH$_2$	Bnz	OBnz	7.481	7.493	−0.012	−0.013	7.495	882.377
2	(CH$_2$)$_2$CONH$_2$	4-FBnz	OBnz	7.854	7.492	0.362	0.410	7.444	883.062
3	(CH$_2$)$_2$CONH$_2$	3,4-diFBnz	OBnz	8.523	7.492	1.031	1.165	7.358	882.859
4	(CH$_2$)$_2$CONH$_2$	CH$_2$-c-Hex	OBnz	6.750	7.368	−0.618	−0.850	7.600	906.641
5[a]	(CH$_2$)$_2$CONH$_2$	Bnz	Me	6.052	5.531	0.520	9.821	−3.770	749.850
6	(CH$_2$)$_2$CONH$_2$	Bnz	c-Pent	7.469	7.194	0.275	0.325	7.144	825.095
7	(CH$_2$)$_2$CONH$_2$	Bnz	[1,3]Dithiolane-2-yl	6.983	7.190	−0.207	−0.245	7.228	824.774
8	(CH$_2$)$_2$CONH$_2$	Bnz	Tetrahydrofuran-2-yl	5.750	7.049	−1.299	−1.550	7.299	814.614
9	(CH$_2$)$_2$CONH$_2$	Bnz	t-Butyl	6.286	7.120	−0.835	−0.991	7.277	819.529
10	(CH$_2$)$_2$CONH$_2$	Bnz	5-Me-Benzoxazol-3-yl	7.796	7.394	0.402	0.466	7.330	845.229
11	(CH$_2$)$_2$CONH$_2$	Bnz	5-Cl-Benzoxazol-3-yl	7.620	7.315	0.305	0.357	7.263	836.004
12	(R)-2-Oxopyrrodine-3-yl	Bnz	OBnz	8.523	7.476	1.047	1.204	7.319	888.453
13	(S)-2-Oxopyrrodine-3-yl	Bnz	OBnz	6.329	7.300	−0.971	−1.592	7.921	914.072

[a]Considered as outlier.

SA was shown to be detrimental to the activity, probably because of the steric problem.

$$pEC_{50} = -670.463(\pm111.246) + 1.568(\pm0.259)SA - 0.001(\pm0.0001)SA^2 \quad (11.41)$$

$N = 12$, $R = 0.905$, $R^2 = 0.819$, $R_A^2 = 0.779$, $F(2, 9) = 20.403$, $P < 0.00045$, SEE $= 0.413$, $q^2 = 0.715$, $Q = 2.191$, $SA_{opt} = 784$, Outlier $=$ Compound **5**

7.2.7 Michael Acceptor Containing Irreversible HRV 3C^pro Inhibitors

Johnson et al. (2002) reported some Michael acceptor containing irreversible HRV 3C^pro inhibitors (Table 11.43). For these inhibitors, the QSAR model [Eq. (11.42)] indicated that the activity of compounds will simply depend upon the presence or absence of β-naphthyl group or chromene ring at the R-position of the compound. Of the two indicator variables, I_1 and I_2, the former with a value of 1 indicated the presence of β-naphthyl group and the latter with a value of unity indicated the presence of chromene ring at the R-position. The positive coefficients of both the variables indicated the favorable contribution of either of the substituent. Both might have steric interactions with the active site of the enzyme.

$$pEC_{50} = 5.951(\pm0.086) + 0.833(\pm0.172)I_1 + 0.819(\pm0.172)I_2 \quad (11.42)$$

$N = 10$, $R = 0.917$, $R^2 = 0.841$, $R_A^2 = 0.796$, $F(2, 7) = 18.528$, $P < 0.00160$, SEE $= 0.210$, $q^2 = 0.765$, $Q = 4.367$, Outlier $=$ Compounds **7, 11**

7.2.8 2-Pyridone Containing Peptidomimetics as HRV 3C^pro Inhibitors

Dragovich et al. (2003) reported a series of 2-pyridone containing peptido-mimetics as HRV 3C^pro inhibitors (Table 11.44). The QSAR model obtained for these compounds was as shown by Eq. (11.43). This model suggested that have less bulky molecules with small X-component of their dipole moment will be favored. Simultaneously, the high value of the PSA of these molecules may be conducive to activity. Further, the positive coefficient of the indicator variable "I" that was defined with a value of unity for a benzyl substituent at R_1-position indicated that such a substituent should be desired for the better activity of the compound. This benzyl group might have steric interaction with the receptor.

$$pEC_{50} = 7.013(\pm2.741) - 0.471(\pm0.091)CMR - 0.329(\pm0.042)D_X \\ + 0.032(\pm0.009)PSA + 0.675(\pm0.165)I \quad (11.43)$$

$N = 18$, $R = 0.947$, $R^2 = 0.897$, $R_A^2 = 0.865$, $F(4, 13) = 28.323$, $P < 0.00000$, SEE $= 0.175$, $q^2 = 0.737$, $Q = 5.411$

TABLE 11.43 Biological Activity and Physicochemical Parameters of Michael Acceptor Containing Irreversible HRV 3C^{pro} Inhibitors for QSAR Model [Eq. (11.42)]
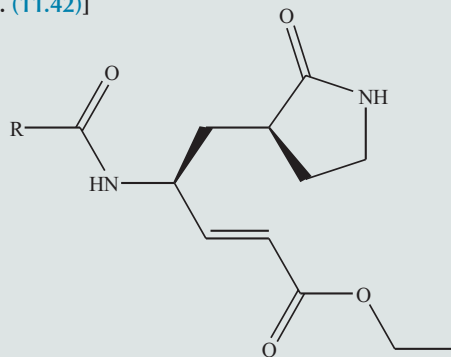
Compound	R	Obsd	Calcd	Res	Del res	Pred	I_1	I_2
1	3-BrPhCH=CH	5.854	5.951	−0.098	−0.117	5.971	0	0
2	3-Br,4-MePhCH=CH	5.889	5.951	−0.062	−0.074	5.964	0	0
3	3-Br,4-FPhCH=CH	6.201	5.951	0.249	0.299	5.902	0	0
4	Benzo[1,3]dioxole	5.742	5.951	0.209	0.251	5.993	0	0
5	5-Bromo-benzo[1,3]dioxole	6.310	5.951	0.358	0.430	5.880	0	0
6	2-Methyl-5-phenyl-furan	5.712	5.951	0.239	0.287	5.999	0	0
7[a]	2H-Chromene-3-yl	5.924	6.488	−0.564	−0.846	6.770	0	1
8	6-Chloro-2H-chromene-3-yl	6.796	6.488	0.308	0.461	6.335	0	1
9	6-Bromo-2H-chromene-3-yl	6.745	6.488	0.256	0.385	6.360	0	1
10	Napthaleny-2-yl	6.824	6.541	0.283	0.424	6.400	1	0
11[a]	6-Methyl-napthaleny-2-yl	6.056	6.541	−0.486	−0.729	6.784	1	0
12	7-Bromo-napthaleny-2-yl	6.745	6.541	0.203	0.305	6.440	1	0

[a]Considered as outlier.

TABLE 11.44 Biological Activity and Physicochemical Parameters of 2-Pyridone Containing Peptidomimetics as HRV 3C^pro Inhibitors for QSAR Model [Eq. (11.43)]
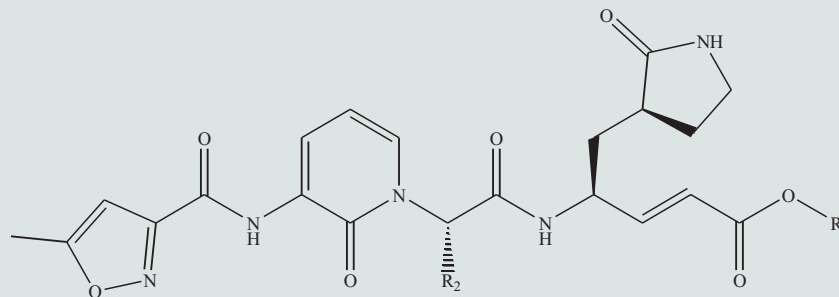
Compound	R_1	R_2	Obsd	Calcd	Res	Del res	Pred	CMR	D_X	PSA	I
1	Et	CH$_2$(3,4-F)Ph	7.959	7.724	0.234	0.463	7.495	15.443	−2.386	226.148	0
2	i-Pr	CH$_2$(3,4-F)Ph	7.108	7.394	−0.286	−0.507	7.615	15.907	−2.400	222.485	0
3	Et	CH$_2$CCH	7.237	7.243	−0.006	−0.008	7.245	13.625	1.971	229.100	0
4	i-Pr	CH$_2$CCH	6.759	6.808	−0.049	−0.054	6.814	14.089	1.926	221.859	0

6	CH$_2$-t-But	CH$_2$CCH	6.559	6.345	0.214	0.312	6.247	15.017	2.128	223.123	0
7	c-But	CH$_2$CCH	7.046	6.959	0.087	0.110	6.936	14.376	0.459	215.681	0
8	c-Pent	CH$_2$CCH	6.759	6.756	0.003	0.003	6.756	14.839	0.494	216.549	0
9	c-Hex	CH$_2$CCH	6.391	6.438	−0.047	−0.056	6.447	15.303	0.536	213.857	0
10	c-Hept	CH$_2$CCH	6.090	6.234	−0.143	−0.200	6.291	15.767	0.581	214.763	0
11	Bnz	CH$_2$CCH	7.444	7.298	0.145	0.292	7.152	15.673	0.533	225.091	1
12	Et	Et	7.328	7.356	−0.028	−0.047	7.375	13.364	2.199	231.167	0
13	i-Pr	Et	6.492	6.808	−0.316	−0.371	6.863	13.828	2.155	220.347	0
14	t-But	Et	6.393	6.402	−0.009	−0.011	6.404	14.292	2.297	215.939	0
15	CH$_2$-t-But	Et	6.509	6.460	0.049	0.071	6.437	14.756	2.353	225.186	0
16	c-But	Et	7.119	6.943	0.176	0.260	6.859	14.115	0.733	214.152	0
17	c-Hex	Et	6.504	6.424	0.080	0.098	6.407	15.042	0.807	212.348	0
18	Bnz	Et	7.194	7.339	−0.145	−0.292	7.486	15.412	0.797	225.237	1

8 OVERVIEW AND CONCLUSIONS

A total of 43 QSAR models (33 for SARS-CoV 3CL[pro] inhibitors and 10 for HRV 3C[pro] inhibitors) have been reported here to get an insight into the relation between the enzyme inhibitory activities of the antiviral compounds and their physicochemical and structural properties. QSAR models exhibited that the physicochemical parameters, such as dipole moment, PSA, polar volume, hydrophobicity, molar refractivity, SA, and molecular volume of the compounds play a crucial role in controlling both SARS-CoV 3CL[pro] and HRV 3C[pro] inhibitory activities. Moreover, some structural indicator variables were found to play an important role for inhibition of these enzymes. In many cases, the dipole moment and the PSA were found to be dominant factors. The bulk of the inhibitors and their flexibility and polarity also appeared to play crucial roles in the inhibition of the enzyme. Most of the QSAR models exhibited a direct correlation of dipole moment with the 3CL[pro] or 3C[pro] inhibitory activity, where a majority of them showed the positive effect of dipole moment on activity but few showed the negative effect, too. These positive and negative effects may be attributed to the orientation of the inhibitor molecules in the active site of the enzyme.

The PSA and the polarity of the inhibitors were some other important factors that were found in some cases to influence the activity. With their positive coefficients in the correlation, they indicated the attractive electronic interactions of the molecules with the enzyme, and with negative coefficient, they indicated the repulsive interaction. In many cases, the polar volume was found to govern the activity. The polar volume also indicated the attractive or repulsive dispersion interaction between the molecule and the receptor.

Among all, the hydrophobicity of the molecules had its own role. In any drug-receptor interaction, hydrophobicity is found to play an important role because in most of the enzymes the active site has a hydrophobic pocket which plays an important role in the activity of the site. In most of the cases, the bulky portion of the molecule tries to occupy this hydrophobic pocket where it may have hydrophobic interaction. The molecular volume, MW, or molar refractivity all sometimes become synonymous to the hydrophobic property of the molecules. If they are not found related to hydrophobicity and are crucial for the activity, then it means that the inhibitor-enzyme interaction involves dispersion interaction. The QSAR models discussed here may be a great help to design some new, more potent compounds in any given category of SARS-CoV 3CL[pro] or HRV 3C[pro] inhibitors.

REFERENCES

Akaji, K., Konno, H., Mitsui, H., Teruya, K., Shimamoto, Y., Hattori, Y., Ozaki, T., Kusunoki, M., Sanjoh, A., 2011. Structure-based design, synthesis, and evaluation of peptide-mimetic SARS 3CL protease inhibitors. J. Med. Chem. 54, 7962–7973.

Allaire, M., Chernaia, M.M., Malcolm, B.A., James, M.N., 1994. Picornaviral 3C cysteine proteinases have a fold similar to chymotrypsin-like serine proteinases. Nature 369, 72–76.

Anand, K., Palm, G.J., Mesters, J.R., Siddell, S.G., Ziebuhr, J., Hilgenfeld, R., 2002. Structure of coronavirus main proteinase reveals combination of a chymotrypsin fold with an extra alpha-helical domain. EMBO J. 21, 3213–3224.

Anand, K., Ziebuhr, J., Wadhwani, P., Mesters, J.R., Hilgenfeld, R., 2003. Coronavirus main proteinase (3CLpro) structure: basis for design of anti-SARS drugs. Science 300, 1763–1767.

Anand, K., Yang, H., Bartlam, M., Rao, Z., Hilgenfeld, R., 2005. Coronavirus main proteinase: target for antiviral drug therapy. In: Schmidt, A., Wolff, M.H., Weber, O. (Eds.), Coronaviruses with Special Emphasis on First Insights Concerning SARS. Birkhauser Verlag, Basel, Switzerland, pp. 173–199.

Atmar, R.L., 2010. Noroviruses—state of the art. Food Environ. Virol. 2, 117–126.

Babcock, G.J., Esshaki, D.J., Thomas, Jr., W.D., Ambrosino, D.M., 2004. Amino acids 270 to 510 of the severe acute respiratory syndrome coronavirus spike protein are required for interaction with receptor. J. Virol. 78, 4552–4560.

Bergmann, E.M., Mosimann, S.C., Chernaia, M.M., Malcolm, B.A., James, M.N., 1997. The refined crystal structure of the 3C gene product from hepatitis A virus: specific proteinase activity and RNA recognition. J. Virol. 71, 2436–2448.

Bisht, H., Roberts, A., Vogel, L., Bukreyev, A., Collins, P.L., Murphy, B.R., Subbarao, K., Moss, B., 2004. Severe acute respiratory syndrome coronavirus spike protein expressed by attenuated vaccinia virus protectively immunizes mice. Proc. Natl. Acad. Sci. USA 101, 6641–6646.

Blanchard, J.E., Elowe, N.H., Huitema, C., Fortin, P.D., Cechetto, J.D., Eltis, L.D., Brown, E.D., 2004. High-throughput screening identifies inhibitors of the SARS coronavirus main proteinase. Chem. Biol. 11, 1445–1453.

Buchholz, U.J., Bukreyev, A., Yang, L., Lamirande, E.W., Murphy, B.R., Subbarao, K., Collins, P.L., 2004. Contributions of the structural proteins of severe acute respiratory syndrome coronavirus to protective immunity. Proc. Natl. Acad. Sci. U.S.A. 101, 9804–9809.

Cavanagh, D., 1997. Nidovirales: a new order comprising Coronaviridae and Arteriviridae. Arch. Virol. 142, 629–633.

Chen, L., Chen, S., Gui, C., Shen, J., Shen, X., Jiang, H., 2006a. Discovering severe acute respiratory syndrome coronavirus 3CL protease inhibitors: virtual screening, surface plasmon resonance, and fluorescence resonance energy transfer assays. J. Biomol. Screen 11, 915–921.

Chen, L., Li, J., Luo, C., Liu, H., Xu, W., Chen, G., Liew, O.W., Zhu, W., Puah, C.M., Shen, X., Jiang, H., 2006b. Binding interaction of quercetin-3-beta-galactoside and its synthetic derivatives with SARS-CoV 3CL (pro): structure–activity relationship studies reveal salient pharmacophore features. Bioorg. Med. Chem. 14, 8295–8306.

Cowley, J.A., Dimmock, C.M., Spann, K.M., Walker, P.J., 2000. Gill-associated virus of *Penaeus monodon* prawns: an invertebrate virus with ORF1a and ORF1b genes related to arteri- and coronaviruses. J. Gen. Virol. 81, 1473–1484.

Dragovich, P.S., Webber, S.E., Babine, R.E., Fuhrman, S.A., Patick, A.K., Matthews, D.A., Lee, C.A., Reich, S.H., Prins, T.J., Marakovits, J.T., Littlefield, E.S., Zhou, R., Tikhe, J., Ford, C.E., Wallace, M.B., Meador, III, J.W., Ferre, R.A., Brown, E.L., Binford, S.L., Harr, J.E., DeLisle, D.M., Worland, S.T., 1998a. Structure-based design, synthesis, and biological evaluation of irreversible human rhinovirus 3C protease inhibitors. 1. Michael acceptor structure–activity studies. J. Med. Chem. 41, 2806–2818.

Dragovich, P.S., Webber, S.E., Babine, R.E., Fuhrman, S.A., Patick, A.K., Matthews, D.A., Reich, S.H., Marakovits, J.T., Prins, T.J., Zhou, R., Tikhe, J., Littlefield, E.S., Bleckman, T.M., Wallace, M.B., Little, T.L., Ford, C.E., Meador, III, J.W., Ferre, R.A., Brown, E.L., Binford, S.L., DeLisle, D.M., Worland, S.T., 1998b. Structure-based design, synthesis, and biological evaluation of irreversible human rhinovirus 3C protease inhibitors. 2. Peptide structure–activity studies. J. Med. Chem. 41, 2819–2834.

Dragovich, P.S., Prins, T.J., Zhou, R., Fuhrman, S.A., Patick, A.K., Matthews, D.A., Ford, C.E., Meador, III, J.W., Ferre, R.A., Worland, S.T., 1999a. Structure-based design, synthesis, and biological evaluation of irreversible human rhinovirus 3C protease inhibitors. 3. Structure–activity studies of ketomethylene-containing peptidomimetics. J. Med. Chem. 42, 1203–1212.

Dragovich, P.S., Prins, T.J., Zhou, R., Webber, S.E., Marakovits, J.T., Fuhrman, S.A., Patick, A.K., Matthews, D.A., Lee, C.A., Ford, C.E., Burke, B.J., Rejto, P.A., Hendrickson, T.F., Tuntland, T., Brown, E.L., Meador, III, J.W., Ferre, R.A., Harr, J.E., Kosa, M.B., Worland, S.T., 1999b. Structure-based design, synthesis, and biological evaluation of irreversible human rhinovirus 3C protease inhibitors. 4. Incorporation of P1 lactam moieties as L-glutamine replacements. J. Med. Chem. 42, 1213–1224.

Dragovich, P.S., Webber, S.E., Prins, T.J., Zhou, R., Marakovits, J.T., Tikhe, J.G., Fuhrman, S.A., Patick, A.K., Matthews, D.A., Ford, C.E., Brown, E.L., Binford, S.L., Meador, III, J.W., Ferre, R.A., Worland, S.T., 1999c. Structure-based design of irreversible, tripeptidyl human rhinovirus 3C protease inhibitors containing N-methyl amino acids. Bioorg. Med. Chem. Lett. 9, 2189–2194.

Dragovich, P.S., Zhou, R., Webber, S.E., Prins, T.J., Kwok, A.K., Okano, K., Fuhrman, S.A., Zalman, L.S., Maldonado, F.C., Brown, E.L., Meador, III, J.W., Patick, A.K., Ford, C.E., Brothers, M.A., Binford, S.L., Matthews, D.A., Ferre, R.A., Worland, S.T., 2000. Structure-based design of ketone-containing, tripeptidyl human rhinovirus 3C protease inhibitors. Bioorg. Med. Chem. Lett. 10, 45–48.

Dragovich, P.S., Prins, T.J., Zhou, R., Brown, E.L., Maldonado, F.C., Fuhrman, S.A., Zalman, L.S., Tuntland, T., Lee, C.A., Patick, A.K., Matthews, D.A., Hendrickson, T.F., Kosa, M.B., Liu, B., Batugo, M.R., Gleeson, J.P., Sakata, S.K., Chen, L., Guzman, M.C., Meador, III, J.W., Ferre, R.A., Worland, S.T., 2002. Structure-based design, synthesis, and biological evaluation of irreversible human rhinovirus 3C protease inhibitors. 6. Structure–activity studies of orally bioavailable, 2-pyridone-containing peptidomimetics. J. Med. Chem. 45, 1607–1623.

Dragovich, P.S., Prins, T.J., Zhou, R., Johnson, T.O., Hua, Y., Luu, H.T., Sakata, S.K., Brown, E.L., Maldonado, F.C., Tuntland, T., Lee, C.A., Fuhrman, S.A., Zalman, L.S., Patick, A.K., Matthews, D.A., Wu, E.Y., Guo, M., Borer, B.C., Nayyar, N.K., Moran, T., Chen, L., Rejto, P.A., Rose, P.W., Guzman, M.C., Dovalsantos, E.Z., Lee, S., McGee, K., Mohajeri, M., Liese, A., Tao, J., Kosa, M.B., Liu, B., Batugo, M.R., Gleeson, J.P., Wu, Z.P., Liu, J., Meador, III, J.W., Ferre, R.A., 2003. Structure-based design, synthesis, and biological evaluation of irreversible human rhinovirus 3C protease inhibitors. 8. Pharmacological optimization of orally bioavailable 2-pyridone-containing peptidomimetics. J. Med. Chem. 46, 4572–4585.

Fan, K., Wei, P., Feng, Q., Chen, S., Huang, C., Ma, L., Lai, B., Pei, J., Liu, Y., Chen, J., Lai, L., 2004. Biosynthesis, purification, and substrate specificity of severe acute respiratory syndrome coronavirus 3C-like proteinase. J. Biol. Chem. 279, 1637–1642.

Finlay, B.B., See, R.H., Brunham, R.C., 2004. Rapid response research to emerging infectious diseases: lessons from SARS. Nat. Rev. Microbiol. 2, 602–607.

Galasiti, Kankanamalage, A.C., Kim, Y., Weerawarna, P.M., Uy, R.A., Damalanka, V.C., Mandadapu, S.R., Alliston, K.R., Mehzabeen, N., Battaile, K.P., Lovell, S., Chang, K.O., Groutas, W.C., 2015. Structure-guided design and optimization of dipeptidyl inhibitors of norovirus 3CL protease.Structure–activity relationships and biochemical, X-ray crystallographic, cell-based, and in vivo studies. J. Med. Chem. 58, 3144–3155.

Ghosh, A.K., Xi, K., Grum-Tokars, V., Xu, X., Ratia, K., Fu, W., Houser, K.V., Baker, S.C., Johnson, M.E., Mesecar, A.D., 2007. Structure-based design, synthesis, and biological evaluation of peptidomimetic SARS-CoV 3CLpro inhibitors. Bioorg. Med. Chem. Lett. 17, 5876–5880.

Grum-Tokars, V., Ratia, K., Begaye, A., Baker, S.C., Mesecar, A.D., 2008. Evaluating the 3C-like protease activity of SARS-Coronavirus: recommendations for standardized assays for drug discovery. Virus Res. 133, 63–73.

Gupta, S.P., 2007. Quantitative structure–activity relationship studies on zinc-containing metalloproteinase inhibitors. Chem. Rev. 107, 3042–3087.

Hegyi, A., Friebe, A., Gorbalenya, A.E., Ziebuhr, J., 2002a. Mutational analysis of the active centre of coronavirus 3C-like proteases. J. Gen. Virol. 83, 581–593.

Hegyi, A., Ziebuhr, J., 2002b. Conservation of substrate specificities among coronavirus main proteases. J. Gen. Virol. 83, 595–599.

Herold, J., Raabe, T., Schelle-Prinz, B., Siddell, S.G., 1993. Nucleotide sequence of the human coronavirus 229E RNA polymerase locus. Virol. 195, 680–691.

Holmes, K.V., 2003. SARS coronavirus: a new challenge for prevention and therapy. J. Clin. Invest. 111, 1605–1609.

Hsu, J.T., Kuo, C.J., Hsieh, H.P., Wang, Y.C., Huang, K.K., Lin, C.P., Huang, P.F., Chen, X., Liang, P.H., 2004. Evaluation of metal-conjugated compounds as inhibitors of 3CL protease of SARS-CoV. FEBS. Lett. 574, 116–120.

Jain, R.P., Pettersson, H.I., Zhang, J., Aull, K.D., Fortin, P.D., Huitema, C., Eltis, L.D., Parrish, J.C., James, M.N., Wishart, D.S., Vederas, J.C., 2004. Synthesis and evaluation of keto-glutamine analogues as potent inhibitors of severe acute respiratory syndrome 3CLpro. J. Med. Chem. 47, 6113–6116.

Jiang, S., He, Y., Liu, S., 2005. SARS vaccine development. Emerg. Infect. Dis. 11, 1016–1020.

Johnson, T.O., Hua, Y., Luu, H.T., Brown, E.L., Chan, F., Chu, S.S., Dragovich, P.S., Eastman, B.W., Ferre, R.A., Fuhrman, S.A., Hendrickson, T.F., Maldonado, F.C., Matthews, D.A., Meador, III, J.W., Patick, A.K., Reich, S.H., Skalitzky, D.J., Worland, S.T., Yang, M., Zalman, L.S., 2002. Structure-based design of a parallel synthetic array directed toward the discovery of irreversible inhibitors of human rhinovirus 3C protease. J. Med. Chem. 45, 2016–2023.

Khan, G., 2013. A novel coronavirus capable of lethal human infections: an emerging picture. Virol. J. 10, 66.

Kim, Y., Shivanna, V., Narayanan, S., Prior, A.M., Weerasekara, S., Hua, D.H., Kankanamalage, A.C., Groutas, W.C., Chang, K.O., 2015. Broad-spectrum inhibitors against 3C-like proteases of feline coronaviruses and feline caliciviruses. J. Virol. 89, 4942–4950.

Lee, N., Hui, D., Wu, A., Chan, P., Cameron, P., Joynt, G.M., Ahuja, A., Yung, M.Y., Leung, C.B., To, K.F., Lui, S.F., Szeto, C.C., Chung, S., Sung, J.J., 2003. A major outbreak of severe acute respiratory syndrome in Hong Kong. N. Engl. J. Med. 348, 1986–1994.

Li, B.J., Tang, Q., Cheng, D., Qin, C., Xie, F.Y., Wei, Q., Xu, J., Liu, Y., Zheng, B.J., Woodle, M.C., Zhong, N., Lu, P.Y., 2005. Using siRNA in prophylactic and therapeutic regimens against SARS coronavirus in Rhesus macaque. Nat. Med. 11, 944–951.

Liu, W., Zhu, H.M., Niu, G.J., Shi, E.Z., Chen, J., Sun, B., Chen, W.Q., Zhou, H.G., Yang, C., 2014. Synthesis, modification and docking studies of 5-sulfonyl isatin derivatives as SARS-CoV 3C-like protease inhibitors. Bioorg. Med. Chem. 22, 292–302.

Lu, I.L., Mahindroo, N., Liang, P.H., Peng, Y.H., Kuo, C.J., Tsai, K.C., Hsieh, H.P., Chao, Y.S., Wu, S.Y., 2006. Structure-based drug design and structural biology study of novel nonpeptide inhibitors of severe acute respiratory syndrome coronavirus main protease. J. Med. Chem. 49, 5154–5161.

Mandadapu, S.R., Gunnam, M.R., Tiew, K.C., Uy, R.A., Prior, A.M., Alliston, K.R., Hua, D.H., Kim, Y., Chang, K.O., Groutas, W.C., 2013a. Inhibition of norovirus 3CL protease by bisulfite adducts of transition state inhibitors. Bioorg. Med. Chem. Lett. 23, 62–65.

Mandadapu, S.R., Weerawarna, P.M., Prior, A.M., Uy, R.A., Aravapalli, S., Alliston, K.R., Lushington, G.H., Kim, Y., Hua, D.H., Chang, K.O., Groutas, W.C., 2013b. Macrocyclic inhibitors of 3C and 3C-like proteases of picornavirus, norovirus, and coronavirus. Bioorg. Med. Chem. Lett. 23, 3709–3712.

Marra, M.A., Jones, S.J., Astell, C.R., Holt, R.A., Brooks-Wilson, A., Butterfield, Y.S., Khattra, J., Asano, J.K., Barber, S.A., Chan, S.Y., Cloutier, A., Coughlin, S.M., Freeman, D., Girn, N., Griffith, O.L., Leach, S.R., Mayo, M., McDonald, H., Montgomery, S.B., Pandoh, P.K., Petrescu, A.S., Robertson, A.G., Schein, J.E., Siddiqui, A., Smailus, D.E., Stott, J.M., Yang, G.S., Plummer, F., Andonov, A., Artsob, H., Bastien, N., Bernard, K., Booth, T.F., Bowness, D., Czub, M., Drebot, M., Fernando, L., Flick, R., Garbutt, M., Gray, M., Grolla, A., Jones, S., Feldmann, H., Meyers, A., Kabani, A., Li, Y., Normand, S., Stroher, U., Tipples, G.A., Tyler, S., Vogrig, R., Ward, D., Watson, B., Brunham, R.C., Krajden, M., Petric, M., Skowronski, D.M., Upton, C., Roper, R.L., 2003. The genome sequence of the SARS-associated coronavirus. Science 300, 1399–1404.

McMinn, P.C., 2012. Recent advances in the molecular epidemiology and control of human enterovirus 71 infection. Curr. Opin. Virol. 2, 199–205.

Mohamed, S.F., Ibrahiem, A.A., Amr Abd El-Galil, E., Abdalla, M.M., 2015. SARS-CoV 3C-like protease inhibitors of some newly synthesized substituted pyrazoles and substituted pyrimidines based on 1-(3-aminophenyl)-3-(1H-indol-3-yl)prop-2-en-1-one. Int. J. Pharmacol. 11, 749–756.

Myint, S.H., 1995. Human coronavirus infections. In: Siddell, S.G. (Ed.), The Coronaviridae. Plenum press, New York, pp. 389–401.

Nguyen, T.T., Ryu, H.J., Lee, S.H., Hwang, S., Cha, J., Breton, V., Kim, D., 2012. Flavonoid-mediated inhibition of SARS coronavirus 3C-like protease expressed in Pichia pastoris. Biotechnol. Lett. 34, 831–838.

Nguyen, T.T., Ryu, H.J., Lee, S.H., Hwang, S., Breton, V., Rhee, J.H., Kim, D., 2011. Virtual screening identification of novel severe acute respiratory syndrome 3C-like protease inhibitors and in vitro confirmation. Bioorg. Med. Chem. Lett. 21, 3088–3091.

Niu, C., Yin, J., Zhang, J., Vederas, J.C., James, M.N., 2008. Molecular docking identifies the binding of 3-chloropyridine moieties specifically to the S1 pocket of SARS-CoV M[pro]. Bioorg. Med. Chem. 16, 293–302.

Patel, M.M., Hall, A.J., Vinjé, J., Parashar, U.D., 2009. Noroviruses: a comprehensive review. J. Clin. Virol. 44, 1–8.

Perlman, S., Netland, J., 2009. Coronaviruses post-SARS: update on replication and pathogenesis. Nat. Rev. Microbiol. 7, 439–450.

Pogrebnyak, N., Golovkin, M., Andrianov, V., Spitsin, S., Smirnov, Y., Egolf, R., Koprowski, H., 2005. Severe acute respiratory syndrome (SARS) S protein production in plants: development of recombinant vaccine. Proc. Natl. Acad. Sci. USA 102, 9062–9067.

Prior, A.M., Kim, Y., Weerasekara, S., Moroze, M., Alliston, K.R., Uy, R.A., Groutas, W.C., Chang, K.O., Hua, D.H., 2013. Design, synthesis, and bioevaluation of viral 3C and 3C-like protease inhibitors. Bioorg. Med. Chem. Lett. 23, 6317–6320.

Ramajayam, R., Tan, K.P., Liu, H.G., Liang, P.H., 2010. Synthesis and evaluation of pyrazolone compounds as SARS-coronavirus 3C-like protease inhibitors. Bioorg. Med. Chem. 18, 7849–7854.

Regnier, T., Sarma, D., Hidaka, K., Bacha, U., Freire, E., Hayashi, Y., Kiso, Y., 2009. New developments for the design, synthesis and biological evaluation of potent SARS-CoV 3CL (pro) inhibitors. Bioorg. Med. Chem. Lett. 19, 2722–2727.

Ren, L., Xiang, Z., Guo, L., Wang, J., 2012. Viral infections of the lower respiratory tract. Curr. Infect. Dis. Rep. 14, 284–291.

Rota, P.A., Oberste, M.S., Monroe, S.S., Nix, W.A., Campagnoli, R., Icenogle, J.P., Peñaranda, S., Bankamp, B., Maher, K., Chen, M.H., Tong, S., Tamin, A., Lowe, L., Frace, M., DeRisi, J.L., Chen, Q., Wang, D., Erdman, D.D., Peret, T.C., Burns, C., Ksiazek, T.G., Rollin, P.E., Sanchez, A., Liffick, S., Holloway, B., Limor, J., McCaustland, K., Olsen-Rasmussen, M., Fouchier, R., Günther, S., Osterhaus, A.D., Drosten, C., Pallansch, M.A., Anderson, L.J., Bellini, W.J., 2003. Characterization of a novel coronavirus associated with severe acute respiratory syndrome. Science 300, 1394–1399.

Ryu, Y.B., Jeong, H.J., Kim, J.H., Kim, Y.M., Park, J.Y., Kim, D., Nguyen, T.T., Park, S.J., Chang, J.S., Park, K.H., Rho, M.C., Lee, W.S., 2010. Biflavonoids from Torreya nucifera displaying SARS-CoV 3CL (pro) inhibition. Bioorg. Med. Chem. 18, 7940–7947.

Shie, J.J., Fang, J.M., Kuo, C.J., Kuo, T.H., Liang, P.H., Huang, H.J., Yang, W.B., Lin, C.H., Chen, J.L., Wu, Y.T., Wong, C.H., 2005a. Discovery of potent anilide inhibitors against the severe acute respiratory syndrome 3CL protease. J. Med. Chem. 48, 4469–4473.

Shie, J.J., Fang, J.M., Kuo, T.H., Kuo, C.J., Liang, P.H., Huang, H.J., Wu, Y.T., Jan, J.T., Cheng, Y.S., Wong, C.H., 2005b. Inhibition of the severe acute respiratory syndrome 3CL protease by peptidomimetic alpha, beta-unsaturated esters. Bioorg. Med. Chem. 13, 5240–5252.

Shigeta, S., Yamase, T., 2005. Current status of anti-SARS agents. Antivir. Chem. Chemother. 16, 23–31.

Solomon, T., Lewthwaite, P., Perera, D., Cardosa, M.J., McMinn, P., Ooi, M.H., 2010. Virology, epidemiology, pathogenesis, and control of enterovirus 71. Lancet. Infect. Dis. 10, 778–790.

St. John, S.E., Tomar, S., Stauffer, S.R., Mesecar, A.D., 2015. Targeting zoonotic viruses: structure-based inhibition of the 3C-like protease from bat coronavirus HKU4-The likely reservoir host to the human coronavirus that causes middle east respiratory syndrome (MERS). Bioorg. Med. Chem. 23, 6036–6048.

Tao, P., Zhang, J., Tang, N., Zhang, B.Q., He, T.C., Huang, A.L., 2005. Potent and specific inhibition of SARS-CoV antigen expression by RNA interference. Chin. Med. J. (Engl.) 118, 714–719.

Thanigaimalai, P., Konno, S., Yamamoto, T., Koiwai, Y., Taguchi, A., Takayama, K., Yakushiji, F., Akaji, K., Chen, S.E., Naser-Tavakolian, A., Schön, A., Freire, E., Hayashi, Y., 2013a. Development of potent dipeptide-type SARS-CoV 3CL protease inhibitors with novel P3 scaffolds: design, synthesis, biological evaluation, and docking studies. Eur. J. Med. Chem. 68, 372–384.

Thanigaimalai, P., Konno, S., Yamamoto, T., Koiwai, Y., Taguchi, A., Takayama, K., Yakushiji, F., Akaji, K., Kiso, Y., Kawasaki, Y., Chen, S.E., Naser-Tavakolian, A., Schön, A., Freire, E., Hayashi, Y., 2013b. Design, synthesis, and biological evaluation of novel dipeptide-type SARS-CoV 3CL protease inhibitors: structure–activity relationship study. Eur. J. Med. Chem. 65, 436–447.

Thiel, V., Herold, J., Schelle, B., Siddell, S.G., 2001. Viral replicase gene products suffice for coronavirus discontinuous transcription. J. Virol. 75, 6676–6681.

Tsai, K.C., Chen, S.Y., Liang, P.H., Lu, I.L., Mahindroo, N., Hsieh, H.P., Chao, Y.S., Liu, L., Liu, D., Lien, W., Lin, T.H., Wu, S.Y., 2006. Discovery of a novel family of SARS-CoV protease inhibitors by virtual screening and 3D-QSAR studies. J. Med. Chem. 49, 3485–3495.

Tsukada, H., Blow, D.M., 1985. Structure of alpha-chymotrypsin refined at 1.68 Å resolution. J. Mol. Biol. 184, 703–711.

Tuboly, T., Yu, W., Bailey, A., Degrandis, S., Du, S., Erickson, L., Nagy, E., 2000. Immunogenicity of porcine transmissible gastroenteritis virus spike protein expressed in plants. Vaccine 18, 2023–2028.

Turlington, M., Chun, A., Tomar, S., Eggler, A., Grum-Tokars, V., Jacobs, J., Daniels, J.S., Dawson, E., Saldanha, A., Chase, P., Baez-Santos, Y.M., Lindsley, C.W., Hodder, P., Mesecar, A.D., Stauffer, S.R., 2013. Discovery of *N*-(benzo [1,2,3]triazol-1-yl)-*N*-(benzyl)acetamido)phenyl) carboxamides as severe acute respiratory syndrome coronavirus (SARS-CoV) 3CLpro inhibitors: identification of ML300 and noncovalent nanomolar inhibitors with an induced-fit binding. Bioorg. Med. Chem. Lett. 23, 6172–6177.

Turner, R.B., Couch, R.B., 2007. Rhiniviruses. In: Knipe, D.M., Howley, P.M. (Eds.), Fields Virology. Lippincott Williams & Wilkins, Philadelphia, PA, pp. 895–909.

Verma, R.P., Hansch, C., 2009. Camptothecins: a SAR/QSAR study. Chem. Rev. 109, 213–235.

Wang, Z., Ren, L., Zhao, X., Hung, T., Meng, A., Wang, J., Chen, Y.G., 2004. Inhibition of severe acute respiratory syndrome virus replication by small interfering RNAs in mammalian cells. J. Virol. 78, 7523–7527.

Webber, S.E., Marakovits, J.T., Dragovich, P.S., Prins, T.J., Zhou, R., Fuhrman, S.A., Patick, A.K., Matthews, D.A., Lee, C.A., Srinivasan, B., Moran, T., Ford, C.E., Brothers, M.A., Harr, J.E., Meador, III, J.W., Ferre, R.A., Worland, S.T., 2001. Design and synthesis of irreversible depsipeptidyl human rhinovirus 3C protease inhibitors. Bioorg. Med. Chem. Lett. 11, 2683–2686.

Winther, B., 2011. Rhinovirus infections in the upper airway. Proc. Am. Thorac. Soc. 8, 79–89.

Wu, C.Y., Jan, J.T., Ma, S.H., Kuo, C.J., Juan, H.F., Cheng, Y.S., Hsu, H.H., Huang, H.C., Wu, D., Brik, A., Liang, F.S., Liu, R.S., Fang, J.M., Chen, S.T., Liang, P.H., Wong, C.H., 2004. Small molecules targeting severe acute respiratory syndrome human coronavirus. Proc. Natl. Acad. Sci. USA 101, 10012–10017.

Wu, C.Y., King, K.Y., Kuo, C.J., Fang, J.M., Wu, Y.T., Ho, M.Y., Liao, C.L., Shie, J.J., Liang, P.H., Wong, C.H., 2006. Stable benzotriazole esters as mechanism-based inactivators of the severe acute respiratory syndrome 3CL protease. Chem. Biol. 13, 261–268.

Yang, H., Yang, M., Ding, Y., Liu, Y., Lou, Z., Zhou, Z., Sun, L., Mo, L., Ye, S., Pang, H., Gao, G.F., Anand, K., Bartlam, M., Hilgenfeld, R., Rao, Z., 2003. The crystal structures of severe acute respiratory syndrome virus main protease and its complex with an inhibitor. Proc. Natl. Acad. Sci. USA 100, 13190–13195.

Yang, Q., Chen, L., He, X., Gao, Z., Shen, X., Bai, D., 2008. Design and synthesis of cinanserin analogs as severe acute respiratory syndrome coronavirus 3CL protease inhibitors. Chem. Pharm. Bull. 56, 1400–1405.

Yang, Z.Y., Kong, W.P., Huang, Y., Roberts, A., Murphy, B.R., Subbarao, K., Nabel, G.J., 2004. A DNA vaccine induces SARS coronavirus neutralization and protective immunity in mice. Nature 428, 561–564.

Zhai, S., Liu, W., Yan, B., 2007. Recent patents on treatment of severe acute respiratory syndrome (SARS). Recent Pat. Antiinfect. Drug Discov. 2, 1–10.

Zhang, J., Pettersson, H.I., Huitema, C., Niu, C., Yin, J., James, M.N., Eltis, L.D., Vederas, J.C., 2007. Design, synthesis, and evaluation of inhibitors for severe acute respiratory syndrome 3C-like protease based on phthalhydrazide ketones or heteroaromatic esters. J. Med. Chem. 50, 1850–1864.

Zhang, J., Huitema, C., Niu, C., Yin, J., James, M.N., Eltis, L.D., Vederas, J.C., 2008. Aryl methylene ketones and fluorinated methylene ketones as reversible inhibitors for severe acute respiratory syndrome (SARS) 3C-like proteinase. Bioorg. Chem. 36, 229–240.

Zhou, L., Liu, Y., Zhang, W., Wei, P., Huang, C., Pei, J., Yuan, Y., Lai, L., 2006. Isatin compounds as noncovalent SARS coronavirus 3C-like protease inhibitors. J. Med. Chem. 49, 3440–3443.

Ziebuhr, J., Snijder, E.J., Gorbalenya, A.E., 2000. Virus-encoded proteinases and proteolytic processing in the *Nidovirales*. J. Gen. Virol. 81, 853–879.

FURTHER READING

Ghosh, A.K., Takayama, J., Aubin, Y., Ratia, K., Chaudhuri, R., Baez, Y., Sleeman, K., Coughlin, M., Nichols, D.B., Mulhearn, D.C., Prabhakar, B.S., Baker, S.C., Johnson, M.E., Mesecar, A.D., 2009. Structure-based design, synthesis, and biological evaluation of a series of novel and reversible inhibitors for the severe acute respiratory syndrome-coronavirus papain-like protease. J. Med. Chem. 52, 5228–5240.

Ghosh, A.K., Takayama, J., Rao, K.V., Ratia, K., Chaudhuri, R., Mulhearn, D.C., Lee, H., Nichols, D.B., Baliji, S., Baker, S.C., Johnson, M.E., Mesecar, A.D., 2010. Severe acute respiratory syndrome coronavirus papain-like novel protease inhibitors: design, synthesis, protein-ligand X-ray structure and biological evaluation. J. Med. Chem. 53, 4968–4979.

Song, Y.H., Kim, D.W., Curtis-Long, M.J., Yuk, H.J., Wang, Y., Zhuang, N., Lee, K.H., Jeon, K.S., Park, K.H., 2014. Papain-like protease (PLpro) inhibitory effects of cinnamic amides from *Tribulus terrestris* fruits. Biol. Pharm. Bull. 37, 1021–1028.